

UNIVERSITY OF THE WESTERN CAPE



UNIVERSITY *of the*
WESTERN CAPE

Imprints of Primordial Non-Gaussianity on Large Scale Structure in the Universe

by

Mahmoud Yousif Ali Wahba Hashim

A thesis submitted in partial fulfillment for the
degree of Doctor of Philosophy

in the
Faculty of Natural Sciences
Physics and Astronomy Department

Supervisor
Prof. Roy Maartens

September 2016

Declaration of Authorship

I, Mahmoud Hashim, declare that this thesis titled, 'Imprints of Primordial Non-Gaussianity on Large Scale Structure in the Universe' and the work presented in it are my own. I confirm that:

- This work was done wholly or mainly while in candidature for a research degree at this University.
- Where any part of this thesis has previously been submitted for a degree or any other qualification at this University or any other institution, this has been clearly stated.
- Where I have consulted the published work of others, this is always clearly attributed.
- Where I have quoted from the work of others, the source is always given. With the exception of such quotations, this thesis is entirely my own work.
- I have acknowledged all main sources of help.
- Where the thesis is based on work done by myself jointly with others, I have made clear exactly what was done by others and what I have contributed myself.

Signed: Mahmoud Hashim

Date: 05 October 2016

“Here it is standing: atoms with consciousness; matter with curiosity. Stands at the sea, wonders at wondering: I, a universe of atoms an atom in the universe.”

Richard Feynman



UNIVERSITY *of the*
WESTERN CAPE

Abstract

Doctor of Philosophy

by [Mahmoud Yousif Ali Wahba Hashim](#)

Large scale structure in the universe is one of the most important probing tools for cosmological modelling. Assuming the hot big bang model of the universe, the expansion history has undergone two phases of acceleration. The primordial phase which had been considered to be responsible for seeding the structure formation and the late phase driven by the mysterious component of the cosmos, Dark Energy. Early inhomogeneity in the structure formation could though leave a signature on the late time universe. We assume the cosmos to have non-Gaussian initial conditions. Gravitational instability is thought to be responsible for late structure evolution. On local scales, non-linear effects dissipate primordial signal of non-Gaussianity, however on very large scales, the signal is well preserved. Initial non-Gaussianity introduce a scale dependent signature on the galaxy power spectrum on very large scales. This could be very useful to constrain non-Gaussianity parameter via upcoming large scale structure surveys. In this thesis, we show that on very large scales, interacting dark energy perturbations induce a scale-dependent effect on the galaxy power spectrum on large scales. This could degenerate with primordial non-Gaussianity signal, though a disentanglement between the two signatures are necessary for observational constraints. On small scales, N-body simulations for standard cosmological models are used to investigate the signature of primordial non-Gaussianity on halo mass function. It has a significant effect on very large halos however it is negligible for small mass halos. Interacting Dark Energy is assumed to have a similar effect on small scales. We prepare the basis for future work that will combine simulations for Interacting Dark Energy models with non-Gaussian initial conditions.

Acknowledgements

I 'd like to thank my supervisor Roy Maartens for his guidance through the work of this thesis, his great support and his continuous encouragement. Also I 'd like to thank Daniele Bertacca for his support and his co-supervision to the early stage of my PhD.

My special thanks goes to Marco Baldi for his help and very useful comments during the simulation work done in this thesis.

My love and deep appreciation to my family for their love, support and encouragement.



Contents

Declaration of Authorship	i
Abstract	iii
Acknowledgements	iv
Publications	vii
List of Figures	viii
List of Tables	xii
1 Introduction	1
1.1 Expansion history of the universe	2
1.1.1 Friedmann equations	2
1.1.2 Λ CDM concordance model	5
1.2 Thesis outline	7
2 Structure formation and gravitational instability	9
2.1 Dynamics of gravitational instability	9
2.1.1 Linear cosmological perturbation theory	10
2.1.1.1 Non-relativistic matter	12
2.1.1.2 Dynamical dark energy	15
2.1.2 Non-linear cosmology	19
2.1.2.1 Spherical collapse	21
2.1.2.2 The mass function of collapsed objects	22
2.2 2–point correlation function and power spectrum	24
2.2.1 Power spectrum evolution in linear perturbation theory	25
2.3 Physical origin of fluctuations from inflation	25
2.3.1 Primordial non-Gaussianity	26
2.3.1.1 Imprints on large-scale structure: scale dependent bias	28
2.4 N-body simulations	30
2.4.1 Initial conditions	31
2.4.1.1 Non-Gaussian initial conditions: local type	31

2.5	Conclusion	32
3	Primordial non-Gaussianity degeneracy with interacting dark sector on large scales	34
3.1	Interacting dark energy dynamics and perturbations	34
3.1.1	Background dynamics	35
3.1.2	Perturbations	35
3.1.3	A simple model of interacting dark energy	37
3.1.4	Initial conditions	39
3.1.5	Growth functions	43
3.2	Large-scale power in interacting dark energy	43
3.2.1	Galaxy overdensity in interacting dark energy and primordial non-Gaussianity	44
3.2.2	Comparing the galaxy power	45
3.2.3	Interacting dark energy mimics primordial non-Gaussianity	45
3.2.4	Breaking the degeneracy between interacting dark energy and primordial non-Gaussianity	46
3.3	Interacting quintessence with an exponential potential	47
3.3.1	Background dynamics	47
3.3.2	Perturbations	49
3.3.3	Galaxy overdensity in interacting quintessence model	50
3.4	Conclusion	51
4	Imprints of primordial non-Gaussianity on non-linear scales	53
4.1	N-body simulation setting	54
4.1.1	Initial conditions generation	55
4.1.1.1	Local non-Gaussianity implementation	55
4.1.2	Simulation settings test	55
4.1.3	CosmoSuite: A toolkit for running and analysing cosmological N-body simulations	56
4.2	Results	58
4.2.1	Halo mass function	67
4.2.2	Non-linear power spectrum	76
4.3	Qualitative comparison with interacting dark energy simulations	85
4.3.1	CoDECS simulations	85
4.3.2	Halo mass function	86
4.4	Conclusion	86
5	Conclusion and future work	89
5.1	Future work	90
	Bibliography	92

Publications

The following paper has been published based on the work done in this thesis:

- **Mahmoud Hashim**, Daniele Bertacca, and Roy Maartens. *Degeneracy between primordial non-Gaussianity and interaction in the dark sector*. Phys. Rev., *D90* (10):103518, 2014. doi: 10.1103/PhysRevD.90.103518.

The following papers are in preparation:

- **Mahmoud Hashim**, Marco Baldi, Daniele Bertacca, and Roy Maartens. *Interacting dark energy N-body simulations with non-Gaussian initial conditions*. In preparation.
- Elisa Chisari, **Mahmoud Hashim** and Julien Devriendt. *Investigating AGN effect on cosmic density and velocity fields in the HORIZON-AGN simulation*. In preparation.



List of Figures

3.1	<i>Upper:</i> Evolution of effective dark energy equation of state, w_x^{eff} , with $w_x = -0.9$ and for different $\Gamma > 0$, in the interacting dark energy model (3.25). The $\Gamma = 0$ limit is $w_x^{\text{eff}} = w_x = -0.9$. <i>Lower:</i> The $\Gamma < 0$ case, with $w_x = -1.1$	38
3.2	<i>Upper:</i> Relative galaxy overdensity [see (3.45)] at $a = 1$ with dark sector interactions, for different $\Gamma > 0$ and with $w_x = -0.9$. The vertical dashed line is the Hubble scale, $k = H_0$. The $\Gamma = 0$ limit is the horizontal line through 0. We used $b(1) = 2$. <i>Lower:</i> The $\Gamma < 0$ case, with $w_x = -1.1$	40
3.3	The relative galaxy overdensity as in Fig. 3.2 but for the case of primordial non-Gaussianity, with $f_{\text{NL}} < 0$ (<i>Up</i>) and $f_{\text{NL}} > 0$ (<i>Down</i>).	41
3.4	<i>Upper:</i> Galaxy power spectrum P_g at $a = 1$ for an interacting dark energy model with $\Gamma = 0.03H_0$ and for a primordial non-Gaussianity model with $f_{\text{NL}} = -7.69$. The black (solid) line is the fiducial w CDM model without interaction or primordial non-Gaussianity. We set $b(1) = 2$ and $w_x = -0.9$. <i>Lower:</i> For $\Gamma = -0.03H_0$ and $f_{\text{NL}} = 4.81$, with $w_x = -1.1$	42
3.5	<i>Upper:</i> Effective primordial non-Gaussianity parameter $f_{\text{NL}}^{\text{eff}}$ corresponding to interaction rate $\Gamma > 0$ at different redshift values. We take $w_x = -0.9$. <i>Lower:</i> For $\Gamma < 0$ and $w_x = -1.1$	44
3.6	The equation of state of interacting quintessence dark energy at different values of the interaction parameter β	49
3.7	Relative galaxy overdensity for interacting quintessence dark energy at $a = 1.0$ for different values of the interacting constant β	50
4.1	Initial matter power spectrum and transfer function at redshift $z = 49.0$ calculated using CAMB.	56
4.2	Halo mass function ratio for $f_{\text{NL}}^{\text{loc}} = 500$ at redshift $z = 1.5$ compared with Wagner et al results [87].	57
4.3	CosmoSuite Graphical User Interface.	57
4.4	Particle projection plot of GADGET-2 output snapshots of redshift series $z = 2.01, 1.0, 0.55, 0.0$ for different values of non-Gaussianity $f_{\text{NL}}^{\text{loc}} = 0.0, 250.0$ from upper-left to lower-right respectively. The projection depth is 7.0 Mpc and the plot is weighted with dark matter halo mass.	59
4.5	Particle projection plot of GADGET-2 output snapshots of redshift series $z = 2.01, 1.0, 0.55, 0.0$ for different values of non-Gaussianity $f_{\text{NL}}^{\text{loc}} = 500.0, 1000.0$ from upper-left to lower-right respectively. The projection depth is 7.0 Mpc and the plot is weighted with dark matter halo mass.	60

- 4.6 Particle projection plot of GADGET-2 output snapshots of redshift series $z = 2.01, 1.0, 0.55, 0.0$ for different values of non-Gaussianity $f_{\text{NL}}^{\text{loc}} = 0.0, -250.0$ from upper-left to lower-right respectively. The projection depth is 7.0 Mpc and the plot is weighted with dark matter halo mass. 61
- 4.7 Particle projection plot of GADGET-2 output snapshots of redshift series $z = 2.01, 1.0, 0.55, 0.0$ for different values of non-Gaussianity $f_{\text{NL}}^{\text{loc}} = -500.0, -1000.0$ from upper-left to lower-right respectively. The projection depth is 7.0 Mpc and the plot is weighted with dark matter halo mass. 62
- 4.8 Particle projection plot of GADGET-2 output snapshots of different values of non-Gaussianity $f_{\text{NL}} = 0.0, 250.0, 500.0, 1000.0$ for redshift series $z = 0.0, 0.55$ from upper-left to lower-right respectively. The projection depth is 7.0 Mpc and the plot is weighted with dark matter halo mass. 63
- 4.9 Particle projection plot of GADGET-2 output snapshots of different values of non-Gaussianity $f_{\text{NL}} = 0.0, 250.0, 500.0, 1000.0$ for redshift series $z = 1.0, 2.01$ from upper-left to lower-right respectively. The projection depth is 7.0 Mpc and the plot is weighted with dark matter halo mass. 64
- 4.10 Particle projection plot of GADGET-2 output snapshots of different values of non-Gaussianity $f_{\text{NL}}^{\text{loc}} = 0.0, -250.0, -500.0, -1000.0$ for redshift series $z = 0.0, 0.55$ from upper-left to lower-right respectively. The projection depth is 7.0 Mpc and the plot is weighted with dark matter halo mass. 65
- 4.11 Particle projection plot of GADGET-2 output snapshots of different values of non-Gaussianity $f_{\text{NL}}^{\text{loc}} = 0.0, -250.0, -500.0, -1000.0$ for redshift series $z = 1.0, 2.01$ from upper-left to lower-right respectively. The projection depth is 7.0 Mpc and the plot is weighted with dark matter halo mass. 66
- 4.12 *Upper:* Cumulative halo mass function for different non-Gaussianity parameter $f_{\text{NL}}^{\text{loc}} = 0.0, 250.0, 500.0, 1000.0$ at redshift $z = 0.0$. Black solid line represents Reed 2007 analytical fit. *Lower:* Cumulative halo mass function residual with respect to Gaussian ΛCDM model at redshift $z = 0.0$. 68
- 4.13 *Upper:* Cumulative halo mass function for different non-Gaussianity parameter $f_{\text{NL}}^{\text{loc}} = 0.0, -250.0, -500.0, -1000.0$ at redshift $z = 0.0$. Black solid line represents Reed 2007 analytical fit. *Lower:* Cumulative halo mass function residual with respect to Gaussian ΛCDM model at redshift $z = 0.0$ 69
- 4.14 *Upper:* Cumulative halo mass function for different non-Gaussianity parameter $f_{\text{NL}}^{\text{loc}} = 0.0, 250.0, 500.0, 1000.0$ at redshift $z = 0.55$. Black solid line represents Reed 2007 analytical fit. *Lower:* Cumulative halo mass function residual with respect to Gaussian ΛCDM model at redshift $z = 0.55$. 70
- 4.15 *Upper:* Cumulative halo mass function for different non-Gaussianity parameter $f_{\text{NL}}^{\text{loc}} = 0.0, -250.0, -500.0, -1000.0$ at redshift $z = 0.55$. Black solid line represents Reed 2007 analytical fit. *Lower:* Cumulative halo mass function residual with respect to Gaussian ΛCDM model at redshift $z = 0.55$ 71
- 4.16 *Upper:* Cumulative halo mass function for different non-Gaussianity parameter $f_{\text{NL}}^{\text{loc}} = 0.0, 250.0, 500.0, 1000.0$ at redshift $z = 1.0$. Black solid line represents Reed 2007 analytical fit. *Lower:* Cumulative halo mass function residual with respect to Gaussian ΛCDM model at redshift $z = 1.0$. 72

4.17	<i>Upper:</i> Cumulative halo mass function for different non-Gaussianity parameter $f_{\text{NL}}^{\text{loc}} = 0.0, -250.0, -500.0, -1000.0$ at redshift $z = 1.0$. Black solid line represents Reed 2007 analytical fit. <i>Lower:</i> Cumulative halo mass function residual with respect to Gaussian Λ CDM model at redshift $z = 1.0$	73
4.18	<i>Upper:</i> Cumulative halo mass function for different non-Gaussianity parameter $f_{\text{NL}}^{\text{loc}} = 0.0, 250.0, 500.0, 1000.0$ at redshift $z = 2.01$. Black solid line represents Reed 2007 analytical fit. <i>Lower:</i> Cumulative halo mass function residual with respect to Gaussian Λ CDM model at redshift $z = 2.01$	74
4.19	<i>Upper:</i> Cumulative halo mass function for different non-Gaussianity parameter $f_{\text{NL}}^{\text{loc}} = 0.0, -250.0, -500.0, -1000.0$ at redshift $z = 2.01$. Black solid line represents Reed 2007 analytical fit. <i>Lower:</i> Cumulative halo mass function residual with respect to Gaussian Λ CDM model at redshift $z = 2.01$	75
4.20	<i>Upper:</i> Non-linear power spectrum for different non-Gaussianity parameter $f_{\text{NL}}^{\text{loc}} = 0.0, 250.0, 500.0, 1000.0$ at redshift $z = 0.0$. Black solid line represents CAMB Halo-fit model prediction. <i>Lower:</i> Non-linear power spectrum residual with respect to Gaussian Λ CDM model at redshift $z = 0.0$	77
4.21	<i>Upper:</i> Non-linear power spectrum for different non-Gaussianity parameter $f_{\text{NL}}^{\text{loc}} = 0.0, -250.0, -500.0, -1000.0$ at redshift $z = 0.0$. Black solid line represents CAMB Halo-fit model prediction. <i>Lower:</i> Non-linear power spectrum residual with respect to Gaussian Λ CDM model at redshift $z = 0.0$	78
4.22	<i>Upper:</i> Non-linear power spectrum for different non-Gaussianity parameter $f_{\text{NL}}^{\text{loc}} = 0.0, 250.0, 500.0, 1000.0$ at redshift $z = 0.55$. Black solid line represents CAMB Halo-fit model prediction. <i>Lower:</i> Non-linear power spectrum residual with respect to Gaussian Λ CDM model at redshift $z = 0.55$	79
4.23	<i>Upper:</i> Non-linear power spectrum for different non-Gaussianity parameter $f_{\text{NL}}^{\text{loc}} = 0.0, -250.0, -500.0, -1000.0$ at redshift $z = 0.55$. Black solid line represents CAMB Halo-fit model prediction. <i>Lower:</i> Non-linear power spectrum residual with respect to Gaussian Λ CDM model at redshift $z = 0.55$	80
4.24	<i>Upper:</i> Non-linear power spectrum for different non-Gaussianity parameter $f_{\text{NL}}^{\text{loc}} = 0.0, 250.0, 500.0, 1000.0$ at redshift $z = 1.0$. Black solid line represents CAMB Halo-fit model prediction. <i>Lower:</i> Non-linear power spectrum residual with respect to Gaussian Λ CDM model at redshift $z = 1.0$	81
4.25	<i>Upper:</i> Non-linear power spectrum for different non-Gaussianity parameter $f_{\text{NL}}^{\text{loc}} = 0.0, -250.0, -500.0, -1000.0$ at redshift $z = 1.0$. Black solid line represents CAMB Halo-fit model prediction. <i>Lower:</i> Non-linear power spectrum residual with respect to Gaussian Λ CDM model at redshift $z = 1.0$	82
4.26	<i>Upper:</i> Non-linear power spectrum for different non-Gaussianity parameter $f_{\text{NL}}^{\text{loc}} = 0.0, 250.0, 500.0, 1000.0$ at redshift $z = 2.01$. Black solid line represents CAMB Halo-fit model prediction. <i>Lower:</i> Non-linear power spectrum residual with respect to Gaussian Λ CDM model at redshift $z = 2.01$	83

- 4.27 *Upper:* Non-linear power spectrum for different non-Gaussianity parameter $f_{\text{NL}}^{\text{loc}} = 0.0, -250.0, -500.0, -1000.0$ at redshift $z = 2.01$. Black solid line represents CAMB Halo-fit model prediction. *Lower:* Non-linear power spectrum residual with respect to Gaussian Λ CDM model at redshift $z = 2.01$ 84
- 4.28 *Upper:* The halo mass function for L-CoDECS simulations of interacting dark energy at $z = 2.01$ for different interaction parameters $\beta = 0.05, 0.1, 0.15$. The solid-dashed line represents Λ CDM mode. *Lower:* The halo mass function residual with respect to Λ CDM model. 87



UNIVERSITY *of the*
WESTERN CAPE

List of Tables

4.1	Cosmological parameters used to generate initial conditions and simulation runs [2].	54
4.2	Set of N-body simulation runs.	54
4.3	Set of L-CoDECS N-body simulation runs.	86



To my kids Omar and Khaled



UNIVERSITY *of the*
WESTERN CAPE

Chapter 1

Introduction

One of the main goals of cosmology is the study of the large scale structure in the universe. Structure formation in the universe mainly arises due to gravitational instabilities on large and small scales [17, 29, 64]. Upcoming galaxy surveys will allow us to better understand the process of the structure formation and to constrain the impacting factors of the initial conditions and the presence of the different components of the cosmos.

Assuming the big bang inflationary model [40], the universe had undergone an early era of cosmic acceleration which led to the amplification of small primordial fluctuations. These seeds of perturbation had grown enormously until they exit the horizon and freeze, keeping all the information about the initial structure of the universe. Simple inflation models suggest that the universe is homogeneous and isotropic. However different models assume that the universe is inhomogeneous with the assumption that the primordial fluctuations are statistically non-Gaussian. Single-field slow-roll inflation model predicts a very small signal of non-Gaussianity, however multi-field inflation models predict large signals [10].

After the inflation era, the universe expands until the frozen primordial signal enters the horizon again and starts to evolve as a seed for late structure formation. Assuming that gravity is the only factor of interaction between late universe components, gravitational instability is the only physical mechanism that produces the observed large scale structures (i.e. galaxies, cluster of galaxies, sheets and filaments). By measuring the statistical nature of the large scale structure, we could constrain the primordial signal of non-Gaussianity on very large scales. Recent studies suggest that the formation of virial objects in the universe is affected by the primordial signal of non-Gaussianity. This leads to a scale dependent bias between galaxies and the dark matter distribution [28].

Current cosmological observations [2] indicate that the cosmos mostly consists of dark components (i.e. dark matter and dark energy), known as the dark sector. These two mysterious components of the universe are responsible for the growth and the decay of the cosmic perturbations. Recently, clustering dark energy has been proven to introduce a scale-dependent signal on very large scales in the galaxy power spectrum [32]. This could be used to determine the nature of dark energy. Interaction between dark energy and dark matter is also introducing a scale dependent signal to the galaxy power spectrum [66].

Other different signals are supposed to affect large scale observables, including general relativistic effects and false gauge effects [18]. This could raise a degeneracy between different signals resulting in misinterpreting parameter constraints.

In this chapter, we give a quick review on the expansion history of the universe assuming homogeneous and isotropic background.

1.1 Expansion history of the universe

The standard model of relativistic big bang cosmology is mainly based on the cosmological principle [31]. It states that the universe is homogeneous and isotropic on very large scales. Cosmic Microwave Background (CMB) radiation observation is one of the main observational tools that support the standard cosmological model (or the Concordance model). By solving the Einstein equations assuming homogeneous and isotropic background, one can reveal the cosmic expansion history.

Observations of the large scale structures in the universe (such as galaxies and cluster of galaxies) indicate that the universe is inhomogeneous in the local regime. These inhomogeneous signatures have evolved in time via gravitational instability. Cosmological perturbation theory suggests that these levels of inhomogeneities can be regarded as small perturbations evolving on homogeneous background universe.

1.1.1 Friedmann equations

In order to describe a relativistic 4-dimensional homogeneous and isotropic space-time, we need to define the Friedmann-Lemaitre-Robertson-Walker (FLRW) line-element as follows

$$ds^2 = g_{\mu\nu} dx^\mu dx^\nu = -dt^2 + a^2(t) \left[\frac{dr^2}{1 - Kr^2} + r^2(d\theta^2 + \sin^2\theta d\phi^2) \right], \quad (1.1)$$

where $a(t)$ is the scale factor which is a function of cosmic time and $g_{\mu\nu}$ is a metric tensor. The curvature constant $K = -1, 0, +1$ corresponds to open, flat and closed universes, respectively.

The Einstein relativistic field equations are given by

$$G_{\nu}^{\mu} = 8\pi G T_{\nu}^{\mu}, \quad (1.2)$$

where T_{ν}^{μ} is the energy-momentum tensor and we assume that $c = 1$. From the metric (1.1), the LHS of (1.2) is given as follows. The Christoffel symbol is given by using the metric $g_{\mu\nu}$

$$\Gamma_{\nu\lambda}^{\mu} = \frac{1}{2}g^{\mu\alpha}(g_{\alpha\nu,\lambda} + g_{\alpha\lambda,\nu} - g_{\nu\lambda,\alpha}), \quad (1.3)$$

where $g_{\alpha\nu,\lambda} \equiv \partial g_{\alpha\nu}/\partial x^{\lambda}$. Note that the metric $g_{\alpha\nu}$ satisfies the relation

$$g^{\mu\alpha}g_{\alpha\nu} = \delta_{\nu}^{\mu}, \quad (1.4)$$

where δ_{ν}^{μ} is Kronecker's delta ($\delta_{\nu}^{\mu} = 1$ for $\mu = \nu$ and $\delta_{\nu}^{\mu} = 0$ for $\mu \neq \nu$).

The non-vanishing components of the Christoffel symbols are

$$\Gamma_{ij}^0 = a^2 H \gamma_{ij}, \quad (1.5)$$

$$\Gamma_{0j}^i = \Gamma_{j0}^i = H \delta_j^i, \quad (1.6)$$

$$\Gamma_{11}^1 = \frac{Kr}{1 - Kr^2}, \quad (1.7)$$

$$\Gamma_{22}^1 = -r(1 - Kr^2), \quad (1.8)$$

$$\Gamma_{33}^1 = -r(1 - Kr^2) \sin^2 \theta, \quad (1.9)$$

$$\Gamma_{33}^2 = -\sin \theta \cos \theta, \quad (1.10)$$

$$\Gamma_{12}^2 = \Gamma_{21}^2 = \Gamma_{13}^3 = \Gamma_{31}^3 = \frac{1}{r}, \quad (1.11)$$

$$\Gamma_{23}^3 = \Gamma_{32}^3 = \cot \theta, \quad (1.12)$$

where γ_{ij} is the 3-dimensional metric given as

$$\gamma_{11} = \frac{1}{1 - Kr^2}, \quad \gamma_{22} = r^2, \quad \gamma_{33} = r^2 \sin^2 \theta, \quad (1.13)$$

and H is the Hubble parameter defined as

$$H \equiv \frac{\dot{a}}{a}, \quad (1.14)$$

where a dot represents a derivative with respect to the cosmic time t .

The Ricci tensor is defined as

$$R_{\mu\nu} = \Gamma_{\mu\nu,\alpha}^{\alpha} - \Gamma_{\mu\alpha,\nu}^{\alpha} + \Gamma_{\mu\nu}^{\alpha}\Gamma_{\alpha\beta}^{\beta} - \Gamma_{\mu\beta}^{\alpha}\Gamma_{\alpha\nu}^{\beta}. \quad (1.15)$$

The non-vanishing components of the Ricci tensor are given by

$$R_{00} = -3(H^2 + \dot{H}), \quad (1.16)$$

$$R_{0i} = R_{i0} = 0, \quad (1.17)$$

$$R_{ij} = a^2 \left(3H^2 + \dot{H} + 2\frac{K}{a^2} \right) \gamma_{ij}. \quad (1.18)$$

The Ricci scalar is defined as the contraction of the Ricci tensor such that

$$R = g^{\mu\nu} R_{\mu\nu}. \quad (1.19)$$

For FLRW metric, it is given by

$$R = 6 \left(2H^2 + \dot{H} + \frac{K}{a^2} \right). \quad (1.20)$$

The Einstein tensor is then defined as

$$G_{\mu\nu} \equiv R_{\mu\nu} - \frac{1}{2}g_{\mu\nu}R. \quad (1.21)$$

The non-vanishing components of the Einstein tensor for FLRW metric are then given by

$$G_0^0 = -3 \left(H^2 + \frac{K}{a^2} \right), \quad (1.22)$$

$$G_i^0 = G_0^i = 0, \quad (1.23)$$

$$G_i^i = - \left(3H^2 + 2\dot{H} + \frac{K}{a^2} \right) \delta_j^i, \quad (1.24)$$

since we used the relation $G_{\nu}^{\mu} = g^{\mu\alpha}G_{\alpha\nu}$. By solving the Einstein equations, we can determine the cosmological dynamics.

By considering the perfect fluid as the background matter in FLRW universe, the energy-momentum tensor is given by

$$T_{\nu}^{\mu} = (\rho + P)u^{\mu}u_{\nu} + P\delta_{\nu}^{\mu}, \quad (1.25)$$

where $u^\mu = \delta_0^\mu$ is the four-velocity of the fluid, ρ is the total energy density and P is the total pressure. The non-vanishing components of T_ν^μ are

$$T_0^0 = -\rho, \quad (1.26)$$

$$T_j^i = P\delta_j^i. \quad (1.27)$$

By substituting in the Einstein field equations (1.2) we obtain

$$H^2 = \frac{8\pi G}{3}\rho - \frac{K}{a^2}, \quad (1.28)$$

$$3H^2 + 2\dot{H} = -8\pi GP - \frac{K}{a^2}, \quad (1.29)$$

which are the Friedmann equations. These equations describe the expansion history of the universe.

From (1.28) and (1.29), we get

$$\frac{\ddot{a}}{a} = -\frac{4\pi G}{3}(\rho + 3P). \quad (1.30)$$

Differentiating with respect to time t and by using (1.29), we find

$$\dot{\rho} + 3H(\rho + P) = 0, \quad (1.31)$$

which is the conservation or continuity equation.

Defining the dimensionless density parameters as follows

$$\Omega_m \equiv \frac{8\pi G\rho}{3H^2}, \quad \Omega_K \equiv -\frac{K}{(aH)^2}, \quad (1.32)$$

we can write (1.28) as

$$\Omega_m + \Omega_K = 1. \quad (1.33)$$

1.1.2 Λ CDM concordance model

We consider a single component universe with equation of state w defined as

$$w \equiv \frac{P}{\rho}. \quad (1.34)$$

For constant w and assume a flat universe ($K = 0$), and from (1.30) and (1.31) we get the following solution

$$\rho \propto a^{-3(1+w)}, \quad a \propto (t - t_i)^{2/3(1+w)}, \quad (1.35)$$

where t_i is the initial cosmic time. For radiation with equation of state $w = 1/3$, the cosmic evolution during the radiation era is given by

$$\rho_r \propto a^{-4}, \quad a \propto (t - t_i)^{1/2}. \quad (1.36)$$

For non-relativistic matter with negligible pressure, i.e $w \simeq 0$, the evolution during the matter domination era is given by

$$\rho_m \propto a^{-3}, \quad a \propto (t - t_i)^{2/3}. \quad (1.37)$$

From (1.30), cosmic acceleration condition is $\ddot{a} > 0$. This leads to

$$P < -\rho/3 \quad \rightarrow \quad w < -1/3, \quad (1.38)$$

since we assume ρ to be always positive. In the case when $w = -1$, i.e. $P = -\rho$, from (1.31) ρ is a constant. This case corresponds to the cosmological constant. In this case, the cosmological evolution is given by

$$H = \sqrt{\frac{8\pi G\rho}{3}}, \quad a \propto \exp(Ht). \quad (1.39)$$

The cosmological constant scenario accounts for late cosmic acceleration and it is one of dark energy models.

For a universe filled with radiation ρ_r , dark matter ρ_m and dark energy ρ_{de} , the evolution equations could be written as

$$\rho_r = \rho_r^0 \left(\frac{a_0}{a}\right)^4 = \rho_r^0 (1+z)^4, \quad (1.40)$$

$$\rho_m = \rho_m^0 \left(\frac{a_0}{a}\right)^3 = \rho_m^0 (1+z)^3. \quad (1.41)$$

The dark energy component satisfies the continuity equation,

$$\dot{\rho}_{de} + 3H(\rho_{de} + P_{de}) = 0. \quad (1.42)$$

where $w_{de} = P_{de}/\rho_{de}$ is the dark energy equation of state.

At radiation-matter equality (i.e $\rho_r = \rho_m$), the corresponding redshift z_{eq} is given by

$$1 + z_{eq} = \frac{\rho_m^0}{\rho_r^0} = \frac{\Omega_m^0}{\Omega_r^0}, \quad (1.43)$$

where Ω_r^0 is defined as

$$\Omega_r^0 \equiv \frac{8\pi G \rho_r^0}{3H_0^2}. \quad (1.44)$$

By Integrating (1.42), we get

$$\rho_{de} = \rho_{de}^0 \exp \left[\int_0^z \frac{3(1+w_{de})}{1+z} dz \right], \quad (1.45)$$

where we used the relation $dt = -dz/[H(1+z)]$.

From (1.28), we get

$$H^2 = \frac{8\pi G}{3}(\rho_r + \rho_m + \rho_{de}), \quad (1.46)$$

since we assume a flat universe with $K = 0$.

The density parameters at present time satisfy the following relation

$$\Omega_r^0 + \Omega_m^0 + \Omega_{de}^0 = 1. \quad (1.47)$$

Equation (1.46) can then be written in the form

$$H^2(z) = H_0^2 \left[\Omega_r^0 (1+z)^4 + \Omega_m^0 (1+z)^3 + \Omega_{de}^0 \exp \left\{ \int_0^z \frac{3(1+w_{de})}{1+z} dz \right\} \right]. \quad (1.48)$$

For cosmological constant with $w_\Lambda = -1$, we get

$$H^2(z) = H_0^2 [\Omega_r^0 (1+z)^4 + \Omega_m^0 (1+z)^3 + \Omega_\Lambda^0]. \quad (1.49)$$

1.2 Thesis outline

This thesis is organized as follows: in chapter 2, a general overview on the linear and non-linear perturbation theory is given. This is to understand the mechanism of gravitational instability responsible for the structure formation in the universe. The perturbation equations are derived for a multi-component dark energy-dark matter universe. For non-linear perturbations, the phenomenological spherical collapse model is presented with derivation of the Press-Schechter halo mass function.

The main results are presented in chapter 3, we present the effect of clustering interacting dark energy on large scale structure observables. We then investigate the degeneracy with primordial non-Gaussianity in galaxy power spectrum on very large scales. Possible disentanglement between the two signals is then discussed with a derivation of effective non-Gaussianity relation.

In chapter 4 we perform a set of N-body simulations to measure the primordial non-Gaussianity imprint on the halo mass function and non-linear power spectrum on non-linear scales. Chapter 5 contains the concluding remarks and future work.



Chapter 2

Structure formation and gravitational instability

The large scale structure of the universe presents one of the observational challenges in modern astrophysics and cosmology. The wealth of information contained in galaxy clustering is very important in constraining different models of cosmological evolution. During late universe, gravitational instability has been widely accepted to be responsible for the observed structure formation. In order to quantitatively understand the dynamics of gravitational instability, one requires a general theory of cosmological perturbations.

In this chapter we review the basic foundations of linear/non-linear cosmological perturbation theory within the context of General Relativity. We discuss its application to different cosmological models including dynamical dark energy. The initial conditions originating from inflation are explained. The statistical properties of the perturbation variables required to link with observations are illustrated with the introduction of the power spectra. We discuss the assumption of the existence of primordial non-Gaussianity signal and its imprints on large scale structure. For full non-linear perturbation solutions, we introduce the numerical N-body simulations. This chapter is mainly based on the following books and reviews [5, 6, 8, 15, 34, 63, 65, 90].

2.1 Dynamics of gravitational instability

Galaxies, superclusters, sheets and filaments are representing the observed large scale structure of the universe. In an expanding universe, gravitational amplifications of primordial fluctuations due to the gravitational interaction of the underlying non-relativistic

cold dark matter is responsible for structure formation seen today [64]. In order to understand the dynamics of the gravitational instability on linear and non-linear scales, cosmological perturbation theory is required.

2.1.1 Linear cosmological perturbation theory

The Friedmann Lematre Robertson Walker (FLRW) metric is given by

$$ds^2 = g_{\mu\nu} dx^\mu dx^\nu = a^2(-d\eta^2 + \delta_{ij} dx^i dx^j), \quad (2.1)$$

where $\eta = \int a^{-1} dt$ is the conformal time and \mathcal{H} is the conformal Hubble parameter defined as

$$\mathcal{H} \equiv \frac{1}{a} \frac{da}{d\eta} = Ha. \quad (2.2)$$

The perturbed FLRW metric at first order is given by

$$g_{\mu\nu} = \bar{g}_{\mu\nu} + \delta g_{\mu\nu}, \quad (2.3)$$

where $\delta g_{\mu\nu}$ is very small with respect to the unperturbed background term.

General relativistic field equations are invariant under a general coordinate transformation which means that the perturbed metric is not unique. In order to keep the background FLRW metric invariant under a general transformation, we choose a set of infinitesimal transformations that leaves $\bar{g}_{\mu\nu}$ invariant, while the perturbed metric $\delta g_{\mu\nu}$ is variant. These set of transformations are called gauge transformations.

The perturbed metric $\delta g_{\mu\nu}$ can generally be defined as

$$\delta g_{\mu\nu} = a^2 \begin{pmatrix} -2\Psi & E_{,i} \\ E_{,i} & 2\Phi\delta_{ij} + D_{ij}B \end{pmatrix}, \quad (2.4)$$

where Ψ , Φ , E and B are spatial scalars functions and D_{ij} is a traceless operator. From these scalar functions one can construct gauge-invariant quantities, which remain invariant under any general coordinate transformation. For simplicity, it is better to work with a specific gauge which could be imposed by putting specific conditions on the metric. These conditions correspond to gauge coordinate transformations. The Newtonian gauge is defined by choosing $E = 0$ and $B = 0$. The perturbed metric in Newtonian gauge is then given by:

$$ds^2 = a^2(\eta) [-(1 + 2\Psi)d\eta^2 + (1 + 2\Phi)\delta_{ij} dx^i dx^j]. \quad (2.5)$$

In order to perturb the Einstein field equations, (1.2), we decompose the Einstein tensor G_ν^μ and the energy-momentum tensor T_ν^μ into background and perturbed parts: $G_\nu^\mu = \bar{G}_\nu^\mu + \delta G_\nu^\mu$ and $T_\nu^\mu = \bar{T}_\nu^\mu + \delta T_\nu^\mu$. The cosmological background evolution is then obtained by solving the background Einstein equations, $\bar{G}_\nu^\mu = 8\pi G\bar{T}_\nu^\mu$, see chapter 1 for details.

The perturbed first-order Einstein equations are given by

$$\delta G_\nu^\mu = 8\pi G\delta T_\nu^\mu. \quad (2.6)$$

In order to compute the perturbed Einstein tensor in (2.6) we first need to calculate the perturbed Christoffel symbols $\delta\Gamma_{\nu\lambda}^\mu$ by using the formula

$$\delta\Gamma_{\nu\lambda}^\mu = \frac{1}{2}\delta g^{\mu\alpha}(g_{\alpha\nu,\lambda} + g_{\alpha\lambda,\nu} - g_{\nu\lambda,\alpha}) + \frac{1}{2}g^{\mu\alpha}(\delta g_{\alpha\nu,\lambda} + \delta g_{\alpha\lambda,\nu} - \delta g_{\nu\lambda,\alpha}). \quad (2.7)$$

The non-vanishing components of perturbed Christoffel symbols for the perturbed FLRW metric (2.5) are

$$\delta\Gamma_{ij}^0 = \delta_{ij} [2\mathcal{H}(\Phi - \Psi) + \dot{\Phi}], \quad (2.8)$$

$$\delta\Gamma_{00}^0 = \dot{\Psi}, \quad (2.9)$$

$$\delta\Gamma_{0i}^0 = \delta\Gamma_{00}^i = \Psi_{,i}, \quad (2.10)$$

$$\delta\Gamma_{j0}^i = \delta_j^i \dot{\Phi}. \quad (2.11)$$

where an overdot here represents the derivative with respect to the conformal time η .

The perturbations in the Ricci tensor and in the Ricci scalar are given by

$$\delta R_{\mu\nu} = \delta\Gamma_{\mu\nu,\alpha}^\alpha - \delta\Gamma_{\mu\alpha,\nu}^\alpha + \delta\Gamma_{\mu\nu}^\alpha\Gamma_{\alpha\beta}^\beta + \Gamma_{\mu\nu}^\alpha\delta\Gamma_{\alpha\beta}^\beta - \delta\Gamma_{\mu\beta}^\alpha\Gamma_{\alpha\nu}^\beta - \Gamma_{\mu\beta}^\alpha\delta\Gamma_{\alpha\nu}^\beta, \quad (2.12)$$

$$\delta R = \delta g^{\mu\alpha}R_{\alpha\mu} + g^{\mu\alpha}\delta R_{\alpha\mu}. \quad (2.13)$$

The perturbed Einstein tensors are then derived by

$$\delta G_{\mu\nu} = \delta R_{\mu\nu} - \frac{1}{2}\delta g_{\mu\nu}R - \frac{1}{2}g_{\mu\nu}\delta R, \quad (2.14)$$

$$\delta G_\nu^\mu = \delta g^{\mu\alpha}G_{\alpha\nu} + g^{\mu\alpha}\delta G_{\alpha\nu}. \quad (2.15)$$

Using the perturbed metric (2.5), we get

$$\delta G_0^0 = 2a^{-2}[3\mathcal{H}(\mathcal{H}\Psi - \dot{\Phi}) + \nabla^2\Phi], \quad (2.16)$$

$$\delta G_i^0 = 2a^{-2}(\dot{\Phi} - \mathcal{H}\Psi)_{,i}, \quad (2.17)$$

$$\delta G_j^i = 2a^{-2}[(\mathcal{H}^2 + 2\dot{\mathcal{H}})\Psi + \mathcal{H}\dot{\Psi} - \ddot{\Phi} - 2\mathcal{H}\dot{\Phi}]\delta_j^i \quad (2.18)$$

$$a^{-2}[\nabla^2(\Psi + \Phi)\delta_j^i]. \quad (2.19)$$

The perturbed energy-momentum tensor δT_ν^μ could be determined for a specified matter source accordingly.

2.1.1.1 Non-relativistic matter

For the energy-momentum tensor $T_{\mu\nu}$ defined in (1.25), the perturbed four-velocity $u^\mu \equiv dx^\mu/ds$ is

$$u^\mu = \left[\frac{1}{a}(1 - \Psi), \frac{v^i}{a} \right], \quad (2.20)$$

where $v^i \equiv dx^i/d\eta$ is the peculiar velocity.

The perturbed quantities are defined as

$$\delta \equiv \frac{\delta\rho}{\rho} = \frac{\rho - \bar{\rho}}{\rho}, \quad \theta \equiv \nabla_i v^i, \quad (2.21)$$

where δ is the density contrast and θ is the velocity divergence.

From (1.25) the perturbed energy-momentum tensor for a perfect fluid with the equation of state $w = P/\rho$ can be written as

$$\delta T_\nu^\mu = \rho[\delta(1 + c_s^2)u_\nu u^\mu + (1 + w)(\delta u_\nu u^\mu + u_\nu \delta u^\mu) + c_s^2 \delta \delta_\nu^\mu]. \quad (2.22)$$

where $c_s^2 \equiv \delta P/\delta\rho$ is the sound speed squared. For barotropic fluid (where $P(\rho)$ is function of time-dependent density $\rho(t)$ only), the sound speed is defined as

$$c_s^2 \equiv \frac{\delta P}{\delta\rho} = \frac{dP}{d\rho} = \frac{\dot{P}}{\dot{\rho}}. \quad (2.23)$$

In general case, where the pressure P can depend on other internal quantities, e.g. entropy s , the sound speed can be defined as

$$c_s^2 = \frac{\delta P(\rho, s)}{\delta\rho} = \frac{\partial P}{\partial\rho} + \frac{\partial P}{\partial s} \frac{\partial s}{\partial\rho} = c_{s(a)}^2 + c_{s(na)}^2, \quad (2.24)$$

where $c_{s(a)}^2 \equiv \dot{P}/\dot{\rho}$ and $c_{s(na)}^2$ are the adiabatic and the non-adiabatic sound speed squared respectively. Given the equation of state $w(a)$ and the sound speed $c_s(a)$ for a fluid, the perturbed Einstein equations are then fully determined.

The energy-momentum tensor components are

$$\delta T_0^0 = -\delta\rho, \quad (2.25)$$

$$\delta T_i^0 = -\delta T_0^i = (1+w)\rho v^i, \quad (2.26)$$

$$\delta T_i^i = c_s^2 \delta\rho. \quad (2.27)$$

From (2.16) and (2.25) the perturbed Einstein equations (2.6) are

$$3\mathcal{H}(\mathcal{H}\Psi - \dot{\Phi}) + \nabla^2\Phi = -4\pi G a^2 \delta\rho, \quad (2.28)$$

$$\nabla^2(\dot{\Phi} - \mathcal{H}\Psi) = 4\pi G a^2 (1+w)\rho\theta, \quad (2.29)$$

$$\Psi = -\Phi, \quad (2.30)$$

$$\ddot{\Phi} + 2\mathcal{H}\dot{\Phi} - \mathcal{H}\dot{\Psi} - (\mathcal{H}^2 + 2\dot{\mathcal{H}})\Psi = -4\pi G a^2 c_s^2 \delta\rho. \quad (2.31)$$

The energy-momentum tensor satisfies the continuity equation $T_{\nu;\mu}^\mu = 0$. The perturbed continuity equation is then

$$\delta T_{\nu;\mu}^\mu = 0. \quad (2.32)$$

The temporal component, i.e. $\delta T_{0;\mu}^\mu = 0$, reads

$$\delta T_{0,\mu}^\mu - \delta\Gamma_{0\beta}^\alpha T_\alpha^\beta - \Gamma_{0\beta}^\alpha \delta T_\alpha^\beta + \delta\Gamma_{0\alpha}^\alpha T_0^0 + \Gamma_{\beta\alpha}^\alpha \delta T_0^\beta = 0. \quad (2.33)$$

By using (2.8), we get

$$\delta\dot{\rho} + 3\mathcal{H}(\delta\rho + \delta P) = -(\rho + P)(\theta + 3\dot{\Phi}), \quad (2.34)$$

In terms of w and c_s^2 and using the background conservation equation $\dot{\rho} + 3\mathcal{H}(\rho + P) = 0$, we get

$$\dot{\delta} + 3\mathcal{H}(c_s^2 - w)\delta = -(1+w)(\theta + 3\dot{\Phi}), \quad (2.35)$$

representing the perturbed continuity equation. For non-relativistic matter where $w = c_s^2 = 0$, the perturbed continuity equation reduces to

$$\dot{\delta} = -\theta - 3\dot{\Phi}. \quad (2.36)$$

On small scales ($k \gg \mathcal{H}$), the $\dot{\Phi}$ term may be neglected.

The spatial component of (2.32) is given by

$$[a(\rho + P)v]^{\cdot} + 3\mathcal{H}[a(\rho + P)v] = -a[av + \Psi](\rho + P), \quad (2.37)$$

where v is a velocity potential since $v^i = \nabla^i v$. By taking the divergence of (2.37), we get

$$\dot{\theta} + \left[\mathcal{H}(1 - 3w) + \frac{\dot{w}}{1 + w} \right] \theta = -\nabla^2 \left(\frac{c_s^2}{1 + w} \delta + \Psi \right). \quad (2.38)$$

Substituting $w = c_s^2 = 0$ for non-relativistic matter we get

$$\dot{\theta} + \mathcal{H}\theta = -\nabla^2 \Psi, \quad (2.39)$$

which represents the Euler equation.

By expanding the perturbation quantities in Fourier space:

$$\Phi = \int e^{i\mathbf{k}\cdot\mathbf{r}} \Phi_{\mathbf{k}} d^3k, \quad (2.40)$$

$$\delta = \int e^{i\mathbf{k}\cdot\mathbf{r}} \delta_{\mathbf{k}} d^3k, \quad (2.41)$$

$$\theta = \int e^{i\mathbf{k}\cdot\mathbf{r}} \theta_{\mathbf{k}} d^3k, \quad (2.42)$$

where \mathbf{k} is the wave-vector, the perturbation equations are defined as follows for each Fourier mode:

$$k^2 \Phi + 3\mathcal{H}(\dot{\Phi} - \mathcal{H}\Psi) = 4\pi G a^2 \rho \delta, \quad (2.43)$$

$$k^2(\dot{\Phi} - \mathcal{H}\Psi) = -4\pi G a^2 (1 + w) \rho \theta, \quad (2.44)$$

$$\dot{\delta} + 3\mathcal{H}(c_s^2 - w)\delta = -(1 + w)(\theta + 3\dot{\Phi}), \quad (2.45)$$

$$\dot{\theta} + \left[\mathcal{H}(1 - 3w) + \frac{\dot{w}}{1 + w} \right] \theta = k^2 \left(\frac{c_s^2}{1 + w} \delta + \Psi \right), \quad (2.46)$$

where $\nabla^2 \rightarrow -k^2$. The relativistic Poisson equation can be derived by combining (2.43) and (2.44), which leads to

$$k^2 \Phi = 4\pi G a^2 \rho \Delta, \quad (2.47)$$

where

$$\Delta = \delta + 3\mathcal{H}(w + 1)\theta/k^2, \quad (2.48)$$

is the total comoving matter density contrast.

2.1.1.2 Dynamical dark energy

For general multi-fluid universe with a general equation of state $w(a)$ and a general sound speed $c_s^2(a)$, the gravitational field is sourced by the total energy densities. In the following, the subscripts m, x represent the dark matter and dynamical dark energy components respectively.

Dark energy density and velocity perturbations in Fourier space obey the following equations [5, 84],

$$\delta'_x + 3(c_x^2 - w)\delta_x = -(1+w)(3\Phi' + \theta_x), \quad (2.49)$$

$$\theta'_x + \left(2 - 3w + \frac{H'}{H} + \frac{w'}{1+w}\right)\theta_x = \left(\frac{k}{aH}\right)^2 \left(\frac{c_x^2}{1+w}\delta_x - \Phi\right), \quad (2.50)$$

where

$$\delta_x \equiv \frac{\delta\rho_x}{\rho_x}, \quad \theta_x \equiv \frac{-k^2}{aH}v_x, \quad (2.51)$$

and v_x is the rotational-free dark energy velocity potential. The prime represents a derivative with respect to the number of folds $N = \ln a$. The gravitational potential Φ perturbation equation is given by

$$\Phi' + \Phi = -\frac{3}{2} \left(\frac{aH}{k}\right)^2 [\Omega_m\theta_m + (1+w)\Omega_x\theta_x]. \quad (2.52)$$

In the Newtonian gauge, the galaxy bias b^1 is defined by $\delta_g(k, a) = b(a)\delta_m(k, a)$. However, this definition fails on very large scales due to gauge-dependence, and we need to identify the correct physical frame in which the bias is scale-independent on all scales [19]. This is the comoving frame, so that a gauge-independent definition of the bias that applies on all (linear) scales is given by

$$\Delta_g = b\Delta_m, \quad \text{where } \Delta_m = \delta_m + (\rho'_m/\rho_m)v_m. \quad (2.53)$$

For dynamical dark energy, the gauge-invariant perturbation variable is given by

$$\Delta_x = \delta_x + 3 \left(\frac{aH}{k}\right)^2 (1+w)\theta_x. \quad (2.54)$$

¹The term bias refers to the observed spatial distribution difference between galaxies and the underline bulk matter.

Equations (2.49) and (2.50) are reformulated in terms of v_x and Δ_x as follows. From (2.51) the first derivative of θ_x with respect to N is given by

$$\begin{aligned}\theta'_x &= -k^2 \left[\frac{(aH)v'_x - (aH' + a'H)v_x}{(aH)^2} \right], \\ &= -\frac{k^2}{aH} \left[v'_x - \left(\frac{H'}{H} + 1 \right) v_x \right],\end{aligned}\quad (2.55)$$

since $a'/a = 1$.

The first derivative of the dark energy overdensity δ_x in terms of Δ_x and v_x is given by

$$\begin{aligned}\delta'_x &= \Delta'_x + 3[(aH)(1+w)v_x]', \\ &= \Delta'_x + 3(aH) \left[(1+w)v'_x + w'v_x + \left(\frac{H'}{H} + 1 \right) (1+w)v_x \right].\end{aligned}\quad (2.56)$$

Using (2.55), (2.52) could be rewritten as

$$\Phi' = -\Phi + \frac{3}{2}(aH) [\Omega_m v_m + (1+w)\Omega_x v_x].\quad (2.57)$$

Using (2.56), the LHS of (2.50) could be rewritten as

$$-\frac{k^2}{aH} v'_x - \frac{k^2}{aH} \left(1 - 3w + \frac{w'}{1+w} \right) v_x.\quad (2.58)$$

While the RHS of (2.50) is given by

$$\left(\frac{k}{aH} \right)^2 \left[\frac{c_x^2}{1+w} \Delta_x \right] + 3 \left(\frac{aH}{k} \right)^2 \frac{c_x^2}{1+w} (aH)(1+w)v_x - \left(\frac{aH}{k} \right)^2 \Phi.\quad (2.59)$$

So we get

$$v'_x + \left[1 + 3(c_x^2 - w) + \frac{w'}{1+w} \right] v_x = \frac{1}{aH} \left[\Phi - \frac{c_x^2}{1+w} \Delta_x \right].\quad (2.60)$$

Using the same technique with (2.49), we have for the LHS

$$\Delta'_x + 3(aH)(1+w)v'_x + 3(c_x^2 - w)\Delta_x + 3(aH) \left[w' + \left(\frac{H'}{H} + 1 \right) (1+w) + 3(c_x^2 - w)(1+w) \right] v_x.\quad (2.61)$$

From (2.57), we get

$$\Delta'_x + 3(c_x^2 - w)\Delta_x - 3c_x^2\Delta_x + 3(1+w)\Phi + 3(aH)\frac{H'}{H}(1+w)v_x.\quad (2.62)$$

For the RHS of (2.49), we have

$$3(1+w)\Phi - \frac{9}{2}(1+w)(aH)[\Omega_m v_m + (1+w)\Omega_x v_x] + \frac{k^2}{aH}(1+w)v_x. \quad (2.63)$$

By combining the two sides, we get

$$\begin{aligned} \Delta'_x - 3w\Delta_x + 3aH\frac{H'}{H}(1+w)v_x &= -\frac{9}{2}(1+w)(aH)[\Omega_m v_m + (1+w)\Omega_x v_x] \\ &\quad + \frac{k^2}{aH}(1+w)v_x. \end{aligned} \quad (2.64)$$

Since

$$\frac{H'}{H} = -\frac{3}{2}(1+w\Omega_x), \quad (2.65)$$

we get

$$\begin{aligned} \Delta'_x - 3w\Delta_x - \frac{9}{2}aH(1+w)(1+w\Omega_x)v_x &= -\frac{9}{2}(1+w)aH\Omega_m v_m \\ &\quad - \frac{9}{2}(1+w)aH(1+w)\Omega_x v_x \\ &\quad + \frac{k^2}{aH}(1+w)v_x. \end{aligned} \quad (2.66)$$

or

$$\Delta'_x - 3w\Delta_x - \frac{k^2}{aH}(1+w)v_x - \frac{9}{2}aH(1+w)(1-\Omega_x)[v_x - v_x] = 0. \quad (2.67)$$

Non-adiabatic sound speed

For imperfect fluids, there exist non-adiabatic entropy perturbations generated from dissipative processes [84]. The speed of sound is defined as,

$$c_x^2 = c_s^2 + 3\left(\frac{aH}{k}\right)^2 (1+w)(c_s^2 - c_a^2)\frac{\theta_x}{\delta_x}, \quad (2.68)$$

where, c_s^2 is the speed of sound squared and c_a^2 is the adiabatic speed squared defined as

$$c_a^2 = w - \frac{w'}{3(1+w)}. \quad (2.69)$$

Equation (2.68) could be written as,

$$c_x^2 = c_s^2 + \mathcal{T}, \quad (2.70)$$

where \mathcal{T} is

$$\begin{aligned}\mathcal{T} &= 3 \left(\frac{aH}{k} \right)^2 (1+w)(c_s^2 - c_a^2) \frac{k^2}{aH} \frac{-v_x}{\Delta_x + 3aH(1+w)v_x}, \\ &= -3aH(1+w)(c_s^2 - c_a^2) \frac{v_x}{\Delta_x + 3aH(1+w)v_x}.\end{aligned}\quad (2.71)$$

By substituting into Eq. (2.60), we get

$$v'_x + \left[1 + 3(c_s^2 - w) + \frac{w'}{1+w} \right] v_x + 3\mathcal{T} \left(v_x + \frac{\Delta_x}{1+w} \right) = \frac{1}{aH} \left[\Phi - \frac{c_s^2}{1+w} \Delta_x \right]. \quad (2.72)$$

Since,

$$\begin{aligned}3\mathcal{T} \left(v_x + \frac{\Delta_x}{1+w} \right) &= -9aH(1+w)(c_s^2 - c_a^2) \frac{v_x^2}{\Delta_x + 3aH(1+w)v_x} \\ &\quad - 3(c_s^2 - c_a^2) \frac{v_x \Delta_x}{\Delta_x + 3aH(1+w)v_x}, \\ &= -3(c_s^2 - c_a^2)v_x,\end{aligned}\quad (2.73)$$

we get,

$$v'_x + \left[1 - 3w + 3c_a^2 + \frac{w'}{1+w} \right] v_x = \frac{1}{aH} \left[\Phi - \frac{c_s^2}{1+w} \Delta_x \right]. \quad (2.74)$$

From (2.69), we have

$$v'_x = -v_x + \frac{1}{aH} \left[\Phi - \frac{c_s^2}{1+w} \Delta_x \right]. \quad (2.75)$$

By defining the dimensionless variables

$$h = \frac{H}{H_0}, \quad u_x = \frac{v_x}{H_0}, \quad \zeta = \frac{k}{H_0}, \quad (2.76)$$

we get,

$$\Phi' = -\Phi + \frac{3}{2}(ah) [\Omega_m u_m + (1+w)\Omega_x u_x], \quad (2.77)$$

$$u'_x = -u_x + \frac{1}{ah} \left[\Phi - \frac{c_s^2}{1+w} \Delta_x \right], \quad (2.78)$$

$$\Delta'_x = 3w\Delta_x + \frac{\zeta^2}{ah} (1+w)u_x + \frac{9}{2}ah(1+w)(1-\Omega_x)[u_x - u_m]. \quad (2.79)$$

Dark matter perturbations

The dark matter perturbations are given by

$$\delta'_m = -3\Phi' - \theta_m, \quad (2.80)$$

$$\theta'_m + \left(2 + \frac{H'}{H}\right)\theta_m = -\left(\frac{k}{aH}\right)^2 \Phi. \quad (2.81)$$

where

$$\delta_m \equiv \frac{\delta\rho_m}{\rho_m}, \quad \theta_m \equiv \frac{-k^2}{aH} v_m, \quad (2.82)$$

and v_m is the rotational-free dark matter velocity potential. The gauge-invariant dark matter overdensity perturbation is defined as

$$\Delta_m = \delta_m + 3\left(\frac{aH}{k}\right)^2 \theta_m. \quad (2.83)$$

By using the same procedure for the dark energy perturbations, we have

$$u'_m = \left[\frac{1}{ah}\Phi - u_m\right], \quad (2.84)$$

$$\Delta'_m = \frac{\zeta^2}{ah}u_m + \frac{9}{2}ah(1+w)\Omega_x[u_m - u_x]. \quad (2.85)$$

The relativistic Poisson equation is given by

$$\Phi = \frac{3}{2}\zeta^2\Delta_t, \quad (2.86)$$

where

$$\Delta_t \equiv \delta_t + 3\zeta^2\theta_t(1 + w_{\text{eff}}). \quad (2.87)$$

The total perturbation variables are given by

$$\delta_t = \sum_i \Omega_i \delta_i, \quad (2.88)$$

$$\theta_t = \sum_i \frac{1 + w_i}{1 + w_{\text{eff}}} \Omega_i \theta_i, \quad (2.89)$$

where $w_{\text{eff}} = \sum_i \Omega_i w_i$ is the total equation of state for $i = m, x$.

2.1.2 Non-linear cosmology

Linear gravitational processes only act on very large cosmological scales. In non-linear regime, gravitational instability responsible for the formation of astrophysical objects is

replaced with a new physical mechanism and new interactions. Therefore the signature of the global structure of the cosmos is lost or dissipated.

An intermediate regime, in which gravitational interaction is still effective beyond linearity, begins to be observable. This regime lies between the linear perturbation theory and the full non-linear dynamics. Full non-linear dynamics can only be dealt with N-body simulations or by studying individual astronomical objects.

In the following, we present the perturbation equations in Newtonian limit without any linearization assumption. The continuity equation and the Euler equation for non-relativistic matter with density ρ moving under a gravitational potential Φ with a velocity \mathbf{v} are given by [5],

$$\dot{\rho} + \nabla \cdot (\rho \mathbf{v}) = 0, \quad (2.90)$$

$$\dot{\mathbf{v}} + (\mathbf{v} \cdot \nabla) \mathbf{v} = -\nabla \Phi, \quad (2.91)$$

where a dot represents derivative with respect to time t and ∇ is the gradient over the physical coordinate. The gravitational potential satisfies the Poisson equation

$$\nabla^2 \Phi = 4\pi G \rho. \quad (2.92)$$

In expanding universe, the the local coordinate is replaced with the expanding coordinate given the following system for perturbation equation

$$\dot{\delta} + \frac{1}{a} \nabla \cdot (1 + \delta) \mathbf{v} = 0, \quad (2.93)$$

$$\dot{\mathbf{v}} + H \mathbf{v} + \frac{1}{a} \mathbf{v} \cdot \nabla \mathbf{v} = \frac{1}{a} \nabla \Phi, \quad (2.94)$$

and the Poisson equation in the expanding universe is given by

$$\nabla^2 \Phi = -4\pi G a^2 \delta \rho, \quad (2.95)$$

where δ is the matter density contrast.

The total derivative of δ with respect to the cosmic time is defined as

$$\frac{d\delta}{dt} \equiv \frac{\partial \delta}{\partial t} + \frac{v^i}{\mathcal{H}} \nabla_i \delta. \quad (2.96)$$

The continuity equation (2.93) is then

$$\frac{d\delta}{dt} = -\Theta(1 + \delta), \quad (2.97)$$

where $\Theta \equiv \nabla^i v_i / H$. By taking the divergence of the Euler equation and make use of the Poisson equation, we get

$$\frac{d\Theta}{dt} = -(1 + \mathcal{H})\Theta - \frac{1}{3}\Theta^2 - \frac{3}{2}\Omega_m\delta. \quad (2.98)$$

From (2.97) and (2.98), we get

$$\frac{d^2\delta}{dt^2} + (1 + \mathcal{H})\frac{d\delta}{dt} - \frac{3}{2}\Omega_m\delta = \frac{4}{3}\frac{1}{1 + \delta}\left(\frac{d\delta}{dt}\right)^2 + \frac{3}{2}\Omega_m\delta^2, \quad (2.99)$$

where the RHS represents the non-linear terms. We assume $\delta = \delta(x, a)$ and only consider radial perturbations. It corresponds to the density contrast evolution.

2.1.2.1 Spherical collapse

By using the Newtonian picture, (2.99) could be derived assuming a shell of matter with uniform density ρ at a distance R from a spherical overdensity center obeying Newton force law

$$\frac{d^2R}{dt^2} = -\frac{GM(R)}{R^2} = -\frac{4}{3}\pi G\rho R, \quad (2.100)$$

where $M(R) = 4\pi\rho R^3/3$ is the constant mass inside the shell. For non-relativistic matter the background density is given by $\rho_0 = (3M(R_0)/4\pi)(R_0a(t))^{-3}$, where R_0 is the initial size of the perturbation. The density contrast inside the shell can be defined as

$$\delta = \left(\frac{a(t)R_0}{R}\right)^3 - 1, \quad (2.101)$$

where $\delta = 0$ outside. By assuming that the density contrast δ is a top-hat function, all spatial derivative are equal to zero. The time derivative for δ is then

$$\delta'' + \left(1 + \frac{\mathcal{H}'}{\mathcal{H}}\right)\delta' - \frac{3}{2}\Omega_m\delta = \frac{4}{3}\frac{\delta'^2}{1 + \delta} + \frac{3}{2}\Omega_m\delta^2, \quad (2.102)$$

which is exactly the same as (2.99) derived from non-linear perturbation theory.

By multiplying (2.100) by $2dR/dt$ and then integrating, we get

$$\left(\frac{dR}{dt}\right)^2 = \frac{2GM}{R} - C, \quad (2.103)$$

where C is an integration constant. This is called the cycloid equation. The parametric solution for $C > 0$ is

$$R = \frac{1}{C}GM(1 - \cos \tau), \quad t = \frac{1}{C^{\frac{3}{2}}}GM(\tau - \sin \tau), \quad (2.104)$$

where the parameter τ is defined within the range $(0, 2\pi)$. The radius R first increases and then reaches a turning point then reduces to zero (perturbation collapses under its gravity). The linear solution for density contrast δ is given by

$$\delta_L = \frac{3}{5} \left[\frac{3}{4} (\tau - \sin \tau) \right]^{\frac{2}{3}} > 0, \quad (2.105)$$

where the integration constant has been set such that $\delta(\tau = 0) = 0$.

The collapse value δ_{coll} is defined as the linear fluctuation δ_L at the time of collapse. In the Press-Schechter theory [67], δ_{coll} is used to calculate the abundance of collapsed objects. From (2.105), at $\tau = 0$, the density perturbation δ vanishes. At $\tau = \pi$ when the perturbation reaches the turnaround, $\delta_L \sim 1.063$. At the collapse when $\tau = 2\pi$, the overdensity becomes singular with a value of

$$\delta_L = \delta_{coll} = \frac{3}{5} \frac{3\pi^{\frac{2}{3}}}{2} \sim 1.686, \quad (2.106)$$

in the Einstein-de Sitter Universe. For other models, δ_{coll} , however, is time dependent [89] and for coupled dark energy models see [58].

2.1.2.2 The mass function of collapsed objects

The critical value of the overdensity of collapsed objects δ_{coll} within the spherical collapse perturbation is important because it is used within the Press-Schechter (PS) formula for the abundance of virialized objects. The importance of the PS formula is that it can be used to estimate the number of collapsed objects created in a random Gaussian field. It is simply done by counting the overdensity regions at any given time that have a value above the collapse threshold δ_{coll} .

At redshift z , a density fluctuation field is distributed over cells of radius R . Each cell has average mass of $M = 4\pi R^3 \rho/3$ where $\rho(z)$ is the background density. The density contrast δ has a variance $\sigma_M^2(z)$. The fraction of collapsed regions with $\delta > \delta_{coll}$ is given by

$$p(M, z)|_{\delta > \delta_{coll}} = \frac{1}{\sigma_M(z)\sqrt{(2\pi)}} \int_{\delta_{coll}}^{\infty} \exp\left(-\frac{\delta_M^2}{2\sigma_M^2(z)}\right) d\delta_M. \quad (2.107)$$

The fraction of objects of mass within the range $[M, M + dM]$ is then given by

$$dp(M, z) = \left| \frac{\partial p(M, z)|_{\delta > \delta_{coll}}}{\partial M} \right| dM, \quad (2.108)$$

where the threshold collapse value δ_{coll} is time dependent in general. The idea then is to use the linear regime to estimate the collapsed objects with $\delta > \delta_{coll}$.

The volume of N collapsed objects is given by

$$NV_M = V dp, \quad (2.109)$$

where $V_M = M/\rho$. The number density dn of collapsed halos with mass function dM is therefore

$$\begin{aligned} dn &= \frac{N}{V} = \frac{dp}{V_M} = \frac{\rho}{M} \left| \frac{\partial p(M, z)|_{\delta > \delta_{coll}}}{\partial M} \right| dM \\ &= \sqrt{\frac{2}{\pi}} \frac{\rho}{M^2} \frac{\delta_{coll}}{\sigma_M} \left| \frac{d \ln \sigma_M}{d \ln M} \right| e^{-\delta_{coll}^2 / (2\sigma_M^2)} dM, \end{aligned} \quad (2.110)$$

which satisfy the condition

$$V \int_0^\infty \left(\frac{dn}{dM} \right) dM = 1. \quad (2.111)$$

The comoving number density is defined as $\tilde{n}(M, z) = a^3 n(M, z)$ and ρ is defined then as the comoving background density.

The number density could be written as

$$\frac{M}{\rho} \left| \frac{dn}{d \ln \sigma_M} \right| = f(\sigma_M, z), \quad (2.112)$$

where

$$f(\sigma_M, z) = \sqrt{\frac{2}{\pi}} \frac{\delta_{coll}}{\sigma_M} \frac{e^{-\delta_{coll}^2}}{2\sigma_M^2}, \quad (2.113)$$

containing all the cosmological information. The mass M is taken to be the virial mass of the observed objects (galaxies and clusters). The PS formula is though dependent on the cosmological model via the term δ_{coll}/σ_M .

Since the PS approach is based on the assumption of spherical collapse with top-hat or step filter, many processes like dissipation or merging are not considered. However, the PS formula is widely used as a first approximation to the abundance obtained via numerical N-body simulations. Many efforts have been done to improve PS formula to include non-linear corrections [44, 78] or by directly fitting N-body simulations. A widely common successful fit is given by [48]

$$f(\sigma_M, z) = 0.315 \exp(-|0.61 - \ln \sigma_M(z)|^{3.8}), \quad (2.114)$$

which holds for a large range of masses, redshifts, and cosmological models, including dynamical dark energy [82].

2.2 2–point correlation function and power spectrum

The large scale structure of the universe could be explained as the present matter distribution in the universe on cosmological scales originates from the propagation of small, primordial seed of fluctuations and then evolved by means of gravitational instability. To test different cosmological theories characterizing these initial conditions, we need to statistically measure the perturbation fields. The idea is to calculate the statistical properties of the current large scale structure which in turn depend on the the primordial perturbations. We then consider the cosmic scalar field, which could be either be the density field, $\delta(\mathbf{x})$, the velocity divergence field or the gravitational potential, to have a statistical nature.

The two-point correlation function is defined as

$$\zeta(\mathbf{r}) = \langle \delta(\mathbf{x})\delta(\mathbf{x} + \mathbf{r}) \rangle, \quad (2.115)$$

which represent the ensemble average of the density field at two different points. In Fourier space, the density contrast $\delta(\mathbf{x})$ is give by (2.41). Since $\delta(\mathbf{k})$ is real we get

$$\delta(\mathbf{k}) = \delta^*(-\mathbf{k}). \quad (2.116)$$

From (2.115), we can determine the density field by determining the statistical properties of the random variable $\delta(\mathbf{k})$.

The two-point correlation function in Fourier space is defined as,

$$\langle \delta(\mathbf{k})\delta(\mathbf{k}') \rangle = \int \frac{d^3\mathbf{x}}{(2\pi)^3} \frac{d^3\mathbf{r}}{(2\pi)^3} \langle \delta(\mathbf{x})\delta(\mathbf{x} + \mathbf{r}) \rangle \exp[-i(\mathbf{k} + \mathbf{k}') \cdot \mathbf{x} - i\mathbf{k}' \cdot \mathbf{r}]. \quad (2.117)$$

From (2.115), we have

$$\begin{aligned} \langle \delta(\mathbf{k})\delta(\mathbf{k}') \rangle &= \int \frac{d^3\mathbf{x}}{(2\pi)^3} \frac{d^3\mathbf{r}}{(2\pi)^3} \zeta(r) \exp[-i(\mathbf{k} + \mathbf{k}') \cdot \mathbf{x} - i\mathbf{k}' \cdot \mathbf{r}] \\ &= \delta_D(\mathbf{k} + \mathbf{k}') \int \frac{d^3\mathbf{r}}{(2\pi)^3} \zeta(\mathbf{r}) \exp(i\mathbf{k} \cdot \mathbf{r}) \equiv \delta_D(\mathbf{k} + \mathbf{k}')P(k), \end{aligned} \quad (2.118)$$

where $P(\mathbf{k})$ is the density power spectrum. The inverse relation is then

$$\zeta(r) = \int d^3\mathbf{k}P(\mathbf{k}) \exp(i\mathbf{k} \cdot \mathbf{r}). \quad (2.119)$$

2.2.1 Power spectrum evolution in linear perturbation theory

The evolution of the power spectrum is simply determined by the perturbation theory, and since we consider only the two-point correlation function, the linear theory is required. We assume that non-linear effects are negligible. The evolution of the density field is given by a simple time-dependent scaling of the linear power spectrum

$$P(k, \eta) = D(\eta)^2 P_L(k), \quad (2.120)$$

where $D(\eta)$ is the linear growth factor. Since the "linear" power spectrum $P_L(k)$ is affected by the linear evolution of density fluctuations during the radiation domination era, this evolution must be determined by solving general relativistic Boltzmann numerical codes [77]. However analytic techniques can be used for a qualitative understanding [45, 46]. So the linear power spectrum is then determined as

$$P_L(k) \propto k^{n_s} T^2(k), \quad (2.121)$$

where $T(k)$ is the transfer function and n_s is the primordial spectral index. The transfer function phenomenological parametrization is very complicated, however in simple cases (assuming the baryonic matter is negligible) it can be fitted using the parameter $\Gamma \equiv \Omega_m h$ [11]. For the Λ CDM scenario, the transfer function is given as follows on small scales [5],

$$T^2 \propto \ln^2(k)/k^4. \quad (2.122)$$

2.3 Physical origin of fluctuations from inflation

In Sec. (2.1.1) we have derived the perturbation equations governing the structure formation of the universe. In order to solve these equations, the initial conditions are required. The theory of inflation can provide the initial seeds of perturbation. In different models of inflation, the random stochastic perturbation fields originate from quantum fluctuations of a scalar field, called the inflaton. Since it is beyond the scope of this thesis to review inflation models in details, we refer to recent reviews for discussion [13, 56].

During inflationary era, the energy density was dominated by the inflaton. The inflaton field has quantum fluctuations which can be decomposed as follows

$$\delta\phi = \int d^3k [a_{\mathbf{k}} \psi_{\mathbf{k}}(t) \exp(i\mathbf{k} \cdot \mathbf{x}) + a_{\mathbf{k}}^\dagger \psi_{\mathbf{k}}^*(t) \exp(-i\mathbf{k} \cdot \mathbf{x})]. \quad (2.123)$$

where $a_{\mathbf{k}}^\dagger$ and $a_{\mathbf{k}}$ are the creation and annihilation operators respectively for a wave mode \mathbf{k} . These operators satisfy the standard commutation relation

$$[a_{\mathbf{k}}, a_{\mathbf{k}'}^\dagger] = \delta_D(\mathbf{k} + \mathbf{k}'), \quad (2.124)$$

and the wave function $\psi_{\mathbf{k}}(t)$ is obtained from the Klein-Gordon equation for $\delta\phi$ in an expanding universe.

In de-Sitter universe, the wave function $\psi_{\mathbf{k}}(t)$ is given by [13]

$$\psi_{\mathbf{k}}(t) = \frac{H}{(2k)^{1/2}k} \left(i + \frac{k}{aH} \right) \exp \left[\frac{i\mathbf{k}}{aH} \right], \quad (2.125)$$

where a and H are, respectively, the expansion factor and the Hubble constant that are determined by the Friedmann equations.

At $k/(aH) = 1$, the perturbation modes exit the Hubble radius and from (2.125) that the dominant perturbation mode is given by

$$\delta\phi_{\mathbf{k}} = \frac{iH}{\sqrt{2}k^{3/2}} (a_{\mathbf{k}} + a_{\mathbf{k}}^\dagger), \quad \delta\phi = \int d^3\mathbf{k} \phi_{\mathbf{k}} e^{i\mathbf{k}\cdot\mathbf{x}}, \quad (2.126)$$

where $\delta\phi_{\mathbf{k}}$ is proportional to $a_{\mathbf{k}} + a_{\mathbf{k}}^\dagger$. Thus the quantum nature of the fluctuations has disappeared [41], since any combination of $\phi_{\mathbf{k}}$ modes commute with each other according to (2.124). So the field ϕ can then be described as a classic stochastic field. The ensemble averages of the primordial perturbation field ϕ is identified with the vacuum expectation values.

Scalar field fluctuations generate a gravitational potential Φ . The imprints of their energy fluctuations and its statistical properties then appears in the gravitational potential. After the inflation, the gravitational modes enter the horizon. The subsequent statistical properties that appears in the late cosmic fields can be expressed in terms of the primordial random variable $\Phi_{\mathbf{k}}$.

2.3.1 Primordial non-Gaussianity

Deviations from Gaussian initial conditions offer an important window into the very early universe and a powerful constraint for the mechanism which generated the primordial perturbations. Large primordial non-Gaussianity could be produced within multi-field inflation models, while standard single-field slow-roll models lead to a small level of primordial non-Gaussianity [12].

The leading signature of non-Gaussianity is presented in the three-point correlation function, or the bispectrum in Fourier space

$$\langle \Phi_{\mathbf{k}_1} \Phi_{\mathbf{k}_2} \Phi_{\mathbf{k}_3} \rangle = B_{\Phi}(\mathbf{k}_1, \mathbf{k}_2, \mathbf{k}_3). \quad (2.127)$$

For homogeneous and isotropic background, the bispectrum only depends on momentum vectors magnitude

$$B_{\Phi}(\mathbf{k}_1, \mathbf{k}_2, \mathbf{k}_3) = (2\pi)^3 \delta_D(\mathbf{k}_1 + \mathbf{k}_2 + \mathbf{k}_3) B_{\Phi}(k_1, k_2, k_3), \quad (2.128)$$

where δ_D is a delta function over the sum of the three momenta, which means it must form a closed triangle shape. For a scale-invariant power spectrum, the shape of the bispectrum depends only on the ratios $x_2 \equiv k_2/k_1$ and $x_3 \equiv k_3/k_1$,

$$B_{\Phi}(k_1, k_2, k_3) = k_1^{-6} B_{\phi}(1, x_2, x_3). \quad (2.129)$$

The bispectrum is rewritten as

$$B_{\Phi}(k_1, k_2, k_3) = \frac{S(k_1, k_2, k_3)}{(k_1 k_2 k_3)^2} \Delta_{\Phi}^2(k_*), \quad (2.130)$$

where $\Delta_{\Phi}^2(k_*) = k_*^3 P_{\Phi}(k_*)$ is the dimensionless power spectrum evaluated at k_* , and S is dimensionless function.

The amplitude of non-Gaussianity is defined as the size of the bispectrum in the equilateral momentum configuration,

$$f_{\text{NL}}(K) = \frac{5}{18} S(K, K, K), \quad (2.131)$$

where f_{NL} depends on the overall momentum. However, for scale-invariant power spectrum, f_{NL} is a constant and the bispectrum is then reads

$$B_{\Phi}(k_1, k_2, k_3) = \frac{18}{5} f_{\text{NL}} \frac{S(k_1, k_2, k_3)}{(k_1 k_2 k_3)^2} \Delta_{\Phi}^2. \quad (2.132)$$

A common phenomenological parametrization of non-Gaussianity is given as a non-linear correction to a Gaussian perturbation ϕ_g ,

$$\Phi = \phi + \frac{3}{5} f_{\text{NL}}^{\text{loc}} [\phi^2 - \langle \phi^2 \rangle]. \quad (2.133)$$

It is called local non-Gaussianity since it is local in space [71].

2.3.1.1 Imprints on large-scale structure: scale dependent bias

In order to probe non-Gaussianity, one way is to investigate its observational signatures on the large scale structure of the universe. On non-linear scales it is difficult to probe the primordial signal of non-Gaussianity due its correlation with non-linear signals. The mass function of massive virialised objects is affected by primordial non-Gaussianity [14, 59, 74]. This is due to the fact that the very massive virialised objects correspond to very rare large peaks in the primordial density field. Therefore the number density is a unique probe of the primordial peak structure.

Another method to probe primordial non-Gaussianity on large scales is by expanding the clustering of rare peaks calculation in a Gaussian field [11] to include the f_{NL} -type non-Gaussianity. The clustering of rare peaks have a scale-dependent bias feature on large scales [28, 79].

We use the peak-background split to determine halo bias on large scales [23]. By splitting the density field into long-wavelength δ_l and short-wavelength δ_s modes, we have

$$\rho = \bar{\rho}(1 + \delta_l + \delta_s). \quad (2.134)$$

The number density of haloes $n(\mathbf{x})$ at position \mathbf{x} can then be written as a function of the long-wavelength perturbation δ_l and the short-wavelength fluctuations statistics $P_s(k_s)$. For large scale matter perturbations, the number density of halos is given by

$$n(\mathbf{x}) = \bar{n}(1 + b_L \delta_l), \quad (2.135)$$

where the Lagrangian bias is defined as

$$b_L = \bar{n}^{-1} \frac{\partial n}{\partial \delta_l}. \quad (2.136)$$

The total or Eulerian bias is then $b = b_L + 1$. This leads to a general scale-independent bias. To specifically determine the bias $b(M)$, the number density function $n(M)$ needs to be specified by large N-body simulations and then differentiating it.

In the presence of non-Gaussian initial conditions, large and small-scale density fluctuations are dependent. In local non-Gaussian form of f_{NL} , the gravitational potential fluctuations could be separated into independent long and short modes,

$$\phi = \phi_l + \phi_s. \quad (2.137)$$

By substituting into (2.133), we get

$$\Phi = \phi_l + f_{\text{NL}}\phi_l^2 + (1 + 2f_{\text{NL}}\phi_l)\phi_s + f_{\text{NL}}\phi_s^2, \quad (2.138)$$

since we assume that f_{NL} -term simply proportional to ϕ^2 . By using Poisson equation, $\delta(\mathbf{k}) = \alpha(k)\Phi(\mathbf{k})$, we can determine the matter density perturbation in non-Gaussian case. For Λ CDM model, α is defined as

$$\alpha(k, z) = \frac{2k^2 T(k) D(z)}{3\Omega_m H_0^2}, \quad (2.139)$$

where $T(k)$ is the transfer function and $D(z)$ the linear growth factor.

For long-wavelength modes, the matter density field is given by

$$\delta_l(\mathbf{k}) = \alpha(k)\phi_l(\mathbf{k}). \quad (2.140)$$

The short-wavelength modes are then

$$\delta_s = \alpha[X_1\phi_s + X_2\phi_s^2], \quad (2.141)$$

where $X_1 = 1 + 2f_{\text{NL}}\phi_l$ and $X_2 = f_{\text{NL}}$.

The halo bias then reads

$$b_L(M, k) = \bar{n}^{-1} \left[\frac{\partial n}{\partial \delta_l} + 2f_{\text{NL}} \frac{d\phi_l}{d\delta_l} \frac{\partial n}{\partial X_1} \right]. \quad (2.142)$$

The second term represents the modified non-Gaussian part which appears to be scale-dependent while first term is the k independent Gaussian bias. By rewriting (2.142) in terms of the cosmic variance σ_8 , we get

$$b_L(M, k) = b_L(M) + 2f_{\text{NL}} \frac{d\phi_l}{d\delta_l} \frac{\partial \ln n}{\partial \ln \bar{\sigma}_8}, \quad (2.143)$$

where $\bar{\sigma}_8(\mathbf{x}) = \sigma_8 X_1(\mathbf{x})$.

By substituting in $d\phi_l/d\delta_l = \alpha^{-1}$ and dropping the local label, we get

$$\Delta b(M, k, z) = \frac{3\Omega_m H_0^2}{c^2 k^2 T(k) D(z)} f_{\text{NL}} \frac{\partial \ln n}{\partial \ln \sigma_8}. \quad (2.144)$$

For halo abundance with a universal mass function, we can use (2.143) to determine the halo bias. Universal mass function is defined as

$$n(M) = n(M, \nu) = M^{-2} \nu f(\nu) \frac{d \ln \nu}{d \ln M}, \quad (2.145)$$

where we use the significance $\nu = \delta_c^2 / \sigma^2(M)$ and $f(\nu)$ is the fraction of collapsed haloes. $\delta_c = 1.686$ is the spherical collapse over-density.

By using (2.136) and (2.145) we get

$$b = 1 - \frac{2}{\delta_c} \nu \frac{d}{d\nu} \ln[\nu f(\nu)]. \quad (2.146)$$

From (2.144), we have

$$\frac{\partial \ln n}{\partial \ln \sigma_8} = -2\nu \frac{d}{d\nu} \ln[\nu f(\nu)], \quad (2.147)$$

assuming the universality of the mass function.

Comparing with (2.146), we have

$$\Delta b(M, k) = 3f_{\text{NL}}(b-1)\delta_c \frac{\Omega_m}{k^2 T(k) D(z)} \left(\frac{H_0}{c}\right)^2, \quad (2.148)$$

which represents the scale dependent halo bias correction due to primordial non-Gaussianity [28].

2.4 N-body simulations

In order to predict the evolution of the structure formation in the universe in the non-linear regime, cosmological dark matter simulations are required. The idea behind numerical simulations is sampling dark matter distributions in the universe by making number of elementary volumes of the phase space and distributing particles with positions and velocities. Then we follow the evolution of this particle distribution due to the effect of gravity and the universe expansion. The mass resolution of the simulation is fixed by the number of distributed particles.

The most basic steps for cosmological N-body simulation are as follows; first implement the initial conditions on the matter distribution [61], then the gravitational force is calculated by solving the Poisson equation Eq. (2.47). Then update particles positions and velocities accordingly. Some energy conservation tests are done by the end of each position and velocities update. The numerical solution of the gravitational force is

usually performed using time integrators. The Leapfrog algorithm is the most common used integrator. For a review on N-body simulations see [16].

Linear perturbation theory breaks down when dark matter perturbations reaches the cosmic mean. In this case full numerical solutions are needed to solve the non-linear structure evolution. Some analytical approaches can be used to predict the mass function in a given spherical collapse function, e.g. Press-Schechter formalism [67].

2.4.1 Initial conditions

In order to set up the initial conditions for an N-body simulation, first a homogeneous distribution of particles is created over a grid. Then density distribution is applied according to the appropriate power spectrum. In order to apply the density perturbations on the homogeneous uniform grid, the Zel'dovich approximation [95] is used which create a discrete density field according to the following relations

$$\mathbf{x} = \mathbf{x}_0 - \frac{D}{4\pi G \rho a^3} \nabla \psi_0, \quad (2.149)$$

$$\mathbf{v} = -\frac{1}{4\pi G \rho a^2} \frac{a\dot{D}}{D} \nabla \psi, \quad (2.150)$$

where x_0 is the initial Lagrangian position and D is the growth function of linear fluctuations. The displacement field ψ is related to the input power spectrum $P(k)$.

2.4.1.1 Non-Gaussian initial conditions: local type

The bispectrum for local form non-Gaussianity, (2.133), is given by,

$$B_{\Phi}(\mathbf{k}_1, \mathbf{k}_2, \mathbf{k}_3) = 2f_{\text{NL}}P_{\Phi}(\mathbf{k}_1)P_{\Phi}(\mathbf{k}_2) + \text{cyc}, \quad (2.151)$$

where $P_{\Phi}(\mathbf{k}_i)$ is the power spectrum at scale \mathbf{k}_i and 'cyc.' denotes cyclic permutations over \mathbf{k}_i .

By defining a quadratic non-local kernel K such that,

$$\Phi = \phi + f_{\text{NL}}K[\phi, \phi]. \quad (2.152)$$

In Fourier space it can be written as

$$\Phi(\mathbf{k}) = \phi(\mathbf{k}) + \int f_{\text{NL}}[\delta_D]K(k_1, k_2)\Phi(\mathbf{k}_1)\Phi(\mathbf{k}_2)d^3k_1d^3k_2, \quad (2.153)$$

where the kernel K is dimensionless in Fourier space, and $[\delta_D] = \delta_D(\mathbf{k} - \mathbf{k}_{12})(\mathbf{k}_{12} \equiv \mathbf{k}_1 + \mathbf{k}_2)$.

From (2.152), the bispectrum simply reads,

$$B_\Phi = 2f_{\text{NL}}K(k_1, k_2)P_\phi(k_1)P_\phi(k_2) + \text{cyc.} \quad (2.154)$$

The kernel K satisfies the exchange symmetry such that $K(\mathbf{k}_1, \mathbf{k}_2) = K(\mathbf{k}_2, \mathbf{k}_1)$. To generate initial conditions, (2.154) is used to find the kernel from a given bispectrum [75].

For local non-Gaussianity, the kernel satisfies the following relation,

$$2f_{\text{NL}}K(k_1, k_2)P_\Phi(k_1)P_\Phi(k_2) + \text{cyc.} = 2f_{\text{NL}}P_\Phi(k_1)P_\Phi(k_2) + \text{cyc.} \quad (2.155)$$

The trivial solution for the exchange symmetric kernel $K(\mathbf{k}_1, \mathbf{k}_2) = 1$. The non-trivial solution is defined such that

$$K(k_1, k_2) = \frac{P_\Phi(k_3)}{2} \left(\frac{1}{P_\Phi(k_1)} + \frac{1}{P_\Phi(k_2)} \right), \quad (2.156)$$

where $P_\Phi(k_3) = P_\Phi(|k_1 + k_2|)$. This leads to a more general definition of the kernel such that

$$K(k_1, k_2) = (1 - u) + u \frac{P_\Phi(k_3)}{2} \left(\frac{1}{P_\Phi(k_1)} + \frac{1}{P_\Phi(k_2)} \right), \quad (2.157)$$

where u is a free parameter. The Bardeen potential for a scale-invariant spectrum is then given by,

$$\Phi = \phi + f_{\text{NL}} [(1 - u)\phi^2 + u\nabla^{-2}\partial^{-1}(\phi\nabla^2\partial\phi)]. \quad (2.158)$$

For $u = 0$, (2.158) leads to the local form of primordial non-Gaussianity. The CMB constraint on local primordial non-Gaussianity from last Planck results is [1]

$$f_{\text{NL}}^{\text{loc}} = 2.5 \pm 5.7 \quad (68\%CL). \quad (2.159)$$

2.5 Conclusion

In this chapter, we review the basic analysis of the cosmological perturbation theory on small and large scales. The linear perturbation equations have been derived for dynamical dark energy models using gauge-invariant variables. On non-linear scales, the mass function has been derived for collapsed objects using phenomenological spherical collapse model. We show that primordial non-Gaussianity introduces a scale dependency in halo bias.

Full numerical solution is required on non-linear scales. N-body simulations are the perfect suit for numerical analysis of structure formations on very small scales. We review the various methods of numerical simulations and illustrate the creation of primordial non-Gaussian initial conditions.



Chapter 3

Primordial non-Gaussianity degeneracy with interacting dark sector on large scales

Forecasts for primordial non-Gaussianity constraints typically assume the standard concordance model, i.e. with dark energy as the cosmological constant. Dynamical dark energy models, i.e. with equation of state $w_x \neq -1$, do not typically introduce significant changes to the power spectrum on large scales (see [32] and references therein). However, if the dark energy interacts with dark matter, then there can be significant effects on the matter overdensity on large scales in some models [33, 66, 85]. This means that we could misinterpret a large-scale signal as evidence of primordial non-Gaussianity when in fact it might be a signature of interacting dark energy.

In this chapter we investigate the large-scale effects on the power spectrum from a class of interacting dark energy models, and consider how to disentangle this signal from that of primordial non-Gaussianity. Our fiducial (non-interacting) model is a w CDM (i.e. $w_x = \text{const}$) model, with $\Omega_{m0} = 0.32$, $\Omega_{\Lambda0} = 0.68$, $n_s = 0.96$ and $H_0 = 67.04 \text{ km s}^{-1} \text{ Mpc}^{-1}$. The interacting dark energy models have the same parameters.

3.1 Interacting dark energy dynamics and perturbations

The transfer of energy density between dark energy and dark matter is not ruled out by current observations (for recent work, see e.g. [25, 72, 73, 86, 88, 91–93]). Baryons, as standard model particles, do not interact non-gravitationally with the dark sector. For

simplicity, and since we are not producing observational constraints, we neglect baryonic matter in our analysis, but it is straightforward to include it via the transfer function.

3.1.1 Background dynamics

For interacting dark fluids with energy density ρ_m (dark matter) and ρ_x (dark energy), the background continuity equations are (where $A = m, x$)

$$\rho'_A + 3(1 + w_A)\rho_A = \frac{aQ_A}{\mathcal{H}}, \quad Q_x = -Q_m. \quad (3.1)$$

Here a prime denotes $d/d \ln a$. The equation of state parameters are $w_A = p_A/\rho_A$ and we assume a constant equation of state for dark energy¹

$$w_m = 0, \quad w_x = \text{const} \neq -1. \quad (3.2)$$

In the non-interacting case, this dark energy model is known as w CDM. The rate of energy density transfer to fluid A is Q_A , and the conservation of total energy enforces $Q_x + Q_m = 0$. We can rewrite (3.1) in terms of an effective equation of state:

$$\rho'_A + 3(1 + w_A^{\text{eff}})\rho_A = 0, \quad w_A^{\text{eff}} = w_A - \frac{aQ_A}{3\mathcal{H}\rho_A}. \quad (3.3)$$

The Friedmann constraint and evolution equations do not contain interaction terms since they govern the total density and pressure:

$$\mathcal{H}^2 = \frac{8\pi G a^2}{3}(\rho_m + \rho_x), \quad (3.4)$$

$$\mathcal{H}' = -\frac{1}{2}(1 + 3w_t)\mathcal{H}, \quad w_t = \sum_A w_A \Omega_A = w_x \Omega_x, \quad (3.5)$$

where w_t is the total equation of state.

3.1.2 Perturbations

Scalar perturbations of the flat background metric in Newtonian gauge are given by (2.5). The A -fluid energy-momentum tensor is

$$T_{A\nu}^\mu = (\rho_A + P_A)u_A^\mu u_\nu^A + P_A \delta_\nu^\mu, \quad (3.6)$$

¹Interacting dark energy models with $w_x = -1$ are also possible, see e.g. [73] and references therein.

where we assume each fluid is a perfect fluid. Here u_A^μ is the A -fluid four-velocity,

$$u_A^\mu = a^{-1} (1 - \Phi, \partial^i v_A), \quad (3.7)$$

where v_A is the peculiar velocity potential.

The covariant form of energy-momentum transfer is given by (we follow the approach of [85])

$$\nabla_\nu T_A^{\mu\nu} = Q_A^\mu, \quad Q_A^\mu = Q_A u_A^\mu + F_A^\mu. \quad (3.8)$$

We have split the energy-momentum transfer 4-vector relative to the total four-velocity, where

$$u^\mu = a^{-1} (1 - \Phi, \partial^i v_t), \quad (3.9)$$

$$(1 + w_t)v_t = \sum_A (1 + w_A)\Omega_A v_A, \quad (3.10)$$

$$Q_A = \bar{Q}_A + \delta Q_A, \quad u_\mu F_A^\mu = 0. \quad (3.11)$$

Here v_t is the total velocity potential, the energy density transfer rate is Q_A and F_A^μ is the momentum density transfer rate, relative to u^μ . For convenience, we drop the overbar on the background \bar{Q}_A from now on.

Then it follows that

$$F_A^\mu = a^{-1} (0, \partial^i f_A), \quad (3.12)$$

$$Q_0^A = -a [Q_A(1 + \Phi) + \delta Q_A], \quad (3.13)$$

$$Q_i^A = a \partial_i [f_A + Q_A v_t], \quad (3.14)$$

where f_A is the momentum transfer potential. Total energy-momentum conservation implies

$$0 = \sum_A Q_A = \sum_A \delta Q_A = \sum_A f_A. \quad (3.15)$$

The perturbed Einstein equations do not explicitly contain interaction terms, since they govern the total density and velocity perturbations. The gravitational potential evolves as

$$\Phi' + \Phi = -\frac{3}{2}\mathcal{H} \sum_A \Omega_A (1 + w_A) v_A, \quad (3.16)$$

and the relativistic Poisson equation is

$$\nabla^2 \Phi = \frac{3}{2}\mathcal{H} \sum_A \Omega_A [\delta_A - 3\mathcal{H}(1 + w_A)v_A], \quad (3.17)$$

where $\delta_A = \delta\rho_A/\rho_A$ is the overdensity in Newtonian gauge. Although there are no explicit interaction terms in (3.16) and (3.17), the gravitational potential Φ and the matter

overdensity δ_m are affected by interaction – via the perturbed conservation equations [(3.21), (3.22) below], which do explicitly contain the interaction.

For general fluid A , it is convenient to use the comoving overdensities, see Sec. 2.1.1.2, defined as

$$\Delta_A = \delta_A + \frac{\rho'_A}{\rho_A} v_A. \quad (3.18)$$

In terms of the comoving overdensities, the Poisson equation becomes

$$\nabla^2 \Phi = \frac{3}{2} \mathcal{H}^2 \left(\sum_A \Omega_A \Delta_A - \mathcal{Q}^\Phi \right), \quad (3.19)$$

$$\mathcal{Q}^\Phi = \frac{a}{\rho_t} \sum_A Q_A v_A = \frac{a}{\rho_t} Q_x (v_x - v_m). \quad (3.20)$$

The interaction is now explicitly present through the velocity terms introduced via the comoving overdensities.

The perturbed conservation equations in [85] are given in terms of δ_A . We re-express these in terms of Δ_A to obtain

$$v'_A + v_A + \frac{c_{sA}^2}{(1+w_A)\mathcal{H}} \Delta_A + \frac{\Phi}{\mathcal{H}} = \mathcal{Q}_A^v, \quad (3.21)$$

$$\Delta'_A - 3w_A \Delta_A - \frac{k^2}{\mathcal{H}} (1+w_A) v_A - \frac{9}{2} \mathcal{H} (1+w_A) (1+w_t) (v_A - v_t) = \mathcal{Q}_A^\Delta, \quad (3.22)$$

where c_{sA} is the sound-speed, i.e. the speed of propagation of fluctuations. For dark matter, $c_{sm} = 0$. For dark energy, we choose the sound-speed of a quintessence scalar field [85], so that $c_{sx} = 1$. The source terms on the right encode the effect of interactions, and are given by

$$\mathcal{Q}_A^v = \frac{a}{(1+w_A)\rho_A\mathcal{H}} \left[Q_A (v_t - v_A) + f_A \right], \quad (3.23)$$

$$\begin{aligned} \mathcal{Q}_A^\Delta &= \frac{aQ_A}{\rho_A} \left[\frac{Q'_A}{Q_A} - \frac{\rho'_A}{\rho_A} \right] v_A - \frac{aQ_A}{\rho_A} \left[3 + \frac{aQ_A}{(1+w_A)\rho_A\mathcal{H}} \right] (v_t - v_A) \\ &\quad - \frac{a}{\rho_A} \left[3 + \frac{aQ_A}{(1+w_A)\rho_A\mathcal{H}} \right] f_A + \frac{aQ_A}{\rho_A} \left[3(1+w_A) + \frac{aQ_A}{\rho_A\mathcal{H}} \right] v_A + \frac{a}{\rho_A\mathcal{H}} \delta Q_A \\ &\quad - \frac{aQ_A}{\rho_A\mathcal{H}} \left[\frac{c_{sA}^2}{(1+w_A)} + 1 \right] \Delta_A + 2 \frac{aQ_A}{\rho_A\mathcal{H}} \Phi. \end{aligned} \quad (3.24)$$

3.1.3 A simple model of interacting dark energy

Dark sector interactions are not ruled out observationally and are theoretically plausible, given the unknown nature of the physics of the dark sector. We do not have guidance from fundamental physics for either the nature of dark energy, or the form of a possible interaction between it and dark matter. Here we choose a simple model of dark energy and a simple interaction model, each with only a single parameter.

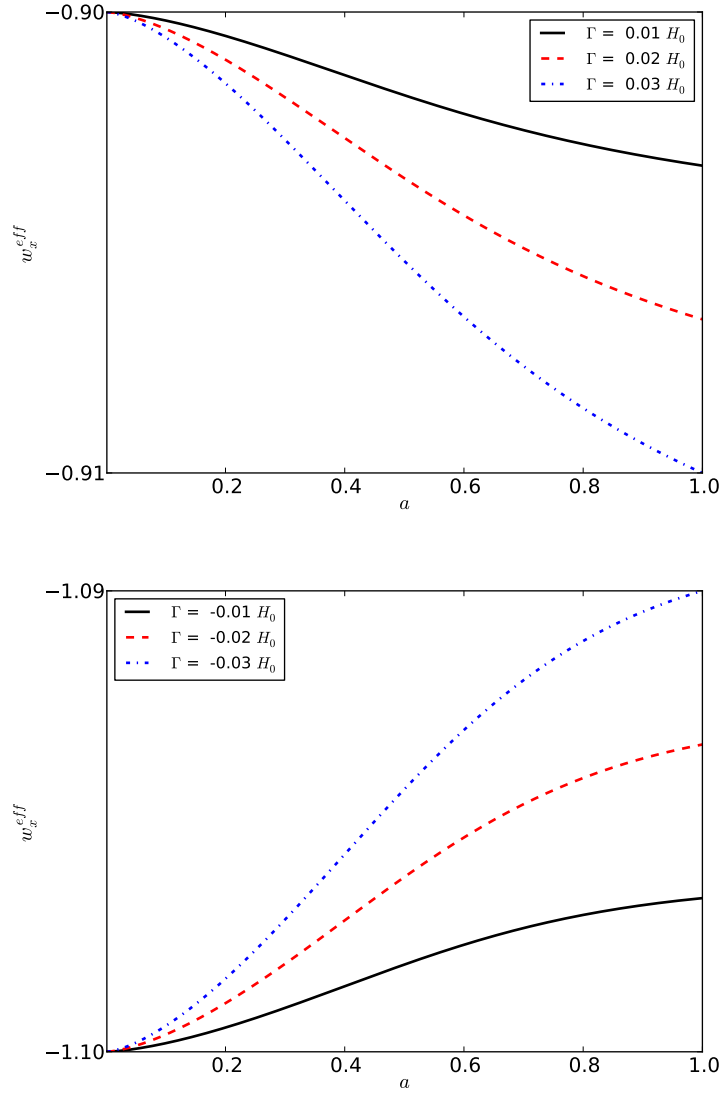


FIGURE 3.1: *Upper:* Evolution of effective dark energy equation of state, w_x^{eff} , with $w_x = -0.9$ and for different $\Gamma > 0$, in the interacting dark energy model (3.25). The $\Gamma = 0$ limit is $w_x^{\text{eff}} = w_x = -0.9$. *Lower:* The $\Gamma < 0$ case, with $w_x = -1.1$.

We adopt the interaction model of [22], defined covariantly by

$$Q_x^\mu = -Q_m^\mu = \Gamma \rho_x u_x^\mu, \quad (3.25)$$

where Γ is a constant interaction rate. (Observational constraints on Γ are given in [22].) Since the dark energy has $w_x = \text{const}$, we call this model $\Gamma w\text{CDM}$.

In the background, (3.25) gives

$$Q_x = \Gamma \rho_x = -Q_m, \quad (3.26)$$

and for the perturbations,

$$\delta Q_x = -\delta Q_m = \Gamma \rho_x \delta_x, \quad f_x = -f_m = \Gamma \rho_x (v_x - v_t). \quad (3.27)$$

Since Q_A^μ is parallel to u_x^μ , there is no momentum transfer in the dark energy frame. This means there is momentum transfer in the dark matter frame, so that the dark matter velocity v_m^i does not obey the same Euler equation as the galaxies, and there is consequently a velocity bias [52]. The alternative model considered in [22] has Q_A^μ parallel to u_m^μ , without momentum transfer in the dark matter frame and thus with no velocity bias.

There are two cases for the Γw CDM model:

- $\Gamma > 0$ – which represents a *transfer of energy density from dark matter to dark energy*, with transfer rate Γ .

Stability of this model requires [22] $w_x > -1$.

- $\Gamma < 0$ – which represents the *decay of dark energy to dark matter*, with decay rate $|\Gamma|$.

Stability of this model requires [22] $w_x < -1$.

From (3.3) and (3.26), we see that $w_x^{\text{eff}} = w_x - a\Gamma/(3\mathcal{H})$. Then it follows that $w_x^{\text{eff}} < w_x$ when $\Gamma > 0$ and $w_x^{\text{eff}} > w_x$ when $\Gamma < 0$. This behaviour is illustrated in Fig. 3.1. The effects of interaction grow with time, as dark energy becomes significant and then dominant. It is clear that $|\Gamma|/H_0 < 1$ is required to avoid a background evolution that will be ruled out by distance measurements. Here we are not concerned with precise limits on Γ (see [22] for these).

3.1.4 Initial conditions

At decoupling, we assume that the dark fluids are adiabatic and have equal peculiar velocities:

$$S_{mx}|_d \equiv \left(\frac{\delta \rho_m}{\rho'_m} - \frac{\delta \rho_x}{\rho'_x} \right)_d = 0, \quad v_{md} = v_{xd}. \quad (3.28)$$

By (3.18), this implies

$$\left(\frac{\rho_m}{\rho'_m} \right)_d \Delta_{md} = \left(\frac{\rho_x}{\rho'_x} \right)_d \Delta_{xd}. \quad (3.29)$$

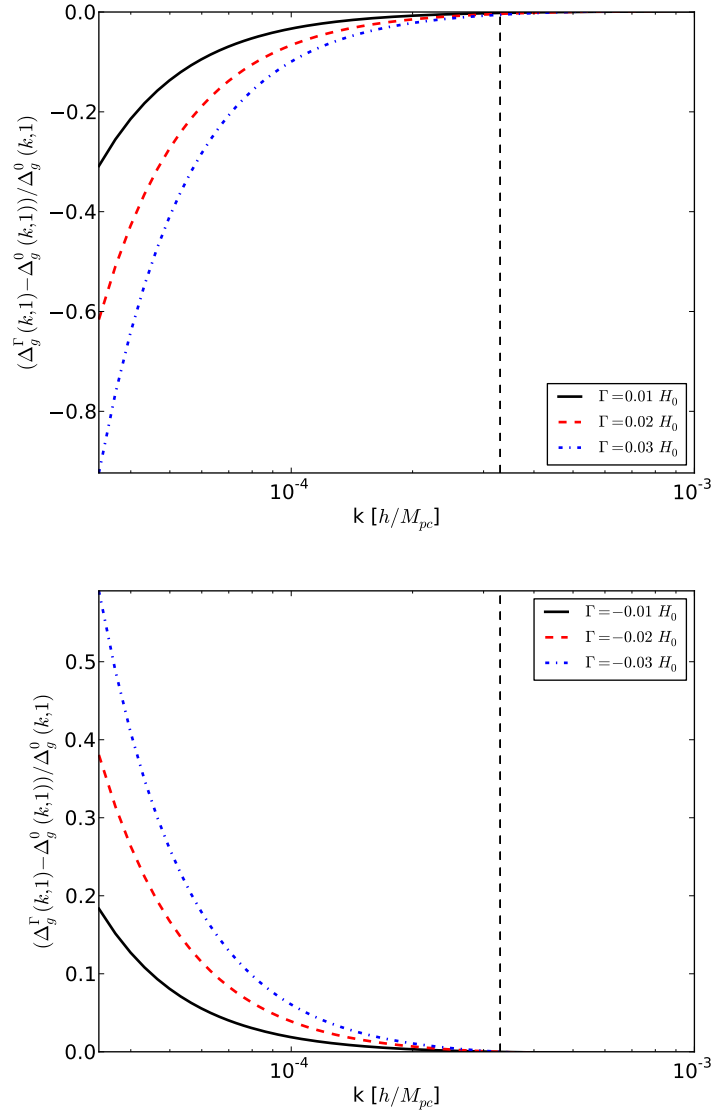


FIGURE 3.2: *Upper:* Relative galaxy overdensity [see (3.45)] at $a = 1$ with dark sector interactions, for different $\Gamma > 0$ and with $w_x = -0.9$. The vertical dashed line is the Hubble scale, $k = H_0$. The $\Gamma = 0$ limit is the horizontal line through 0. We used $b(1) = 2$. *Lower:* The $\Gamma < 0$ case, with $w_x = -1.1$.

Using the Poisson equation (3.19), we get

$$\Delta_{md} = -\frac{2}{3} \left(\frac{k}{\mathcal{H}_d} \right)^2 \frac{(1 + \mu)}{\Omega_{md}} \Phi_d, \quad (3.30)$$

$$\Delta_{xd} = -\frac{2}{3} \left(\frac{k}{\mathcal{H}_d} \right)^2 \frac{\mu}{\Omega_{xd}} \Phi_d, \quad (3.31)$$

where we have defined

$$\mu = \left(\frac{\rho'_x}{\rho'_m} \right)_d \left[1 - \left(\frac{\rho'_x}{\rho'_m} \right)_d \right]^{-1} \ll 1. \quad (3.32)$$

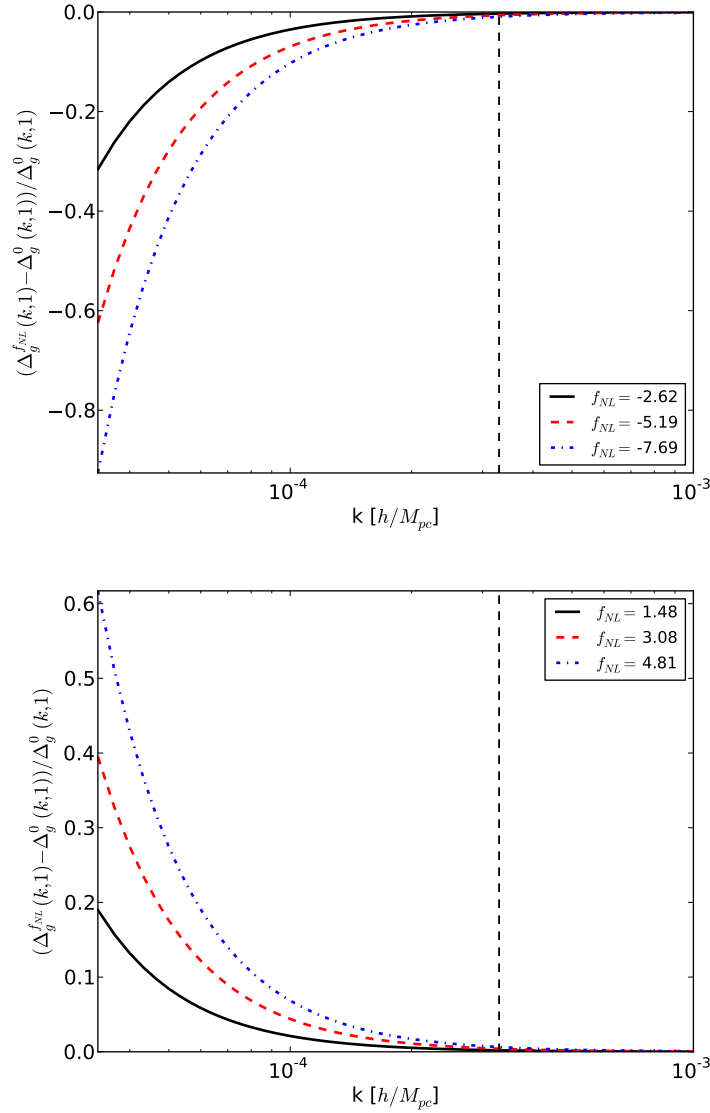


FIGURE 3.3: The relative galaxy overdensity as in Fig. 3.2 but for the case of primordial non-Gaussianity, with $f_{\text{NL}} < 0$ (Up) and $f_{\text{NL}} > 0$ (Down).

We find that $\mu \sim 10^{-9}$ for $|\Gamma|/H_0 \lesssim 0.03$ and $w_x = -0.9$. For $w_x = -1.1$, $\mu \sim -10^{-11}$.

The gravitational potential at decoupling is related to the primordial potential as follows:

$$\Phi_d(k) = \frac{9}{10} T(k) \Phi_p(k), \quad (3.33)$$

$$\Phi_p(k) = A \left(\frac{k}{H_0} \right)^{(n_s-4)/2}, \quad (3.34)$$

where T is the transfer function ($\rightarrow 1$ on very large scales), n_s is the spectral index of the primordial spectrum and A is an amplitude determined by the primordial curvature perturbation.

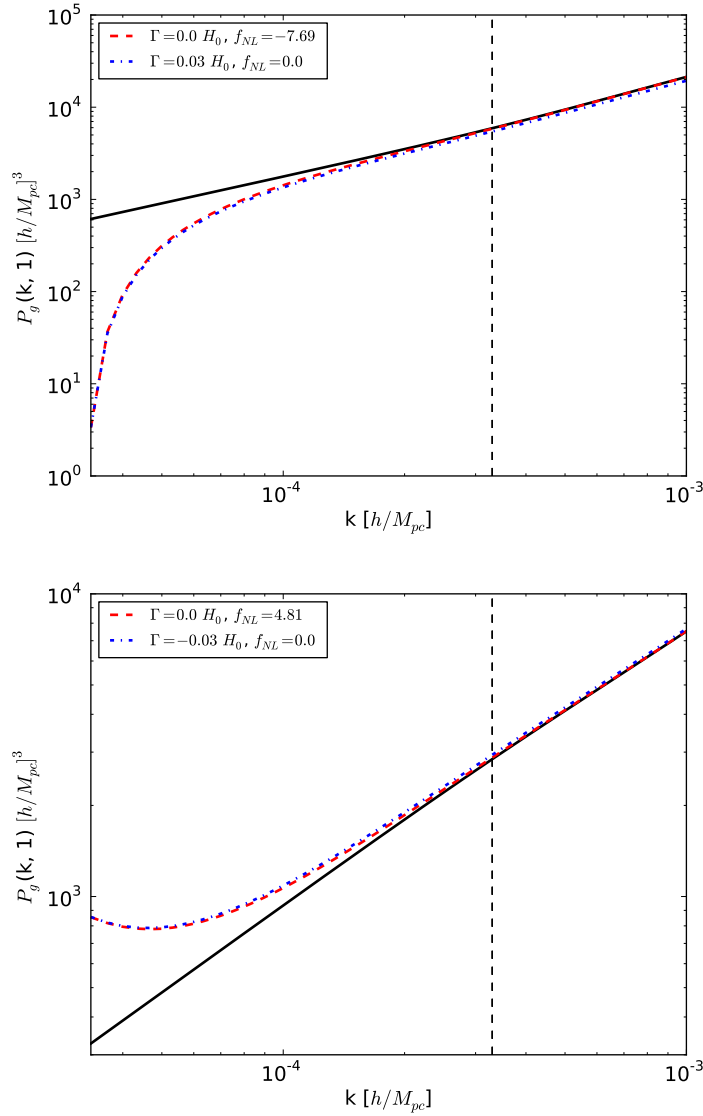


FIGURE 3.4: *Upper:* Galaxy power spectrum P_g at $a = 1$ for an interacting dark energy model with $\Gamma = 0.03H_0$ and for a primordial non-Gaussianity model with $f_{\text{NL}} = -7.69$. The black (solid) line is the fiducial w CDM model without interaction or primordial non-Gaussianity. We set $b(1) = 2$ and $w_x = -0.9$. *Lower:* For $\Gamma = -0.03H_0$ and $f_{\text{NL}} = 4.81$, with $w_x = -1.1$.

We can neglect dark energy and the interaction at decoupling provided that $\mu \ll 1$ and $|\Gamma|/H_0 \lesssim 0.03$. This is equivalent to assuming that the universe at decoupling is well described as matter-dominated, and it implies that $\Phi'_d = 0$. Then from (3.16), (3.20) and (3.28), we find

$$v_{md} = -\frac{2}{3(1 + w_x \Omega_{xd})\mathcal{H}_d} \Phi_d = v_{xd}, \quad (3.35)$$

$$\mathcal{Q}_d^\Phi = 0. \quad (3.36)$$

3.1.5 Growth functions

The potential growth function D_Φ is defined by

$$\Phi(k, a) = \frac{D_\Phi(k, a)}{a} \Phi_d(k), \quad (3.37)$$

so that $D_{\Phi_d} = a_d$.

We define dark matter and dark energy growth functions

$$D_m(k, a) = \frac{\Delta_m(k, a)}{\Delta_{md}(k)} a_d, \quad (3.38)$$

$$D_x(k, a) = \frac{\Delta_x(k, a)}{\Delta_{xd}(k)} a_d, \quad (3.39)$$

where we normalize at decoupling. Then it follows from the Poisson equation (3.19) that

$$D_m = \frac{\Omega_{md}}{\Omega_m(1+\mu)} \left[\frac{a_d \mathcal{H}_d^2}{a \mathcal{H}^2} D_\Phi - \mu \frac{\Omega_x}{\Omega_{xd}} D_x - B \frac{a_d \mathcal{H}_d^2}{T(k) k^{n_s/2}} \mathcal{Q}^\Phi \right], \quad (3.40)$$

$$\mathcal{Q}^\Phi = a \Gamma \Omega_x (v_x - v_m). \quad (3.41)$$

Here $B = 5H_0^{(4-n_s)/2}/(3A)$ is a constant. In the limiting case of the concordance model Λ CDM ($\Gamma = 0, w_x = -1$), we have $\mu = 0 = D_x$ and $\mathcal{H}^2 \Omega_m = a^{-1} H_0^2 \Omega_{m0}$. Thus (3.40) recovers the Λ CDM relation $D_m = D_\Phi$. In Λ CDM, the matter growth function is scale-independent, $D_m = D_m(a)$. This also holds approximately for the non-interacting $w_x = \text{const}$ models, w CDM. The effect of dark sector interactions on the growth of the comoving matter overdensity is encoded in the \mathcal{Q}^Φ term (3.41).

3.2 Large-scale power in interacting dark energy

We show below that dark sector interactions in our model do lead to a growth or decrease of matter power on large scales – which is similar to the effect of primordial non-Gaussianity on the galaxy power spectrum. This illustrates the point that if we are unaware of the possibility of interacting dark energy, then a detection of primordial non-Gaussianity from the galaxy power spectrum could in fact be a signal of dark sector interaction with Gaussian primordial perturbations. We need to be able to distinguish the two possibilities, i.e. to break the potential degeneracy between the signals of interacting dark energy and primordial non-Gaussianity in the large-scale galaxy power. First we need to characterize the galaxy power in the two scenarios.

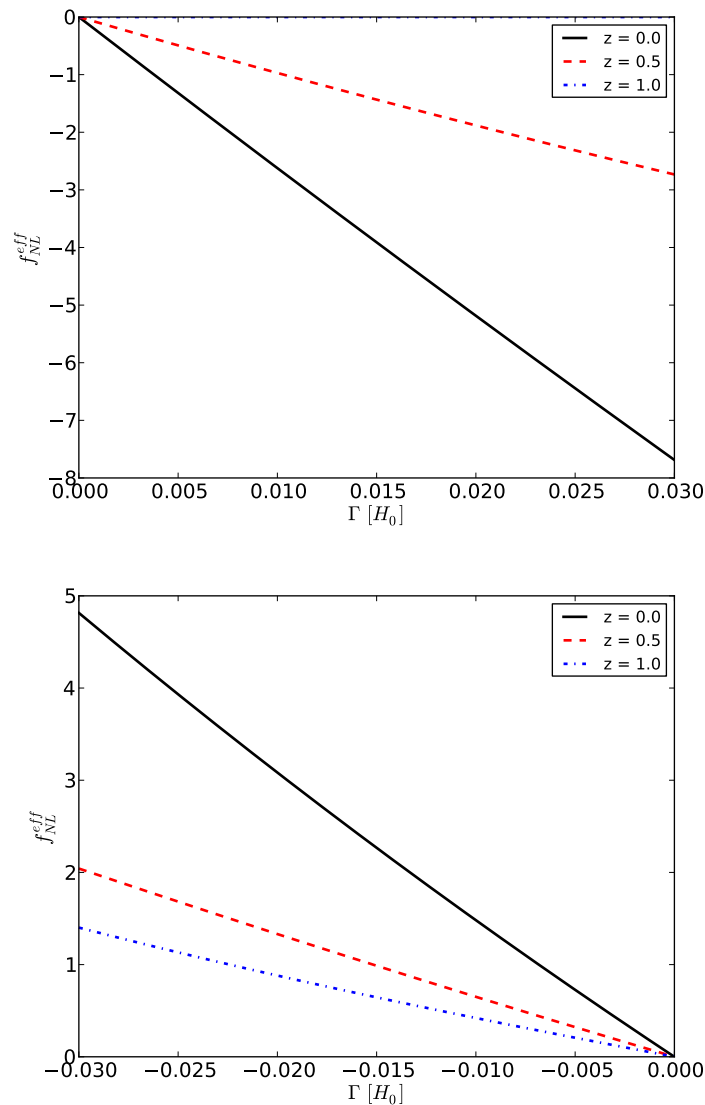


FIGURE 3.5: *Upper:* Effective primordial non-Gaussianity parameter f_{NL}^{eff} corresponding to interaction rate $\Gamma > 0$ at different redshift values. We take $w_x = -0.9$. *Lower:* For $\Gamma < 0$ and $w_x = -1.1$.

3.2.1 Galaxy overdensity in interacting dark energy and primordial non-Gaussianity

In the absence of primordial non-Gaussianity, the galaxy overdensity in Γw CDM is related to the matter overdensity on linear scales by

$$\Delta_g^\Gamma(k, a) = b(a)\Delta_m(k, a), \quad (3.42)$$

where b is the scale-independent bias. We have introduced a Γ superscript to distinguish this galaxy overdensity from the non-interacting primordial non-Gaussianity case.

In the presence of primordial non-Gaussianity, the bias becomes scale-dependent on large scales (2.148). On very large scales, where $T \rightarrow 1$, we have $b \propto f_{\text{NL}} k^{-2}$. Equation (2.148) is derived in Λ CDM but can also be applied to w CDM with the replacement

$$D_m(a) \rightarrow (1 + \mu)D_m(k, a), \quad (3.43)$$

where μ is given by (3.32) and $D_m(k, a)$ is the growth function for non-interacting dark energy (i.e., $\Gamma = 0$). This replacement makes only a small change provided w_x is close to -1 and $c_{sx} = 1$. Thus for non-interacting w CDM with primordial non-Gaussianity

$$\Delta_g^{f_{\text{NL}}}(k, a) = b(a) \left[1 + \frac{\Delta b(k, a)}{b(a)} \right] \Delta_m^0(k, a), \quad (3.44)$$

where Δ_m^0 is the matter overdensity in w CDM. We will call this model $f_{\text{NL}}w$ CDM.

3.2.2 Comparing the galaxy power

Now we investigate whether the large-scale behaviour is qualitatively similar in the two cases, i.e. the Γw CDM and $f_{\text{NL}}w$ CDM models. In order to do this, we define for each model the galaxy overdensity relative to w CDM, i.e.,

$$\frac{\Delta_g^\Gamma(k, a) - \Delta_g^0(k, a)}{\Delta_g^0(k, a)} \quad \text{and} \quad \frac{\Delta_g^{f_{\text{NL}}}(k, a) - \Delta_g^0(k, a)}{\Delta_g^0(k, a)}, \quad (3.45)$$

where $\Delta_g^0(k, a) = b(a)\Delta_m^0(k, a)$ denotes the w CDM galaxy overdensity ($\Gamma = 0 = f_{\text{NL}}$). These relative overdensities are shown in Figs. 3.2 and 3.3.

3.2.3 Interacting dark energy mimics primordial non-Gaussianity

Figures 3.2 and 3.3 confirm that the effects of Γ and of f_{NL} are qualitatively similar, giving a growth ($\Gamma < 0, f_{\text{NL}} > 0$) or suppression ($\Gamma > 0, f_{\text{NL}} < 0$) on super-Hubble scales ($k \ll \mathcal{H}$). The effect is stronger as $|\Gamma|$ or $|f_{\text{NL}}|$ are increased. By comparing the galaxy power spectra, we find numerically the effective primordial non-Gaussianity parameters that correspond most closely to $|\Gamma|/H_0 = 0.03$. The correspondence is confined to scales that are not too far beyond the Hubble radius, since this regime is well outside the reach of observations.

In Fig. 3.4, we compare the resulting galaxy power spectra, where $P_g(k, a) = \langle |\Delta_g(k, a)|^2 \rangle$.

Figure 3.4 indicates that we can successfully extract an effective primordial non-Gaussianity parameter when $|\Gamma|/H_0 = 0.03$. We extend this over the range $|\Gamma|/H_0 < 0.03$ to produce

a curve of the effective primordial non-Gaussianity parameter against Γ . We do this for a range of redshifts, and the results are shown in Fig. 3.5. To account for the redshift evolution of the (Gaussian) bias on linear scales, we adopt the ansatz

$$b = b_0 \sqrt{1+z} = b_0 a^{-1/2}, \quad (3.46)$$

where $b_0 = 2$.

3.2.4 Breaking the degeneracy between interacting dark energy and primordial non-Gaussianity

Figure 3.5, shows a key feature:

- As redshift increases, the value of $|f_{\text{NL}}^{\text{eff}}|$ decreases, approaching zero at redshifts $z \gtrsim 1$. This follows since the dark sector interaction begins to have an effect on the galaxy power spectrum only at late times. By contrast, the primordial non-Gaussianity signal is ‘frozen’ into the power spectrum at primordial times so that f_{NL} is independent of redshift.

This feature should be generic for interacting dark energy models that cause large-scale deviations in the power spectrum. It is exactly what allows us to break the degeneracy between primordial non-Gaussianity and interacting dark energy using the galaxy power spectrum. If we establish a value of $f_{\text{NL}}^{\text{eff}}$ at redshift $z = 0$, then we can compare the observed power at another redshift, e.g. $z = 0.5$, with that predicted by primordial non-Gaussianity with $f_{\text{NL}} = f_{\text{NL}}^{\text{eff}}$. Significant disagreement indicates that the large-scale signal is not due to primordial non-Gaussianity, but could be a smoking gun for dark sector interaction.

For our interacting dark energy model, the relationship between $f_{\text{NL}}^{\text{eff}}$ and Γ can be estimated analytically as follows. We take the limit $k \ll \mathcal{H}$, so that (3.44) implies $\Delta_g^{f_{\text{NL}}} \rightarrow \Delta b \Delta_m^0$. In the Poisson equation (3.19), we neglect $k^2 \Phi$ to obtain $\Delta_m \rightarrow \mathcal{Q}^\Phi / \Omega_m$. Thus by (3.42), $\Delta_g^\Gamma \rightarrow b \mathcal{Q}^\Phi / \Omega_m$. Then we can write (for $k \ll \mathcal{H}$)

$$\Delta_g^{f_{\text{NL}}^{\text{eff}}} \approx \Delta_g^\Gamma \Rightarrow \Delta b \Delta_m^0 \approx b \frac{\mathcal{Q}^\Phi}{\Omega_m}. \quad (3.47)$$

From (3.38) we have $\Delta_m^0 = D_m^0 \Delta_{md}^0 / a_d$. Then (3.30), (3.33) and (2.148) (with $T = 1$) imply

$$f_{\text{NL}}^{\text{eff}} \approx \left[\frac{5a_d}{9A} \frac{a\Omega_{md}\mathcal{H}_d^2}{\Omega_{m0}H_0^2} \frac{b}{(b-1)\delta_c} \frac{\Omega_x}{\Omega_m} \left(\frac{k}{H_0} \right)^{(4-n_s)/2} (v_x - v_m) \right] \Gamma$$

(3.48)

Clearly $f_{\text{NL}}^{\text{eff}}$ is in general redshift dependent, and this is confirmed by Fig. 3.5.

3.3 Interacting quintessence with an exponential potential

As an alternative model for dynamical dark energy, we consider the quintessence model. Quintessence is defined as a canonical scalar field ϕ governed by a potential $V(\phi)$ that is responsible for the late-time acceleration of the universe [21]. The equation of state of quintessence varies with time. The background dynamics of the various quintessence dark energy models could be understood using the dynamical system approach [36, 69].

Interaction between dark energy and dark matter has been proposed in several forms. One proposal is the interaction between quintessence dark energy field ϕ and dark matter of the form $Q\rho_m\phi'$ [4]. This type of interaction is familiar within scalar-tensor theories context [3]. In Brans-Dicke theory, the interaction between a Ricci scalar and a scalar field introduces a constant interaction with non-relativistic dark matter in the Einstein frame [83].

Another phenomenological approach to the interaction between dark energy and dark matter is in the form $\Gamma\rho_m$, where Γ is normalized such that Γ/H is dimensionless [20, 27]. This represents the fluid description of interacting dark energy models (see Sec. 3.1.3).

3.3.1 Background dynamics

The interaction between quintessence scalar field and dark matter is given by

$$\nabla_\mu T_{\nu(\phi)}^\mu = -QT_{(m)}\nabla_\nu\phi, \quad \nabla_\mu T_{\nu(m)}^\mu = QT_{(m)}\nabla_\nu\phi, \quad (3.49)$$

where $T_{\nu(\phi)}^\mu$ and $T_{\nu(m)}^\mu$ are quintessence and dark matter energy-momentum tensors respectively.

Interacting quintessence Lagrangian density is given as

$$\mathcal{L}_\phi = -\frac{1}{2}g^{\mu\nu}\partial_\mu\phi\partial_\nu\phi - V(\phi) + \mathcal{L}_{\text{int}}, \quad (3.50)$$

where \mathcal{L}_{int} is the interacting Lagrangian. We assume the exponential potential form for the quintessence field given by

$$V(\phi) = V_0 \exp(-\lambda\phi), \quad (3.51)$$

where λ is taken to be a positive constant [5].

In FLRW metric, the background continuity equations for interacting quintessence dark energy and dark matter are given by

$$\rho'_\phi + 3(1 + w_\phi)\rho_\phi = \frac{a}{\mathcal{H}}Q_\phi, \quad (3.52)$$

$$\rho'_m + 3\rho_m = \frac{a}{\mathcal{H}}Q_m, \quad (3.53)$$

where $\rho_{\phi,m}$ is the energy density for quintessence field ϕ and dark matter respectively and $w_\phi = P_\phi/\rho_\phi$ is quintessence equation of state. The interaction terms $Q_{\phi,m}$ are defined as

$$Q_\phi = \sqrt{\frac{2}{3}}\beta\rho_m\frac{\phi'}{\mathcal{H}}, \quad Q_m = -Q_\phi, \quad (3.54)$$

where β is the interaction constant. The scalar field ϕ satisfies Klein-Gordon equation in the interacting form

$$\phi'' + 3\mathcal{H}\phi' + V_{,\phi} = \sqrt{\frac{2}{3}}\beta\rho_m\frac{\phi'}{\mathcal{H}}. \quad (3.55)$$

The Friedman constraint equation is

$$\mathcal{H}^2 = \frac{8\pi G a^2}{3}(\rho_m + \rho_\phi), \quad (3.56)$$

where G is the Newtonian constant.

In order to solve for the background dynamics, we introduce the dynamical variables ξ, ϵ defined as

$$\xi \equiv \frac{\phi'}{\sqrt{6}}, \quad \epsilon \equiv \frac{a}{\mathcal{H}}\sqrt{\frac{V}{3}}. \quad (3.57)$$

Equations (3.52) could be written as follows,

$$\xi' = \frac{3}{2}\xi(\xi^2 - \epsilon^2 - 1) + V_{,\phi}\epsilon^2 + \beta(1 - \xi^2 - \epsilon^2), \quad (3.58)$$

$$\epsilon' = \frac{3}{2}\epsilon(\xi^2 - \epsilon^2 + 1) - V_{,\phi}\xi\epsilon, \quad (3.59)$$

and the Hubble evolution equation is given by

$$\mathcal{H}' = -\frac{3}{2}\mathcal{H}(\xi^2 - \epsilon^2 + 1). \quad (3.60)$$

Form the definitions (3.57), the dimensionless density parameters $\Omega_{\phi,m}$ are given by

$$\Omega_\phi = \xi^2 + \epsilon^2, \quad \Omega_m = 1 - \xi^2 - \epsilon^2, \quad (3.61)$$

for quintessence dark energy and dark matter respectively. The equation of state for the scalar field ϕ is given as follows

$$w_\phi = \frac{\xi^2 - \epsilon^2}{\xi^2 + \epsilon^2}. \quad (3.62)$$

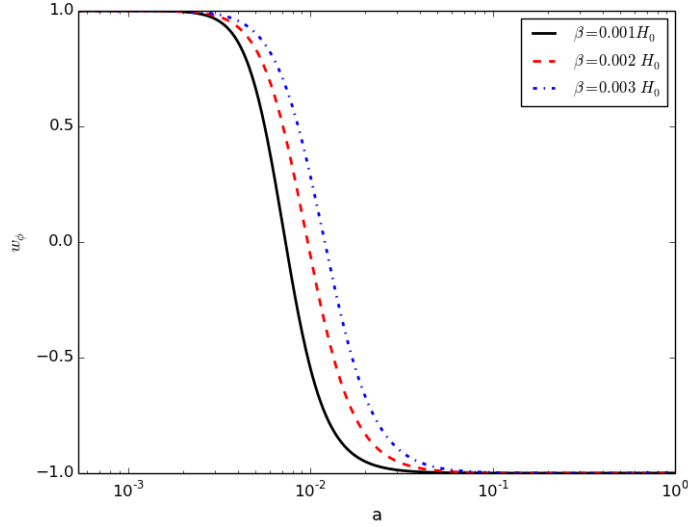


FIGURE 3.6: The equation of state of interacting quintessence dark energy at different values of the interaction parameter β .

Fig. 3.6 shows the equation of state of interacting quintessence dark energy models at values of interacting constant $\beta = 1.0, 2.0, 3.0 \times 10^{-3} H_0$. It appears that the quintessence field has a tracker solution towards $w_\phi = 1.0$ at the initial redshift. The equation of state approaches the value $w_\phi = -1.0$ at redshift $z = 0.0$. The initial conditions for the dynamical system has been chosen such that the current values of the density parameters are the same as Λ CDM model.

3.3.2 Perturbations

For quintessence field ϕ , we define the fluid variables as follows

$$\rho_\phi \equiv -\frac{1}{2}g^{\alpha\beta}\phi_{,\alpha}\phi_{,\beta} + V, \quad (3.63)$$

$$P_\phi \equiv -\frac{1}{2}g^{\alpha\beta}\phi_{,\alpha}\phi_{,\beta} - V, \quad (3.64)$$

$$u_\mu \equiv \frac{\phi_{,\mu}}{|g^{\alpha\beta}\phi_{,\alpha}\phi_{,\beta}|^{1/2}}. \quad (3.65)$$

The energy-momentum tensor is given by

$$T_{\phi\mu\nu} = (\rho_\phi + P_\phi)u_\mu u_\nu + g_{\mu\nu}P_\phi. \quad (3.66)$$

The perturbed energy density and pressure for quintessence dark energy are given by

$$\delta\rho_\phi = H^2(\phi'\delta\phi' - \phi'^2\Phi) + V_{,\phi}\delta\phi, \quad (3.67)$$

$$\delta P_\phi = H^2(\phi'\delta\phi' - \phi'^2\Phi) - V_{,\phi}\delta\phi. \quad (3.68)$$

The sound speed is therefore defined as

$$c_{s,\phi}^2 = \frac{\delta P_\phi}{\delta\rho_\phi} = \frac{H^2(\phi'\delta\phi' - \phi'^2\Phi) - V_{,\phi}\delta\phi}{H^2(\phi'\delta\phi' - \phi'^2\Phi) + V_{,\phi}\delta\phi} \quad (3.69)$$

For interacting fluids with generic equations of state and sound speed, the perturbation equations are given by (3.16), (3.21), (3.22). For interacting quintessence model (3.54), the perturbed coupling terms are given by,

$$\delta Q_m = -\delta Q_\phi = Q_m \left(\delta_m + \frac{3}{2}\Phi + 3\Omega_\phi \frac{\delta_\phi}{2\phi'^2(1+c_{s,\phi}^2)} \right), \quad (3.70)$$

$$f_m = -f_\phi = Q_m(u - u_\phi). \quad (3.71)$$

where $\delta_\phi = \delta\rho_\phi/\rho_\phi$ is the quintessence overdensity.

3.3.3 Galaxy overdensity in interacting quintessence model

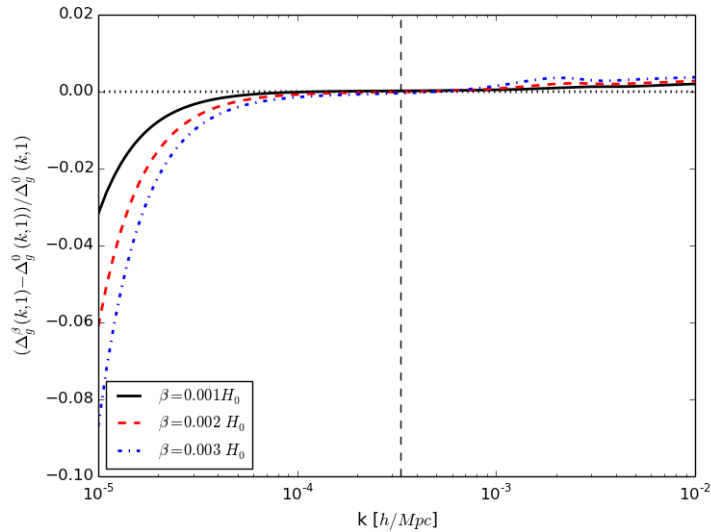


FIGURE 3.7: Relative galaxy overdensity for interacting quintessence dark energy at $a = 1.0$ for different values of the interacting constant β .

Fig. 3.7 shows the relative galaxy overdensity for interacting quintessence dark energy defined as

$$\frac{\Delta_g^\beta(k, a) - \Delta_g^0(k, a)}{\Delta_g^0(k, a)}, \quad (3.72)$$

where $\Delta_g^0(k, a)$ represents the galaxy overdensity for quintessence model with no interaction. On super-horizon scales, the galaxy overdensity (and so the galaxy power spectrum) shows a scale dependent effect decreasing with the interaction parameter increase. On sub-horizon scales, the galaxy overdensity also shows an increasing deviations with respect to the background model with interaction. These signs of interacting effects allow for possible observational constraints on super and sub horizon scales via upcoming large scales surveys. Approaching non-linear scales, interacting quintessence dark energy is assumed to leave an imprint on small structure formation as well. See Sec. 4.3 for further details.

3.4 Conclusion

We have shown that for a simple class of models, interaction in the dark sector causes a growth or suppression of matter power on very large scales, relative to the non-interacting case. Furthermore, these large-scale deviations can be approximately mimicked by primordial non-Gaussianity in a non-interacting model. This raises a potential problem for attempts to constrain primordial non-Gaussianity through the galaxy power spectrum – such attempts could be confused by interaction in the dark sector. One way to break this degeneracy is by looking at the power spectra at two redshifts. If the two effective parameters $f_{\text{NL}}^{\text{eff}}$ are not equal, then this is a strong indication of interacting dark energy.

We also considered interacting quintessence dark energy models with constant interaction rate. The galaxy overdensity shows that the interaction between quintessence scalar field and dark matter leaves a scale-dependent signal on super-horizon scales. On sub-horizon scales, interacting quintessence model shows deviation from the non-interacting case, which could be a very suitable constraint within current large scale observational limits.

There are serious obstacles to the observability of any effect that arises only on very large scales – including interacting dark energy effects and primordial non-Gaussianity. The fundamental problem is cosmic variance, which grows on large scales and typically swamps any small signal. The current state of the art in constraining primordial non-Gaussianity via galaxy surveys [37] is unable to detect $|f_{\text{NL}}| \lesssim 20$, and Planck has already placed the constraint $|f_{\text{NL}}| \lesssim 10$ (2.159). In the interacting dark energy model that we investigate here, $f_{\text{NL}}^{\text{eff}}$ is in the range compatible with Planck, and therefore not

currently detectable. In order to overcome the problem of cosmic variance in galaxy surveys, we need either three-dimensional data (i.e., the power spectrum measured over a significant range of redshifts) or the application of the multi-tracer method [60, 76], or both. (The multi-tracer method requires that we have two or more different tracers of the underlying dark matter overdensity.) Future surveys such as Euclid and the SKA will be needed in order to detect primordial non-Gaussianity or large-scale interacting dark energy effects at the level $|f_{\text{NL}}^{\text{eff}}| \lesssim 10$ considered here.

There is an important further point about observability on very large scales: on these scales, there are general relativistic corrections to the standard power spectrum, which are also potentially degenerate with primordial non-Gaussianity [19, 49, 68, 94]. Therefore one needs to include the relativistic effects in any analysis of primordial non-Gaussianity, as in [19, 49, 68, 94]. The same applies to an analysis of interacting dark energy on very large scales. The relativistic effects for our interacting dark energy model and others are investigated in [33].



Chapter 4

Imprints of primordial non-Gaussianity on non-linear scales

The abundance of galaxy clusters in the universe is considered as one of the large scale structure observational probes of non-Gaussianity. Since large objects formation originate from the initial density distribution tails, which is nearly Gaussian, it is sensitive to primordial non-Gaussianity [59]. The abundance of large objects, i.e. galaxy clusters and large voids, allows to measure primordial non-Gaussianity on small scales of order 10 *Mpc*. Different estimates of $f_{\text{NL}}^{\text{loc}}$ have been derived from very massive galaxy clusters observations which is $f_{\text{NL}}^{\text{loc}} \sim 400$ [35, 62].

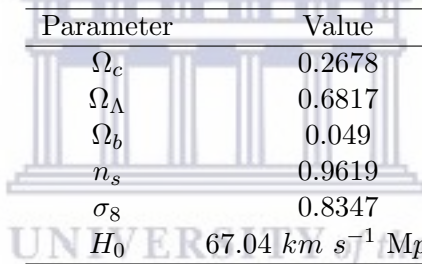
On non-linear scales, where the fluctuations are not governed only via gravitational interactions, numerical simulations are required for more accurate predictions. Since the abundance probe of non-Gaussianity are affected by non-linear gravitational evolution, N-body simulations are considered. Local type non-Gaussianity N-body simulations have been considered with good agreement with the analytical predictions [28, 39, 87].

In this chapter we study the effect of non-Gaussian initial conditions on non-linear dynamics via a set of cosmological dark matter only N-body simulations. We show the effect of non-Gaussianity on non-linear power spectrum and cumulative halo mass function.

4.1 N-body simulation setting

Cosmological N-body simulations consist of an expanding box containing N particles with periodic initial conditions. The mutual interaction between particles, which traces the matter density, are only via Newtonian gravity. The Friedmann equation is used to determine the expansion rate of the expanding box. On non-linear scales, other physical processes are considered such as hydrodynamics which is referred to as baryonic physics. Except on very small scales, baryonic physics are less important and hence gravity-only N-body simulations are good enough for the purpose of this thesis.

Two common algorithms are used for the solution of the N-body problem, the particle-mesh (PM) and the tree particle mesh (tree-PM). The PM method is very good in speed and error control, however it has limits on force resolution. Tree-PM method is used to combine long-range and short-range force computations. Short range force computations are done by tree algorithm. In this thesis we are going to use the tree-PM publicly available code GADGET-2 [81] for all simulation runs.



Parameter	Value
Ω_c	0.2678
Ω_Λ	0.6817
Ω_b	0.049
n_s	0.9619
σ_8	0.8347
H_0	$67.04 \text{ km s}^{-1} \text{ Mpc}^{-1}$

TABLE 4.1: Cosmological parameters used to generate initial conditions and simulation runs [2].

The choice of cosmological parameters are for a flat Λ CDM cosmology with Planck results [2], see Table 4.1. We consider different sets of medium resolution simulations for different local non-Gaussianity realizations to measure the effect on non-linear scales. Table 4.2 contains the setting of the simulations suits done in this thesis.

Name	z_{ini}	$B \text{ [Mpc}^3\text{]}$	N_{part}	$m_{part} [M_\odot]$	$\epsilon_{soft} \text{ [Mpc]}$	f_{NL}
Λ CDM	49.0	250^3	256^3	6.92×10^{12}	0.0244	0.0
f_{NL} - Λ CDM0	49.0	250^3	256^3	6.92×10^{11}	0.0244	250.0
f_{NL} - Λ CDM1	49.0	250^3	256^3	6.92×10^{11}	0.0244	500.0
f_{NL} - Λ CDM2	49.0	250^3	256^3	6.92×10^{11}	0.0244	1000.0
f_{NL} - Λ CDM3	49.0	250^3	256^3	6.92×10^{11}	0.0244	-250.0
f_{NL} - Λ CDM4	49.0	250^3	256^3	6.92×10^{11}	0.0244	-500.0
f_{NL} - Λ CDM5	49.0	250^3	256^3	6.92×10^{11}	0.0244	-1000.0

TABLE 4.2: Set of N-body simulation runs.

All the simulation runs have been done on SCIAMA cluster at Portsmouth University via CosmoSuite code (see Sec. 4.1.3). The total running time on 128 cores is around six hours. Since high resolution simulations are very computationally consuming, we restrict our set of runs to medium resolution setting. We considered high values of the primordial non-Gaussianity parameter $f_{\text{NL}} > 100$, which are ruled out by recent Planck results (2.159), in order to have a qualitative measurable effect on a medium resolution box considered in our simulation runs. For near-Planck f_{NL} values, it requires very high resolution simulations, which is very time and computational consuming and will be considered for future work [30].

4.1.1 Initial conditions generation

The initial conditions for our set of N-body simulations are generated by displacing N number of particles on a regular grid using the Zel'dovich approximation (2.149). We use a realization of a random Gaussian field for the Bardeen potential. The transfer function $T(k)$ for the initial power spectrum is numerically computed using the numerical code CAMB [54], see Fig. 4.1. The initial redshift has been selected at $z = 49.0$ so radiation could be safely neglected.

4.1.1.1 Local non-Gaussianity implementation

For local type non-Gaussianity, we used 2LPT-PNG code to generate initial conditions [75]. It simply computes the non-Gaussian contribution using the kernel defined in (2.158) to compute the non-Gaussian density field from a given Bardeen potential.

4.1.2 Simulation settings test

In order to test our simulation setting for local primordial non-Gaussianity model, we compare our results with [87] for the halo mass function.

Fig. 4.2 shows the the ratio between Gaussian and non-Gaussian halo mass function at redshift $z = 1.5$ for local $f_{\text{NL}}^{\text{loc}} = 500$. The plot shows that our results are in agreement with [87], considering the same setting for initial conditions generation and N-body simulation runs. We used the same halo finder (AHF halo finder) as in [87] to avoid numerical errors.

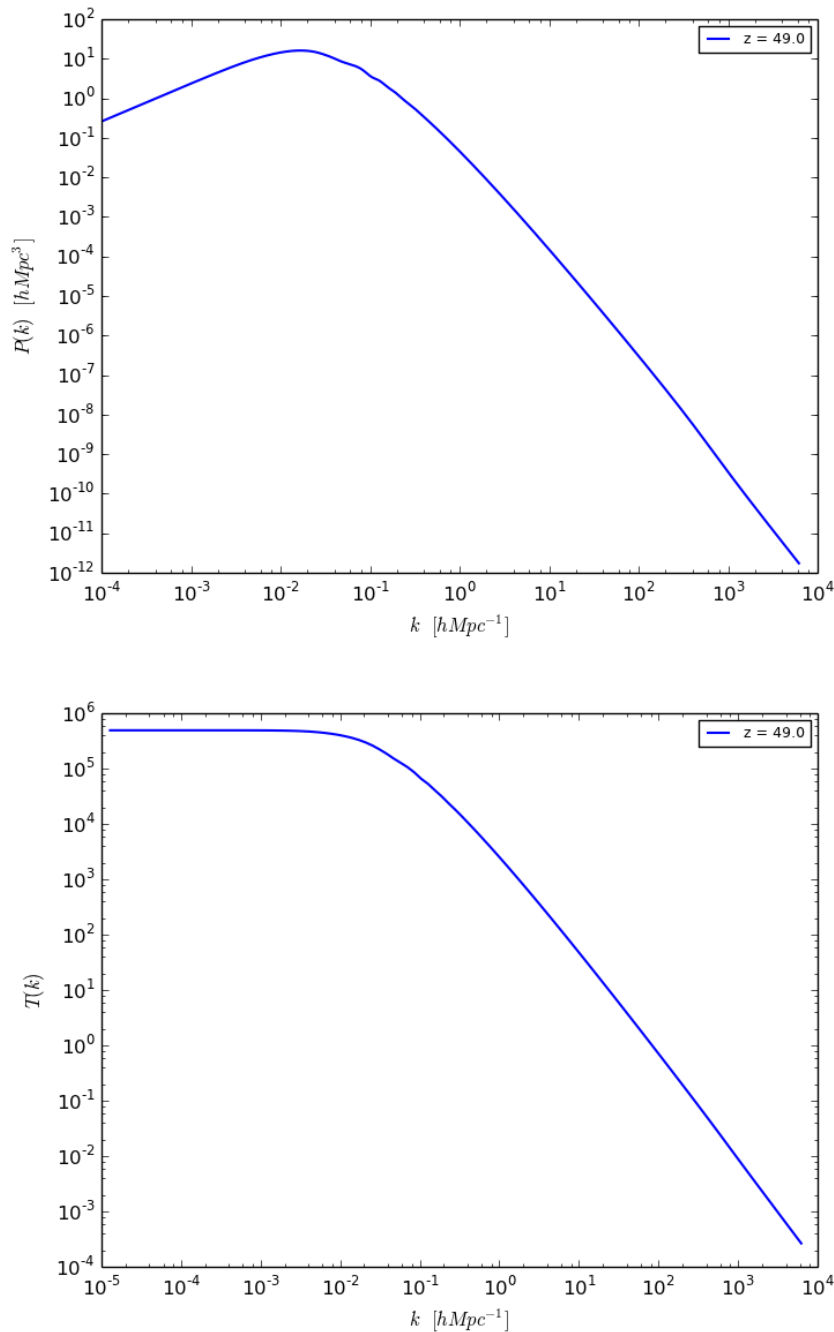


FIGURE 4.1: Initial matter power spectrum and transfer function at redshift $z = 49.0$ calculated using CAMB.

4.1.3 CosmoSuite: A toolkit for running and analysing cosmological N-body simulations

For the simulations done in this thesis, a Python package with Graphical User Interface (GUI) has been developed for the purpose of creating the initial conditions, running the simulations and doing the post-analysis including snapshots visualization and data

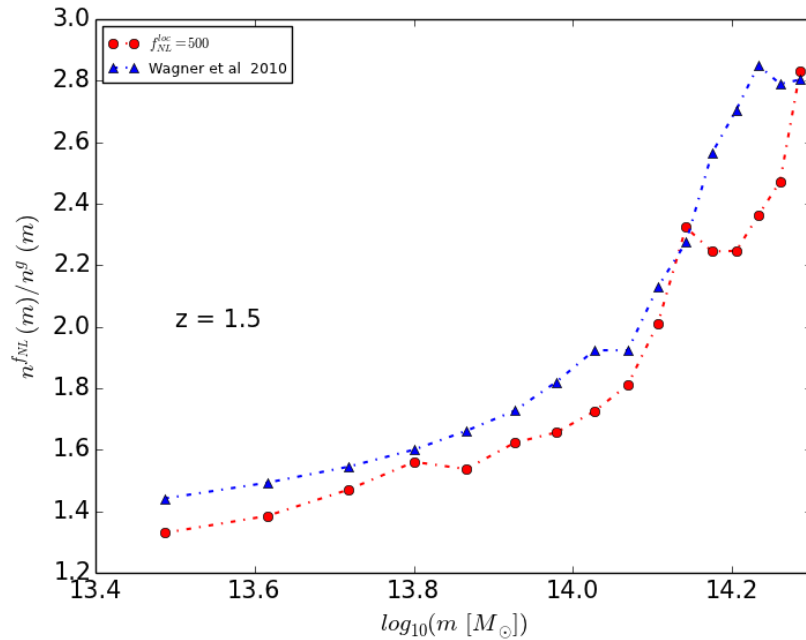


FIGURE 4.2: Halo mass function ratio for $f_{NL}^{loc} = 500$ at redshift $z = 1.5$ compared with Wagner et al results [87].

plotting, halo mass function and non-linear power spectrum calculations. Fig. 4.3 shows the GUI for CosmoSuite code. The code is publicly available on the following address, <https://github.com/mwhashim/CosmoSuite>.

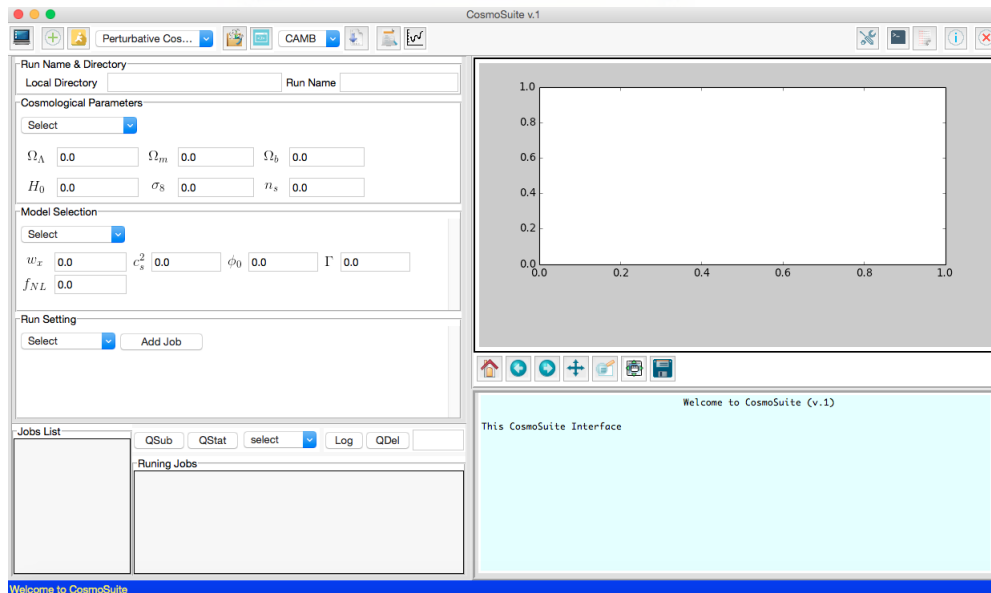


FIGURE 4.3: CosmoSuite Graphical User Interface.

The GUI is user friendly and allows for entering all the simulation settings without any file editing. The code runs over three stages. The first stage is code compilation; in which editing to makefile options of the various codes supported by the GUI is simply done

by multi-choice buttons. Then after choosing the running platform from the settings, selected code could be compiled by a simple click. The GUI is supported with different compiler settings for different platforms.

The second stage of the GUI run is the simulation parameter entering. All parameter files for the various supported codes are implemented in the GUI. Common parameter fields are filed simultaneously. The GUI support different model and cosmological parameters. Then, by adding tasks to the task menu, you can run or submit your simulation job to the running cluster.

The final stage includes the post-analysis of the simulations output. Many different analysing functions are supported, including the calculations of the non-linear power spectrum and the halo mass function. Snapshot projection plotting is also implemented. The code is supported with remote connection for parallel computation.

4.2 Results

We study the effect of primordial non-Gaussianity via a set of dark matter only N-body simulations for different values of non-Gaussianity parameter $f_{\text{NL}}^{\text{loc}} = 0, \pm 250, \pm 500, \pm 1000$. We plot the output snapshots at four different redshifts $z = 0.0, 0.55, 1.0, 2.01$. In Figs. 4.4, 4.5, 4.6, 4.7, we plot time evolution of particle distribution in a box with size 250^3 Mpc^3 and projection depth on the z -axis 7 Mpc at different redshifts. The particle distribution changes between Gaussian and non-Gaussian cases. Also structure formation differs with the inclusion of non-Gaussianity.

Figs. 4.8, 4.9, 4.10, 4.11 represent the four different realizations of non-Gaussianity for positive and negative values at different redshifts. The particle projection plots show that the structure formation at higher redshifts are sensitive to the non-Gaussianity parameter than at low redshifts. The statistical properties of structure formation at higher redshifts is a very good probe of non-Gaussianity parameter. Also higher mass objects distribution differs with different non-Gaussianity parameters.

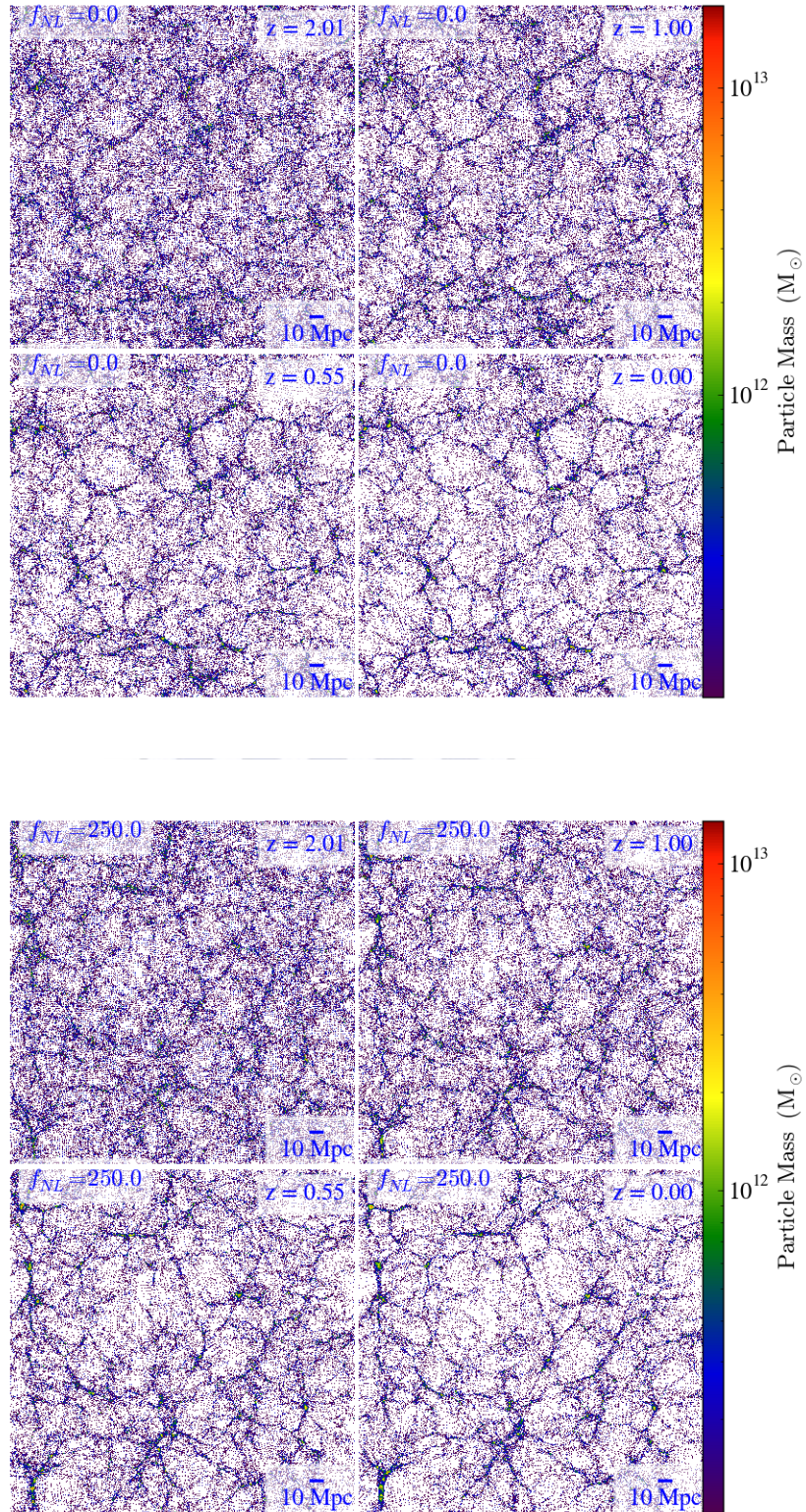


FIGURE 4.4: Particle projection plot of GADGET-2 output snapshots of redshift series $z = 2.01, 1.0, 0.55, 0.0$ for different values of non-Gaussianity $f_{\text{NL}}^{\text{loc}} = 0.0, 250.0$ from upper-left to lower-right respectively. The projection depth is 7.0 Mpc and the plot is weighted with dark matter halo mass.

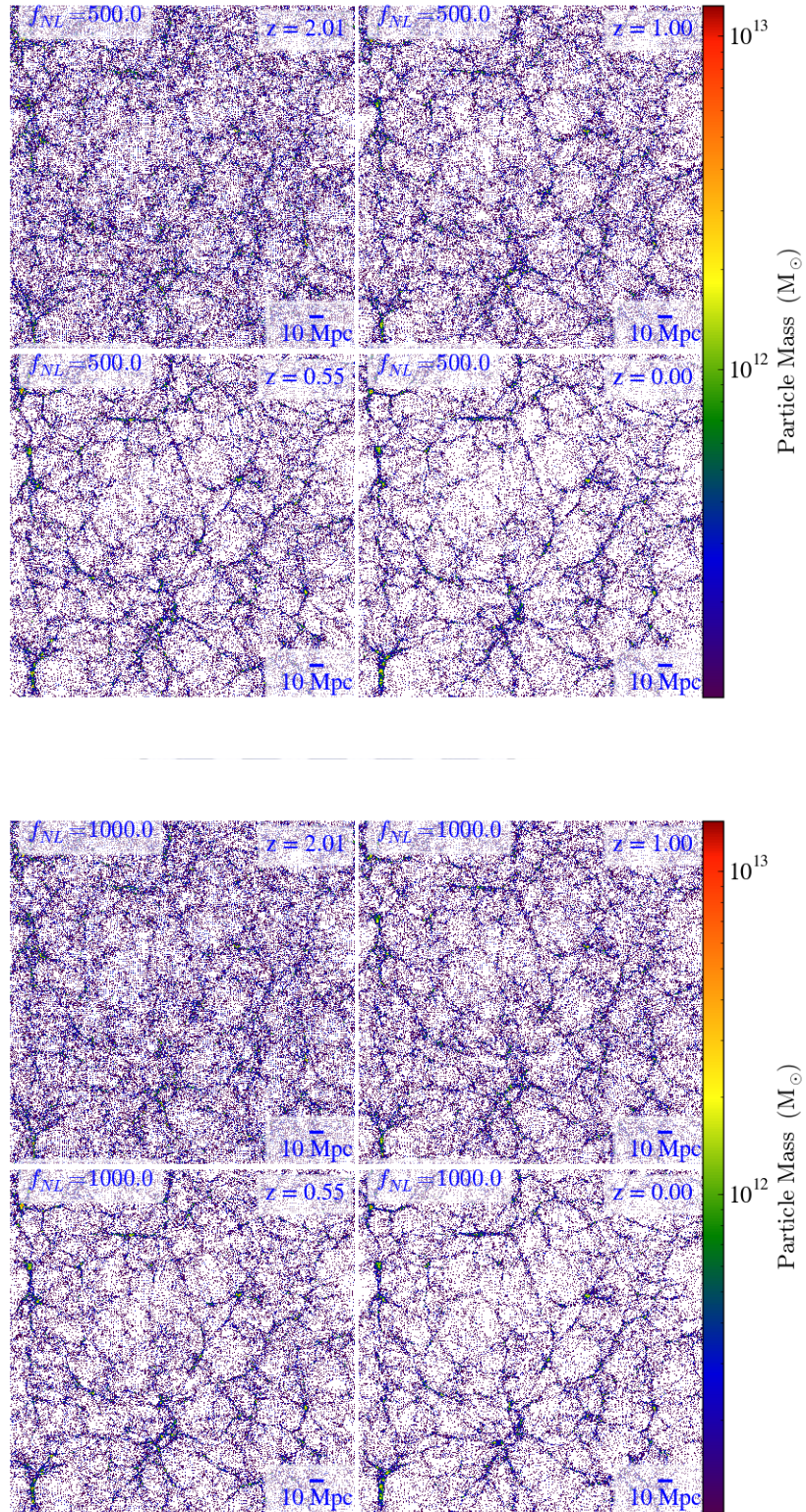


FIGURE 4.5: Particle projection plot of GADGET-2 output snapshots of redshift series $z = 2.01, 1.0, 0.55, 0.0$ for different values of non-Gaussianity $f_{\text{NL}}^{\text{loc}} = 500.0, 1000.0$ from upper-left to lower-right respectively. The projection depth is 7.0 Mpc and the plot is weighted with dark matter halo mass.

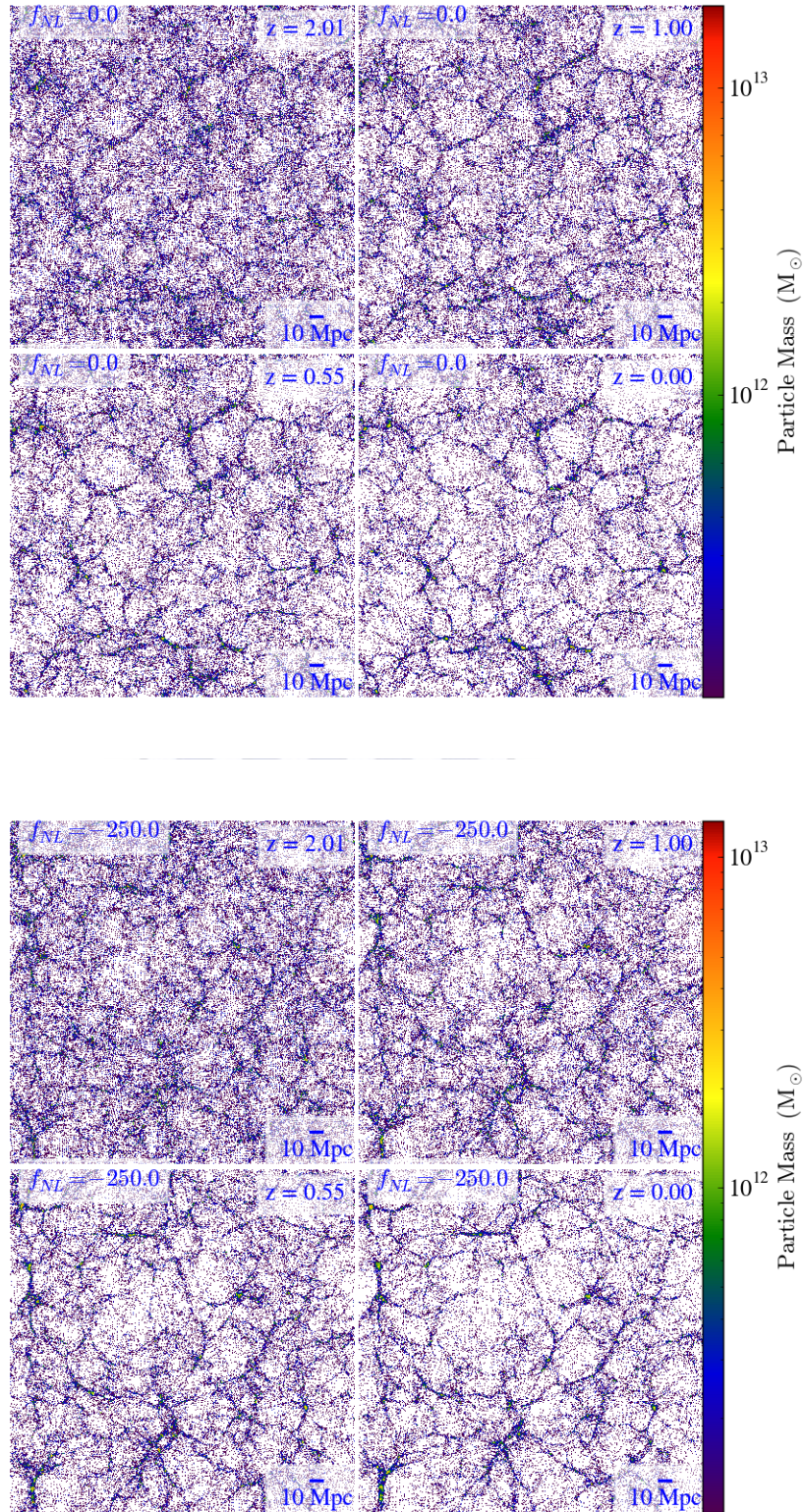


FIGURE 4.6: Particle projection plot of GADGET-2 output snapshots of redshift series $z = 2.01, 1.0, 0.55, 0.0$ for different values of non-Gaussianity $f_{NL}^{loc} = 0.0, -250.0$ from upper-left to lower-right respectively. The projection depth is 7.0 Mpc and the plot is weighted with dark matter halo mass.

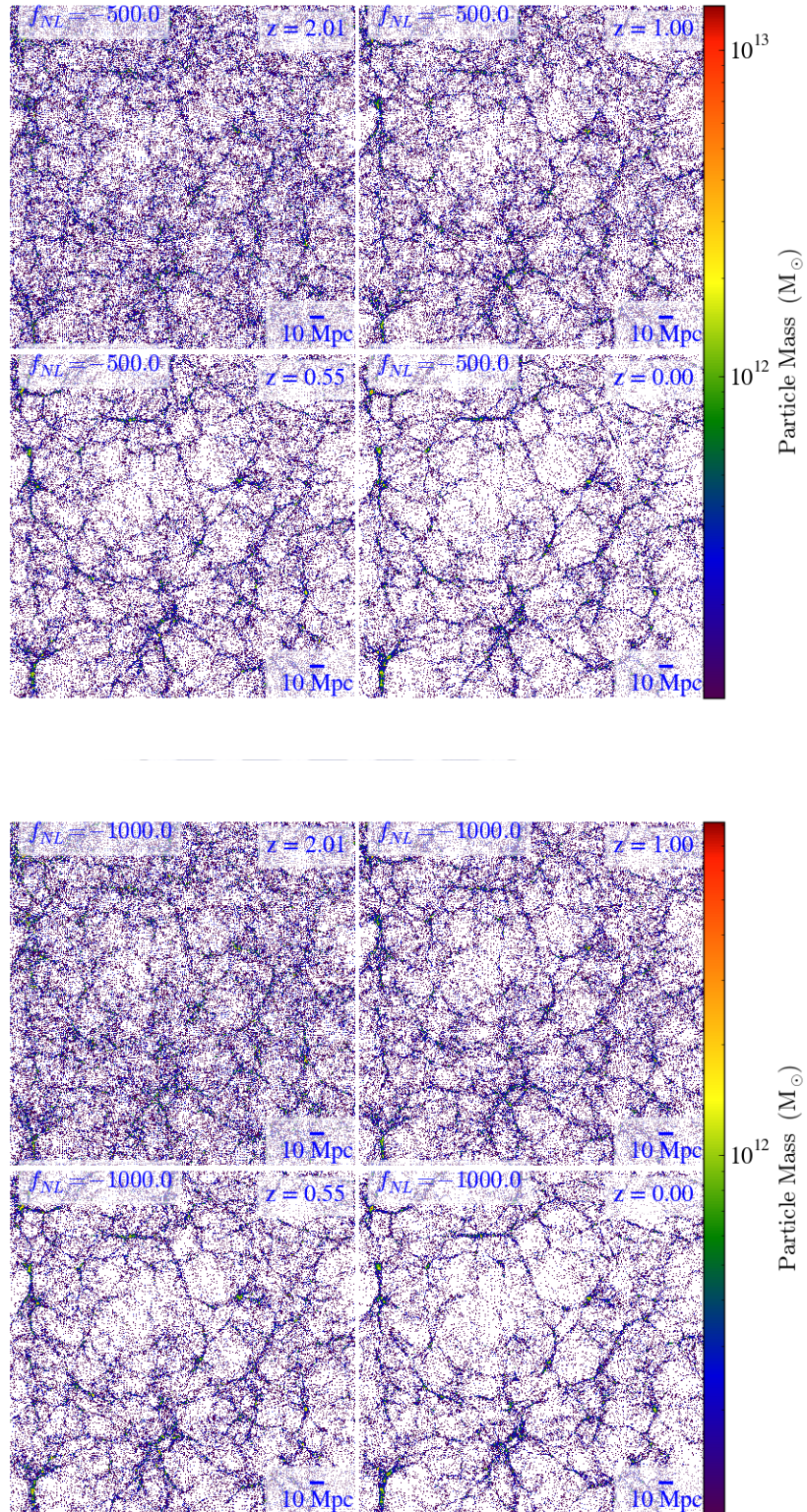


FIGURE 4.7: Particle projection plot of GADGET-2 output snapshots of redshift series $z = 2.01, 1.0, 0.55, 0.0$ for different values of non-Gaussianity $f_{\text{NL}}^{\text{loc}} = -500.0, -1000.0$ from upper-left to lower-right respectively. The projection depth is 7.0 Mpc and the plot is weighted with dark matter halo mass.

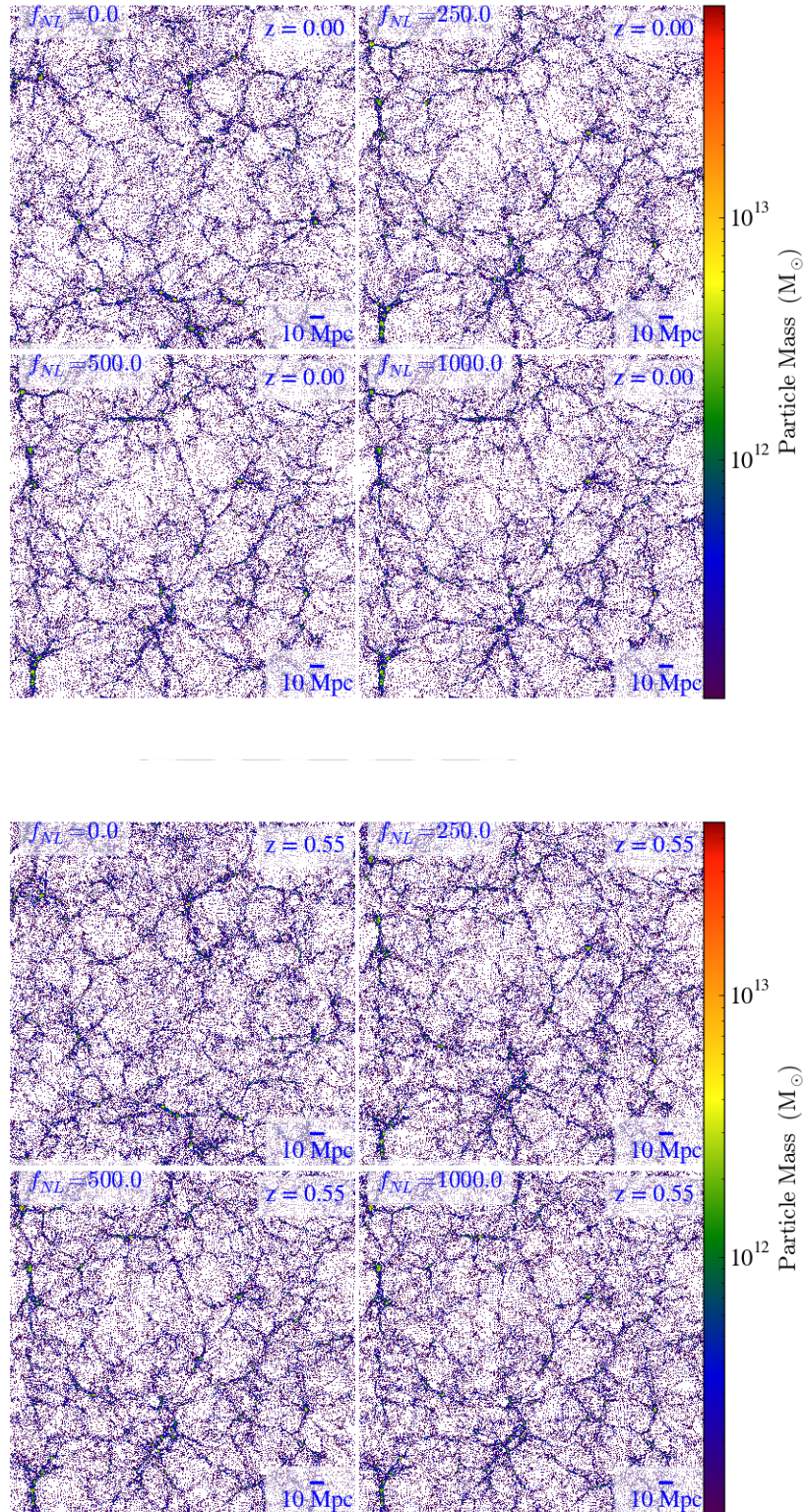


FIGURE 4.8: Particle projection plot of GADGET-2 output snapshots of different values of non-Gaussianity $f_{NL} = 0.0, 250.0, 500.0, 1000.0$ for redshift series $z = 0.0, 0.55$ from upper-left to lower-right respectively. The projection depth is 7.0 Mpc and the plot is weighted with dark matter halo mass.

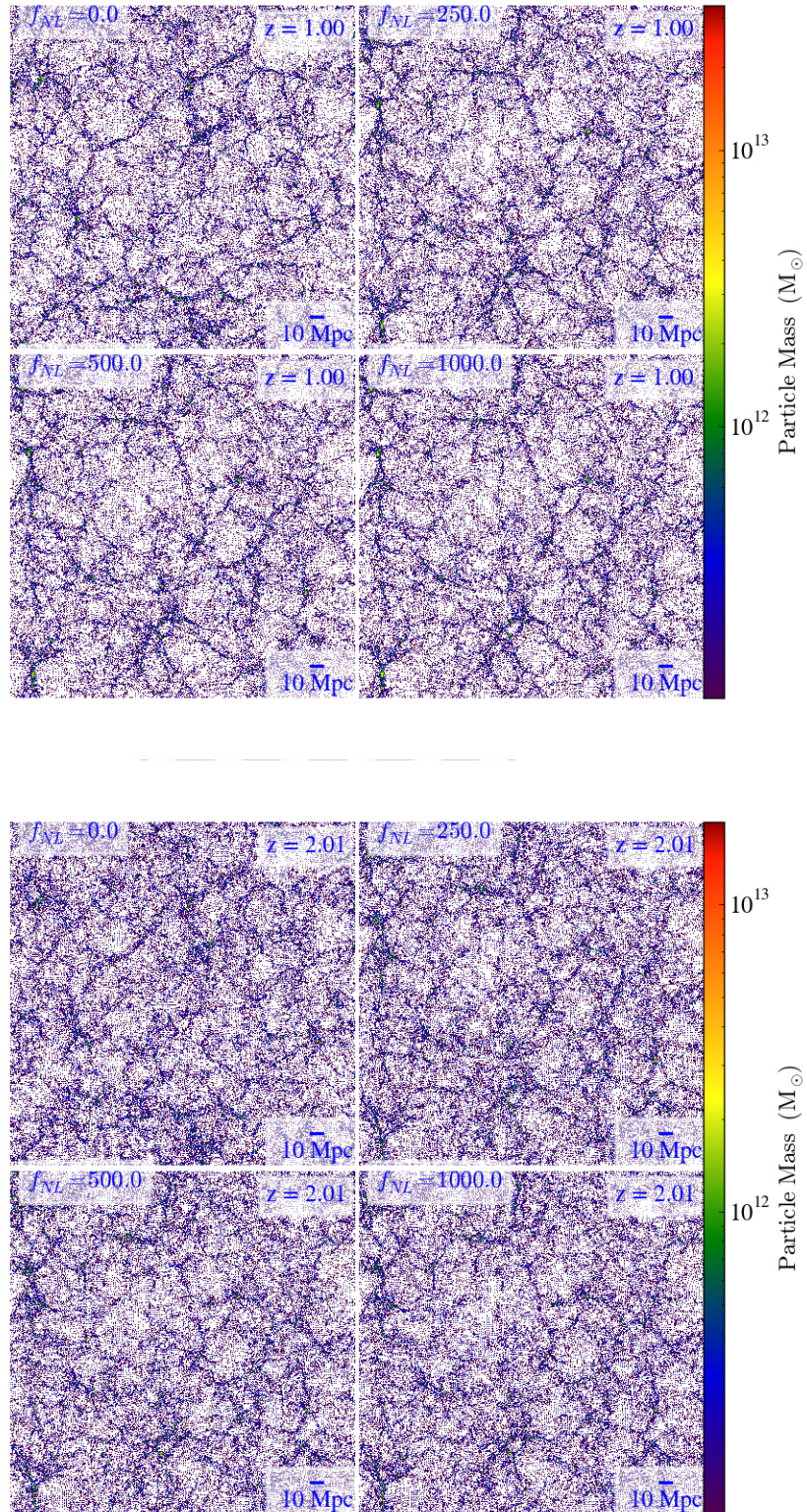


FIGURE 4.9: Particle projection plot of GADGET-2 output snapshots of different values of non-Gaussianity $f_{NL} = 0.0, 250.0, 500.0, 1000.0$ for redshift series $z = 1.0, 2.01$ from upper-left to lower-right respectively. The projection depth is 7.0 Mpc and the plot is weighted with dark matter halo mass.

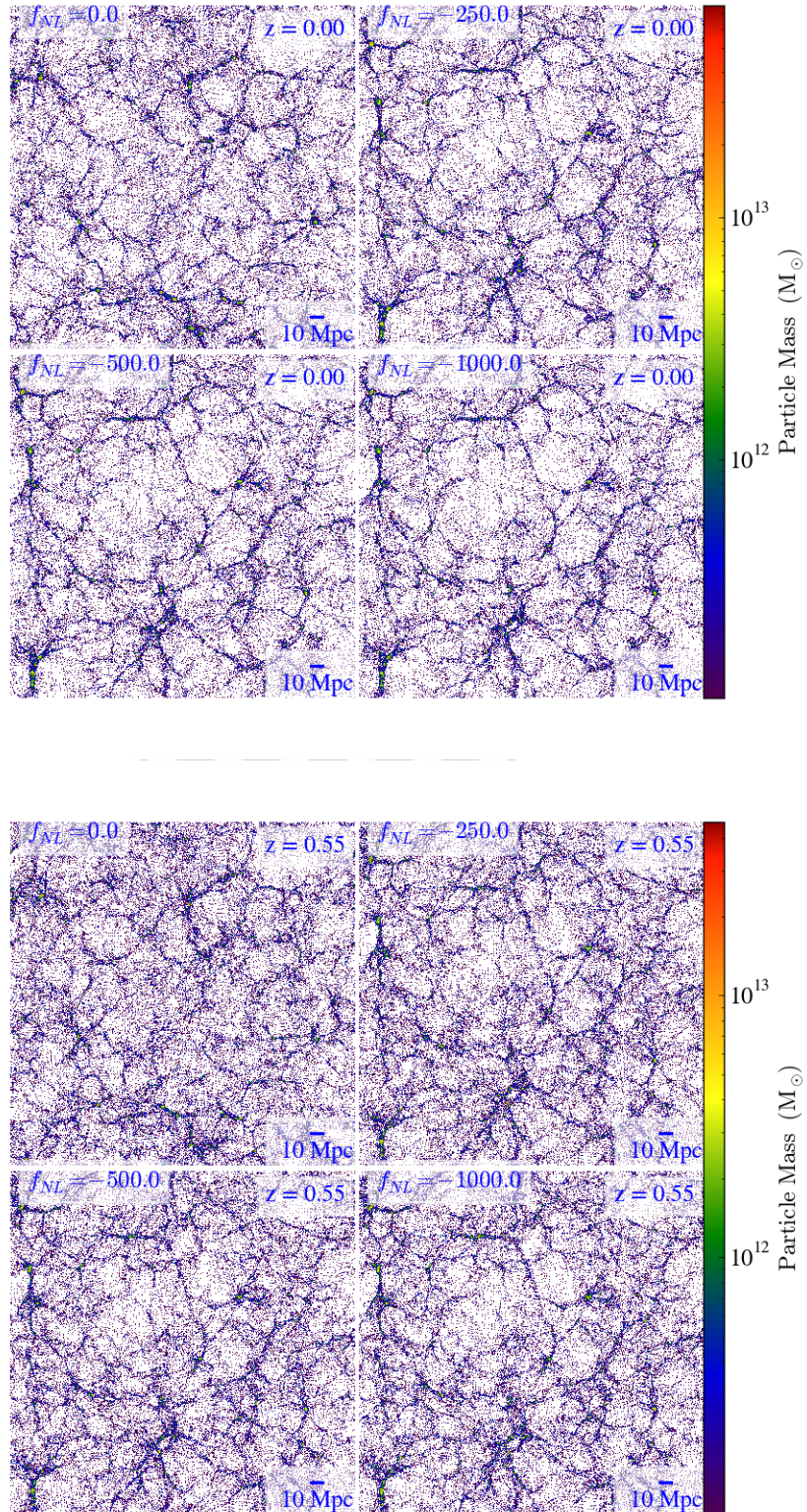


FIGURE 4.10: Particle projection plot of GADGET-2 output snapshots of different values of non-Gaussianity $f_{\text{NL}}^{\text{loc}} = 0.0, -250.0, -500.0, -1000.0$ for redshift series $z = 0.0, 0.55$ from upper-left to lower-right respectively. The projection depth is 7.0 Mpc and the plot is weighted with dark matter halo mass.

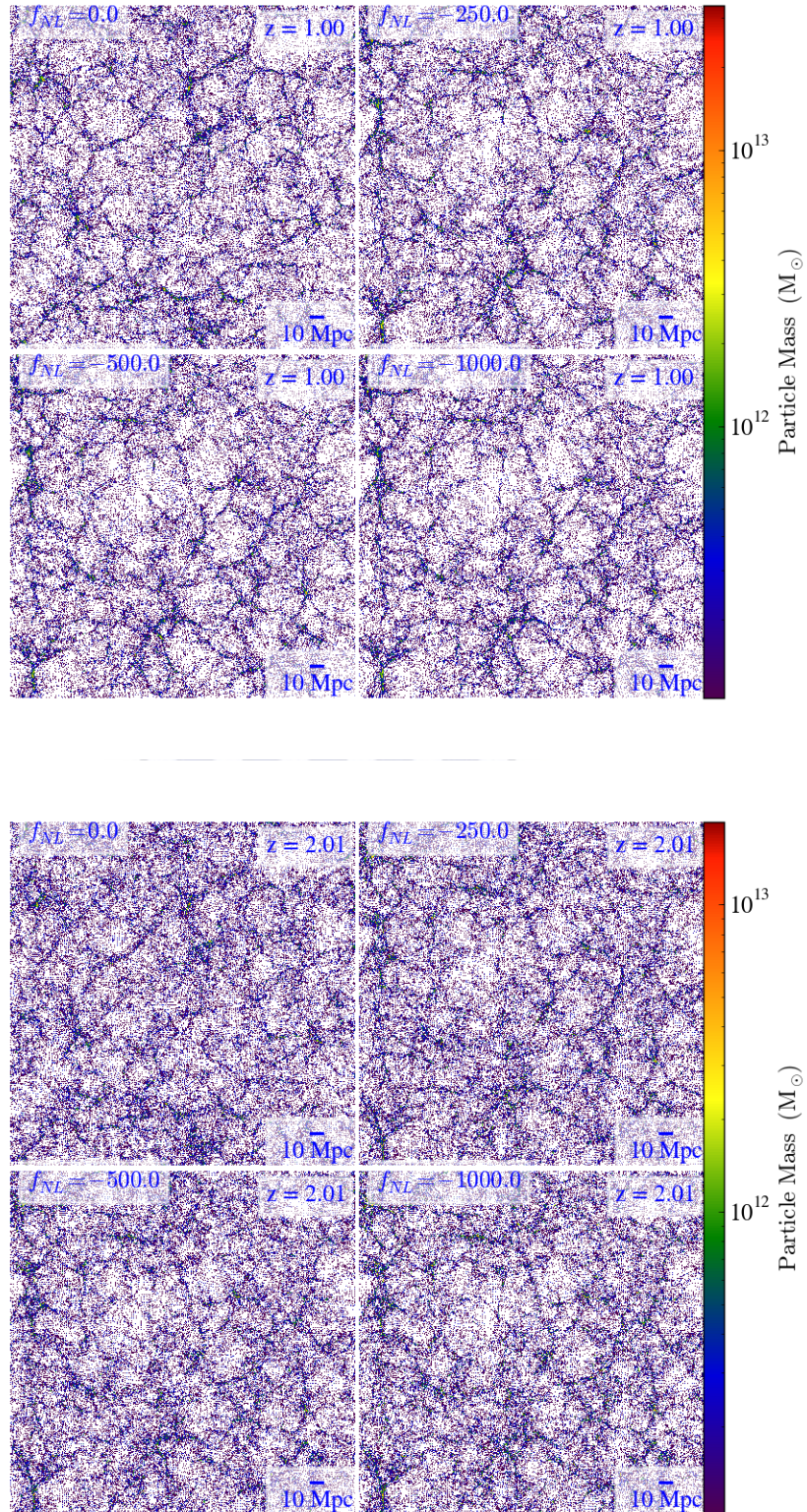


FIGURE 4.11: Particle projection plot of GADGET-2 output snapshots of different values of non-Gaussianity $f_{\text{NL}}^{\text{loc}} = 0.0, -250.0, -500.0, -1000.0$ for redshift series $z = 1.0, 2.01$ from upper-left to lower-right respectively. The projection depth is 7.0 Mpc and the plot is weighted with dark matter halo mass.

4.2.1 Halo mass function

Large gravitationally bound objects are supposed to be sensitive to the value of primordial non-Gaussianity parameter. In this section we study the effect of non-Gaussian initial conditions on the halo mass function. In order to identify halos in the simulation data we use AHF [38, 50], the publicly available Amiga's Halo Finder. AHF identifies halos as gravitationally bound objects with spherical overdensity. Redshift dependent virial overdensity is used to calculate the specific overdensity for a bounded object. We assume the minimal number of particles inside a halo to be 20 particles. The halo masses for the set of simulations are larger than $10^{13} M_{\odot}/h$.

The high mass tail of the halo mass function is very sensitive to primordial non-Gaussianity. Galaxy cluster surveys are very good probe of the primordial non-Gaussianity parameter.

In Figs. 4.12, 4.13, 4.14, 4.15, 4.16, 4.17, 4.18, 4.19, we present the cumulative halo mass function for different values of f_{NL} at four different redshifts. The bottom panel in each plot shows the residual with respect to the Gaussian case. The black solid line represents Reed analytical fit [70]. At redshift $z = 0.0$, the large mass tail of the halo mass function with masses $> 10^{13.5} M_{\odot}$ increase with increasing positive $f_{\text{NL}}^{\text{loc}}$ and decrease with decreasing negative $f_{\text{NL}}^{\text{loc}}$. At very large masses, the halo mass function diffuse due to stochastic effects originate from medium resolution masses. For higher resolution simulations, the systematic errors decrease with higher mass resolutions.

At higher redshifts, the change in the mass function shifts towards lower mass halos, $< 10^{13} M_{\odot}$ and the change increases with a factor of 20% for large mass halos. Future galaxy surveys at higher redshifts will be a sensitive probe to the early universe physics.

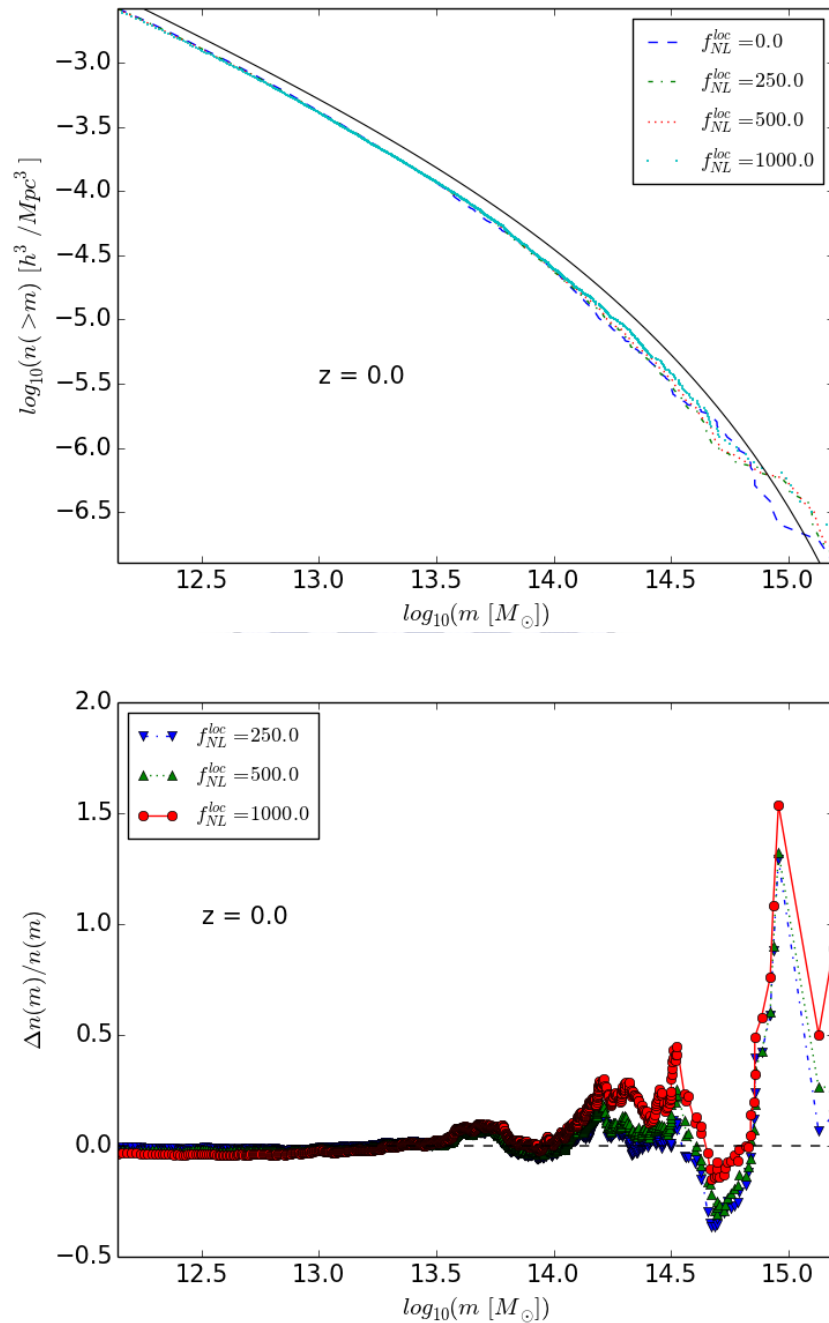


FIGURE 4.12: *Upper:* Cumulative halo mass function for different non-Gaussianity parameter $f_{NL}^{loc} = 0.0, 250.0, 500.0, 1000.0$ at redshift $z = 0.0$. Black solid line represents Reed 2007 analytical fit. *Lower:* Cumulative halo mass function residual with respect to Gaussian Λ CDM model at redshift $z = 0.0$.

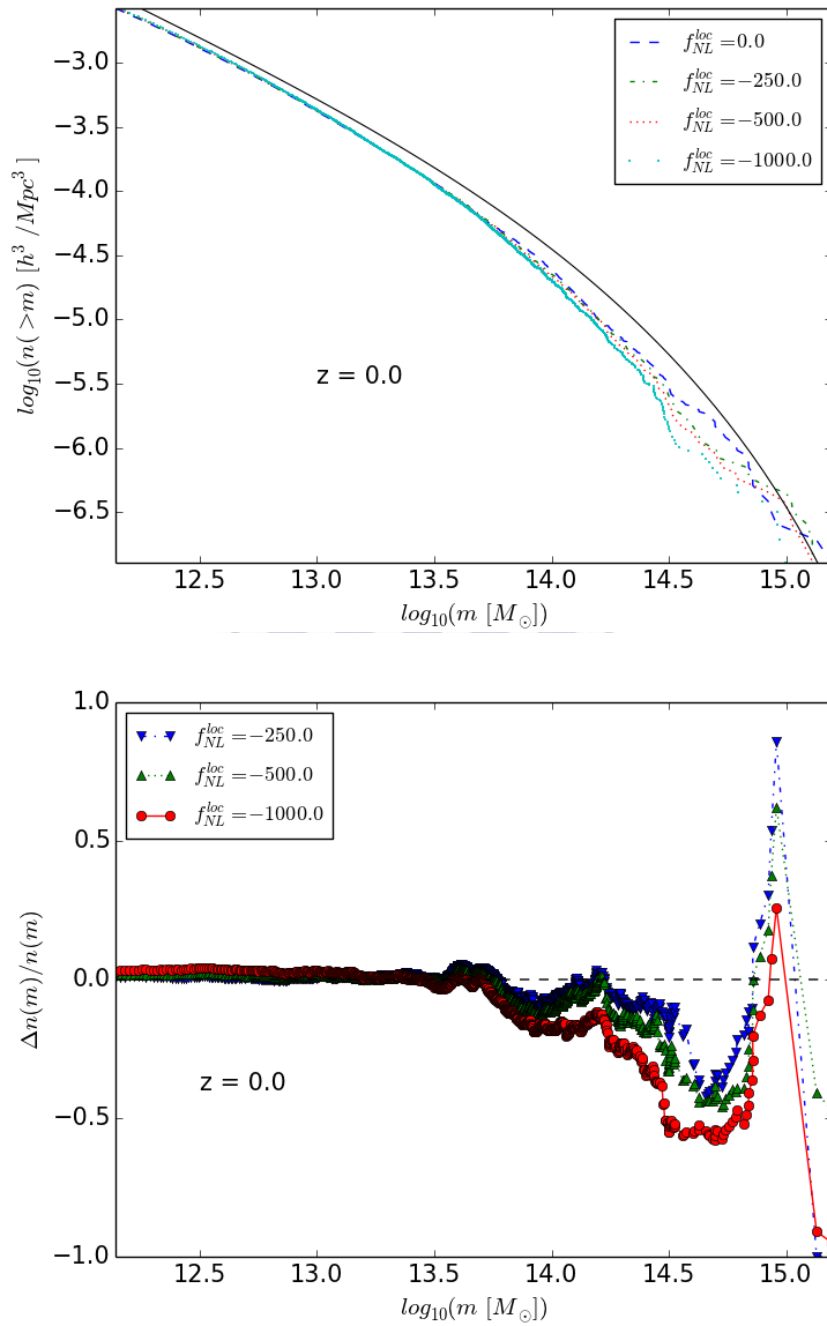


FIGURE 4.13: *Upper*: Cumulative halo mass function for different non-Gaussianity parameter $f_{NL}^{loc} = 0.0, -250.0, -500.0, -1000.0$ at redshift $z = 0.0$. Black solid line represents Reed 2007 analytical fit. *Lower*: Cumulative halo mass function residual with respect to Gaussian Λ CDM model at redshift $z = 0.0$.

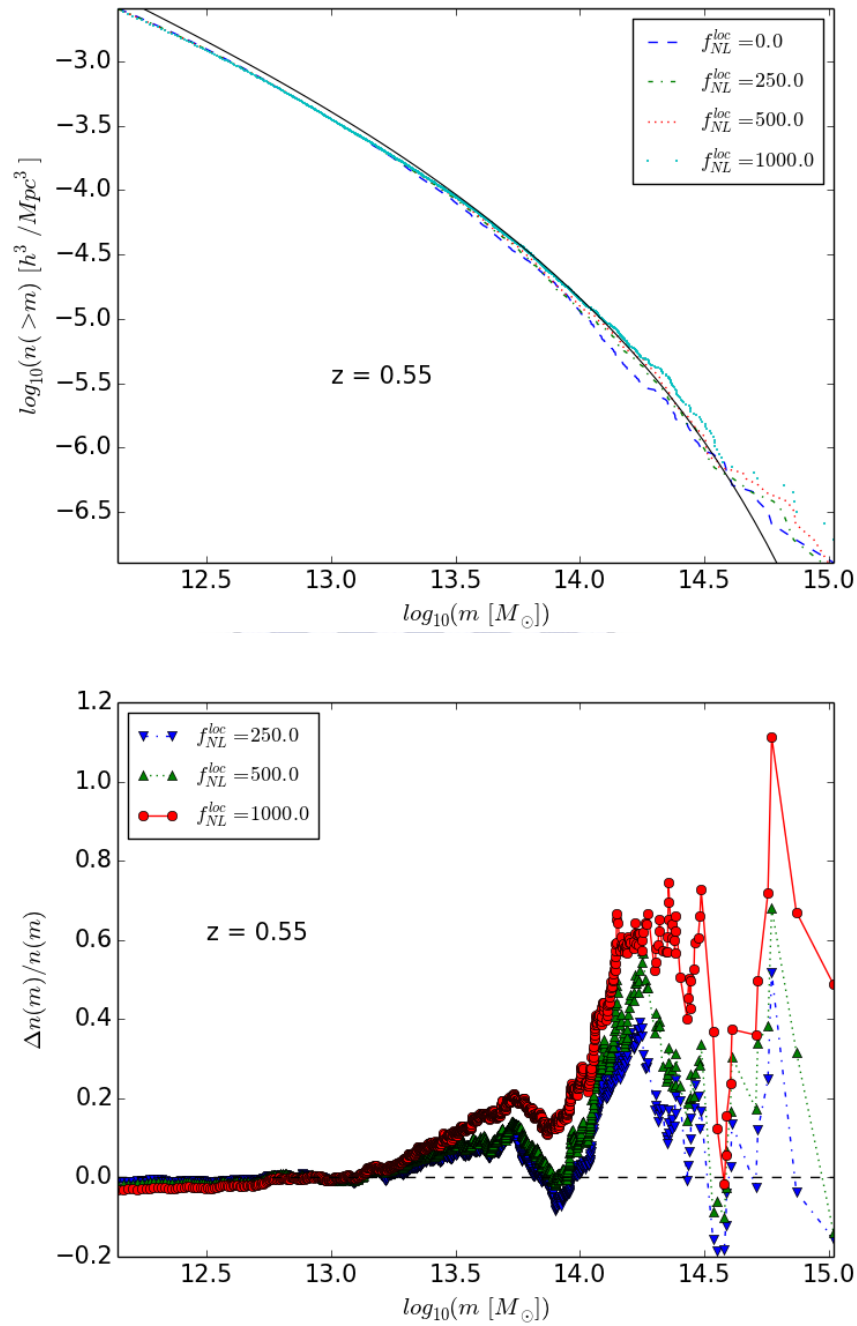


FIGURE 4.14: *Upper*: Cumulative halo mass function for different non-Gaussianity parameter $f_{NL}^{loc} = 0.0, 250.0, 500.0, 1000.0$ at redshift $z = 0.55$. Black solid line represents Reed 2007 analytical fit. *Lower*: Cumulative halo mass function residual with respect to Gaussian Λ CDM model at redshift $z = 0.55$.

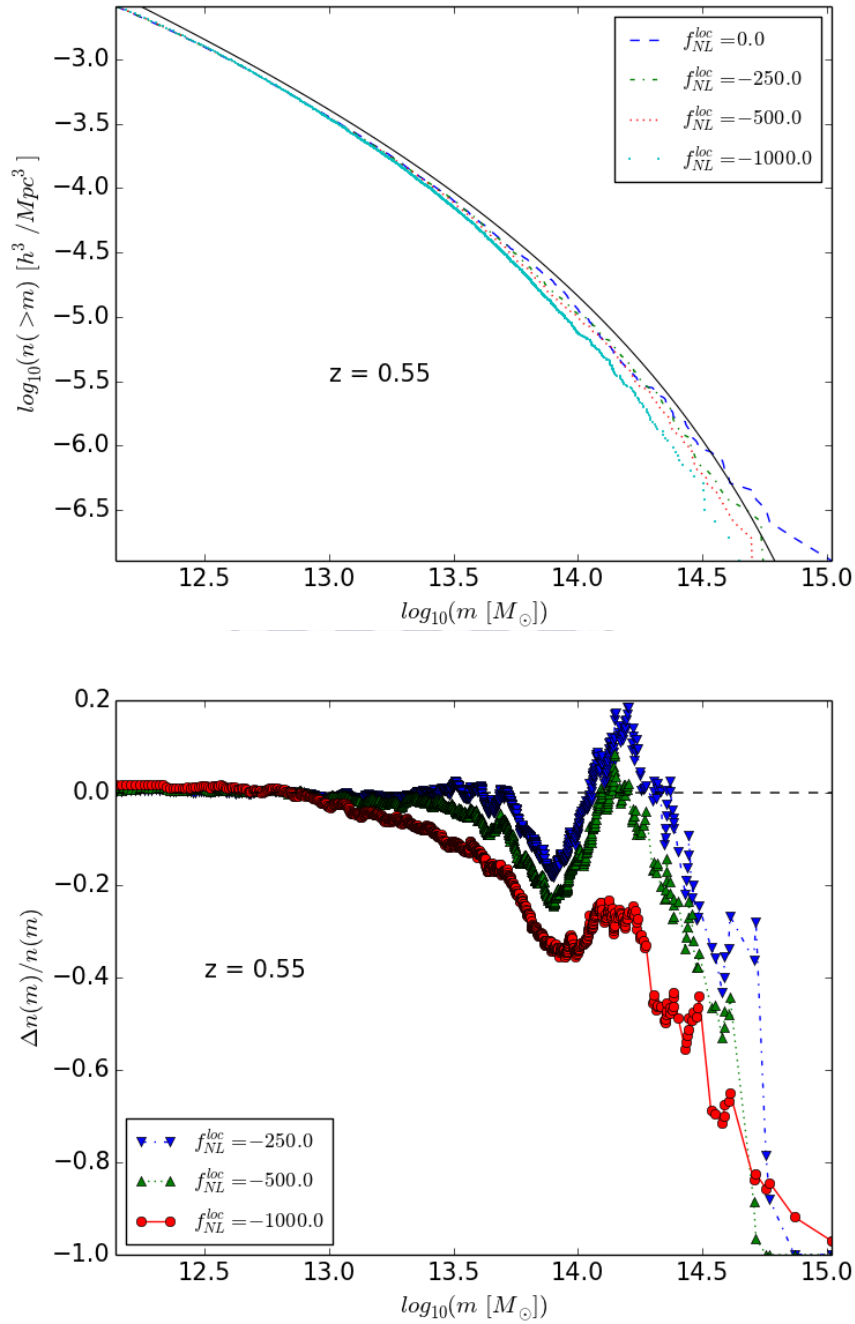


FIGURE 4.15: *Upper:* Cumulative halo mass function for different non-Gaussianity parameter $f_{NL}^{loc} = 0.0, -250.0, -500.0, -1000.0$ at redshift $z = 0.55$. Black solid line represents Reed 2007 analytical fit. *Lower:* Cumulative halo mass function residual with respect to Gaussian Λ CDM model at redshift $z = 0.55$.

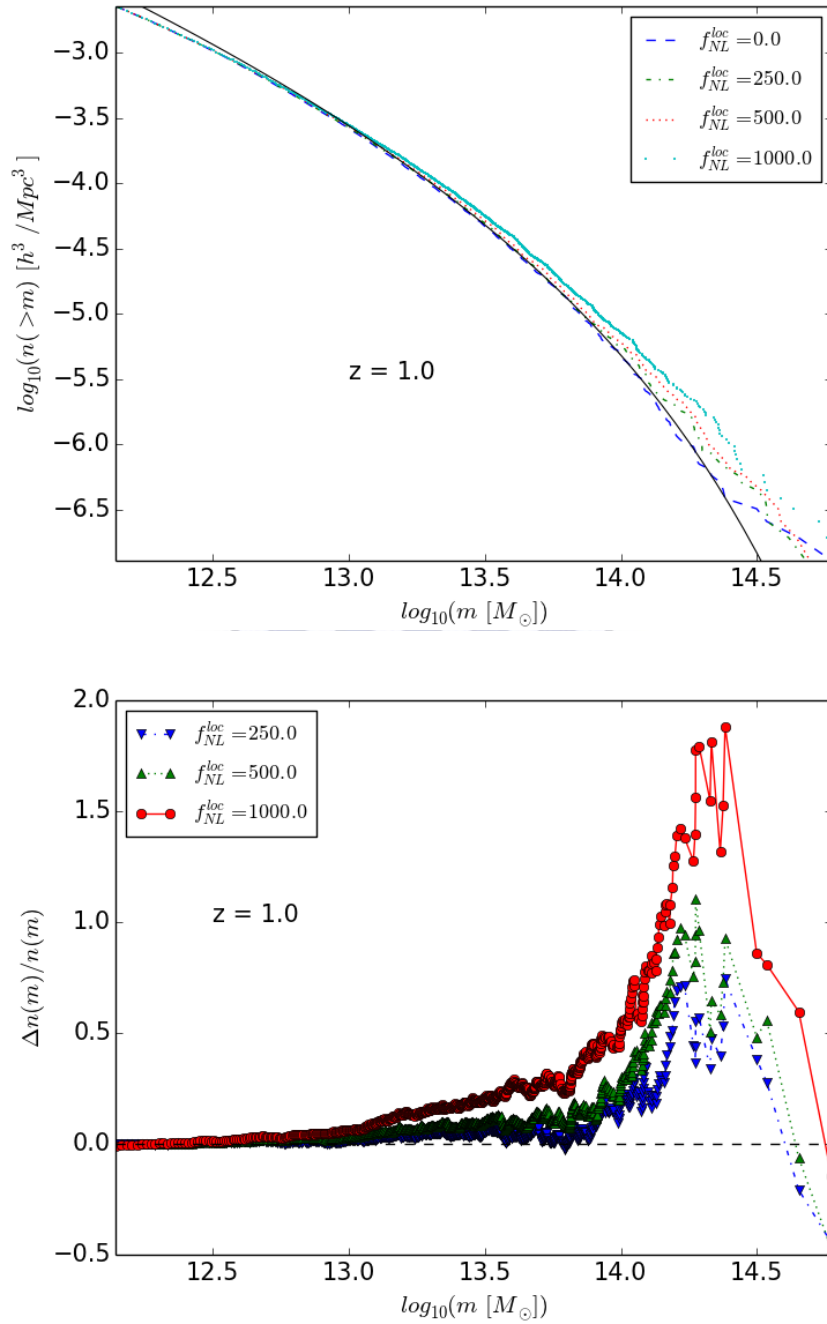


FIGURE 4.16: *Upper:* Cumulative halo mass function for different non-Gaussianity parameter $f_{NL}^{loc} = 0.0, 250.0, 500.0, 1000.0$ at redshift $z = 1.0$. Black solid line represents Reed 2007 analytical fit. *Lower:* Cumulative halo mass function residual with respect to Gaussian Λ CDM model at redshift $z = 1.0$.

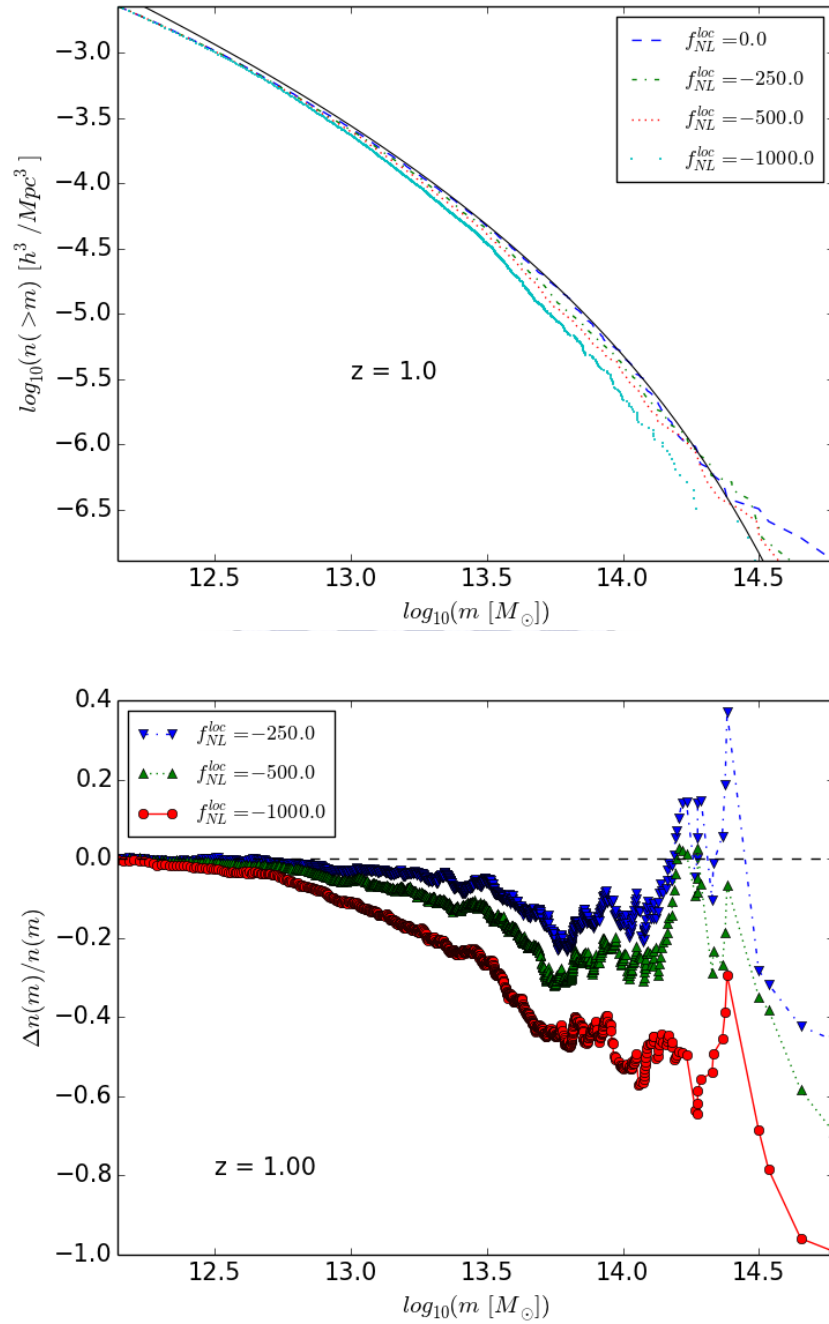


FIGURE 4.17: *Upper:* Cumulative halo mass function for different non-Gaussianity parameter $f_{NL}^{loc} = 0.0, -250.0, -500.0, -1000.0$ at redshift $z = 1.0$. Black solid line represents Reed 2007 analytical fit. *Lower:* Cumulative halo mass function residual with respect to Gaussian Λ CDM model at redshift $z = 1.0$.

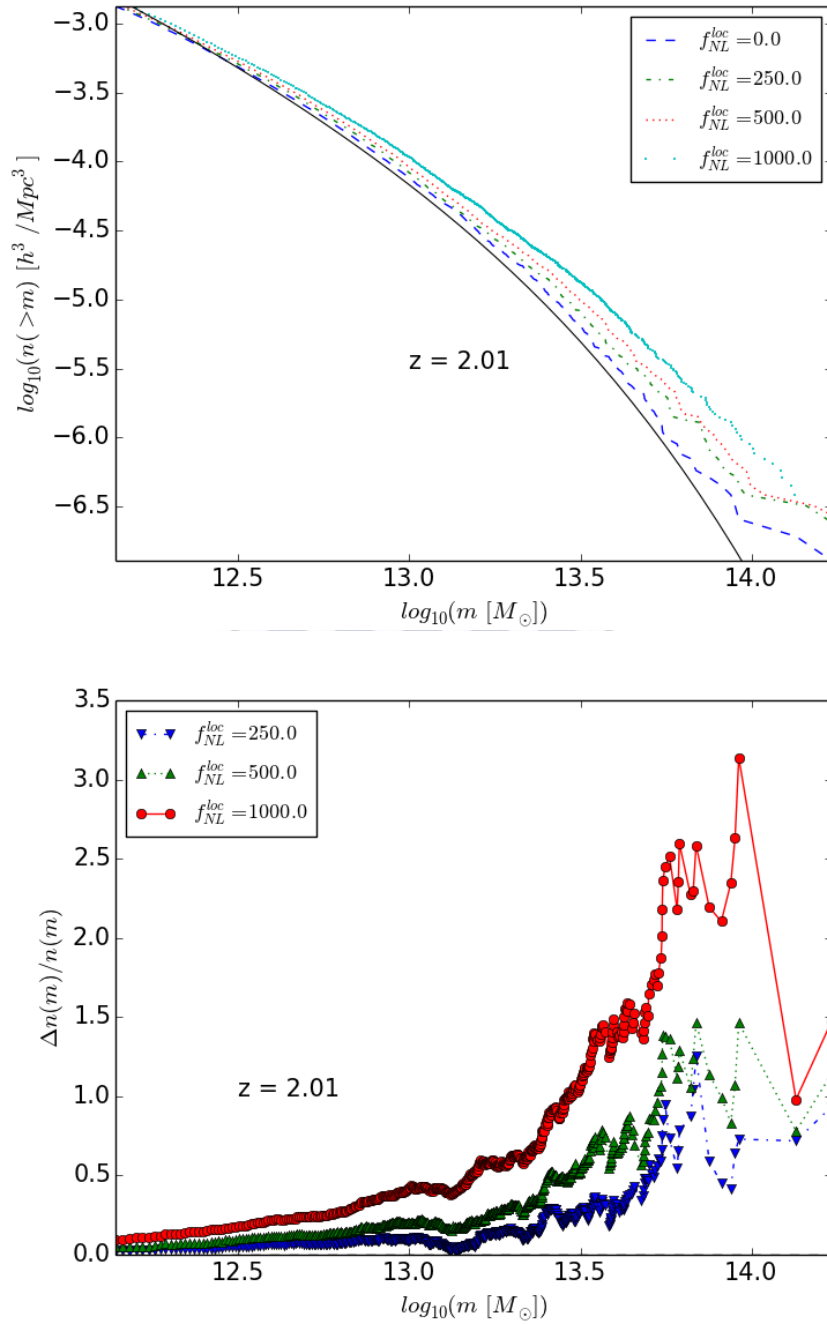


FIGURE 4.18: *Upper*: Cumulative halo mass function for different non-Gaussianity parameter $f_{NL}^{loc} = 0.0, 250.0, 500.0, 1000.0$ at redshift $z = 2.01$. Black solid line represents Reed 2007 analytical fit. *Lower*: Cumulative halo mass function residual with respect to Gaussian Λ CDM model at redshift $z = 2.01$.

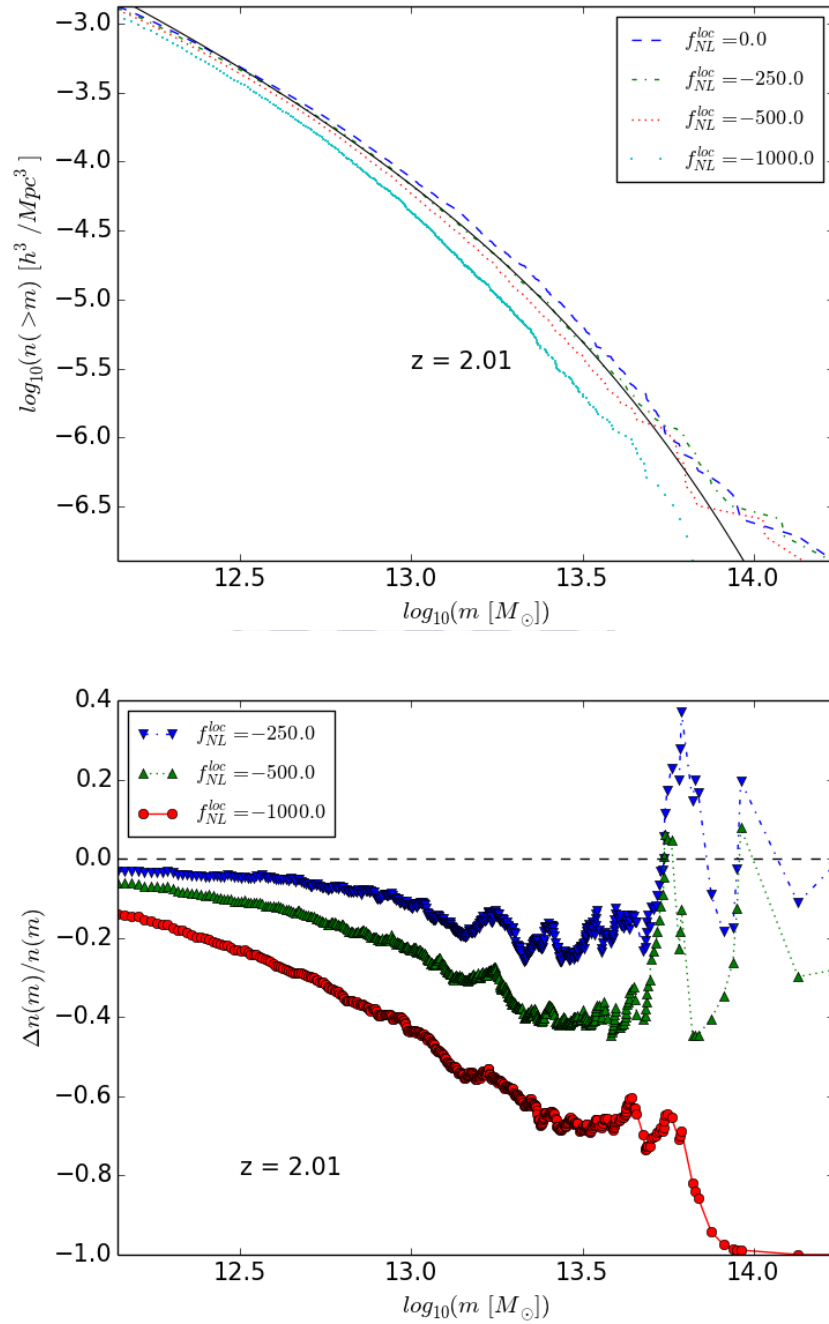


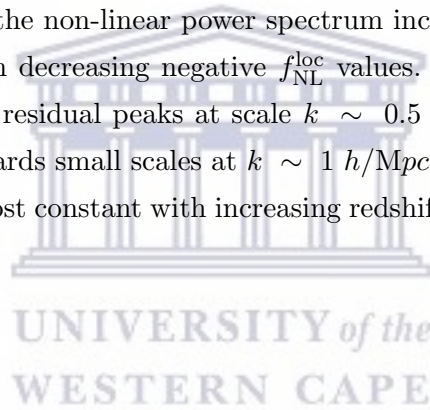
FIGURE 4.19: *Upper*: Cumulative halo mass function for different non-Gaussianity parameter $f_{NL}^{loc} = 0.0, -250.0, -500.0, -1000.0$ at redshift $z = 2.01$. Black solid line represents Reed 2007 analytical fit. *Lower*: Cumulative halo mass function residual with respect to Gaussian Λ CDM model at redshift $z = 2.01$.

4.2.2 Non-linear power spectrum

Non-linear power spectrum prediction at high precision is required to estimate the unbiased results from weak-lensing and Lyman-alpha forest surveys [47]. Primordial non-Gaussianity affects the non-linear power spectrum at a few-percent level. In this section we calculate the non-linear power spectrum for the simulation runs using POWMES code [24]. This power spectrum estimator relies on a Taylor expansion of the trigonometric functions.

In Figs. 4.20, 4.21, 4.22, 4.23, 4.24, 4.25, 4.26, 4.27, we show non-linear power spectrum for different values of the non-Gaussianity parameter at different redshifts. The black solid line represents the analytical non-linear perturbation theory with HaloFit model prediction [80]. In the bottom panel, we calculate the residual with respect to the Gaussian case.

The non-linear power spectrum changes with different values of $f_{\text{NL}}^{\text{loc}}$. On scales larger than $k > 10^{-1} h/\text{Mpc}$ the non-linear power spectrum increases with increasing positive $f_{\text{NL}}^{\text{loc}}$ and decreases with decreasing negative $f_{\text{NL}}^{\text{loc}}$ values. At redshift $z = 0.0$, the non-linear power spectrum residual peaks at scale $k \sim 0.5 h/\text{Mpc}$. This peak shifts with increasing redshift towards small scales at $k \sim 1 h/\text{Mpc}$. The change in the non-linear power spectrum is almost constant with increasing redshift and it stabilize on very small scales $k > 1 h/\text{Mpc}$.



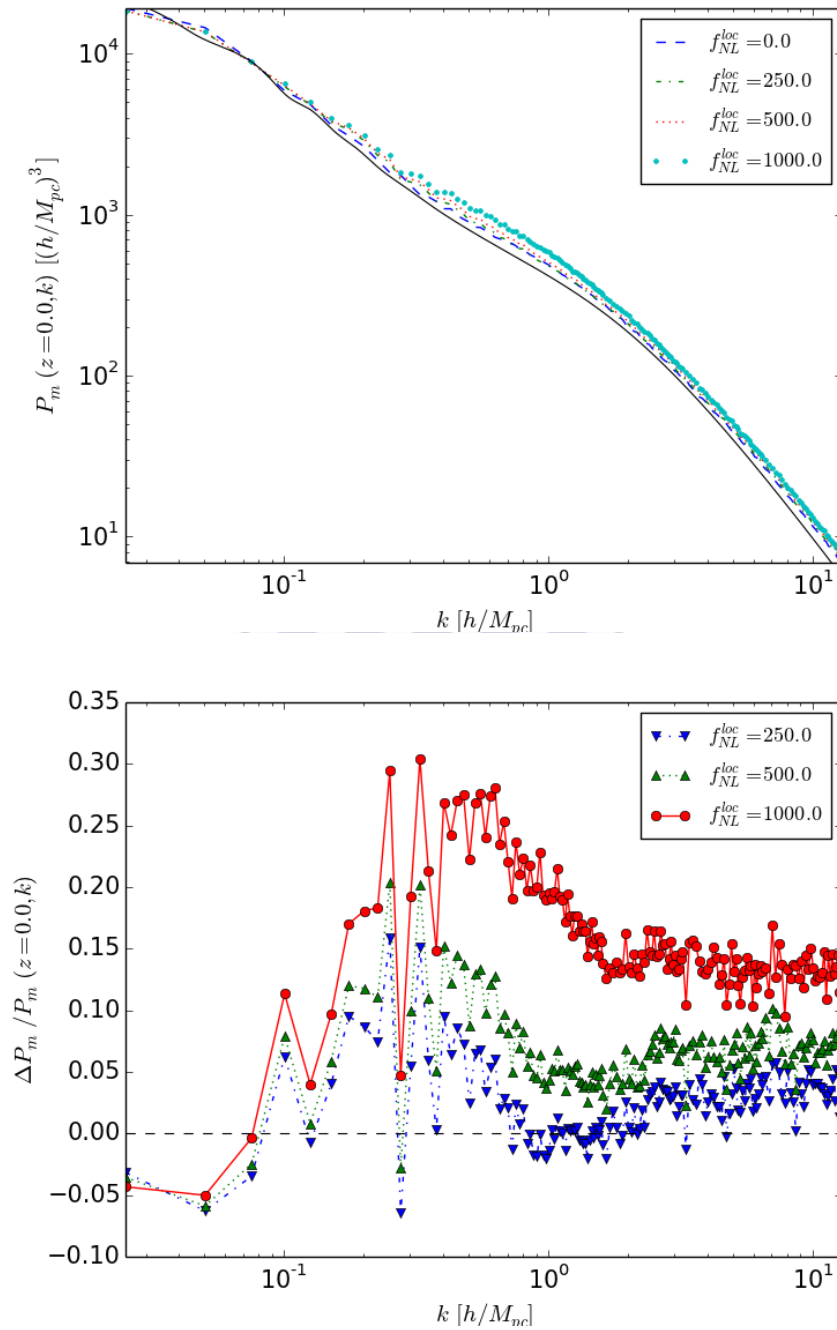


FIGURE 4.20: *Upper*: Non-linear power spectrum for different non-Gaussianity parameter $f_{NL}^{loc} = 0.0, 250.0, 500.0, 1000.0$ at redshift $z = 0.0$. Black solid line represents CAMB Halo-fit model prediction. *Lower*: Non-linear power spectrum residual with respect to Gaussian Λ CDM model at redshift $z = 0.0$.

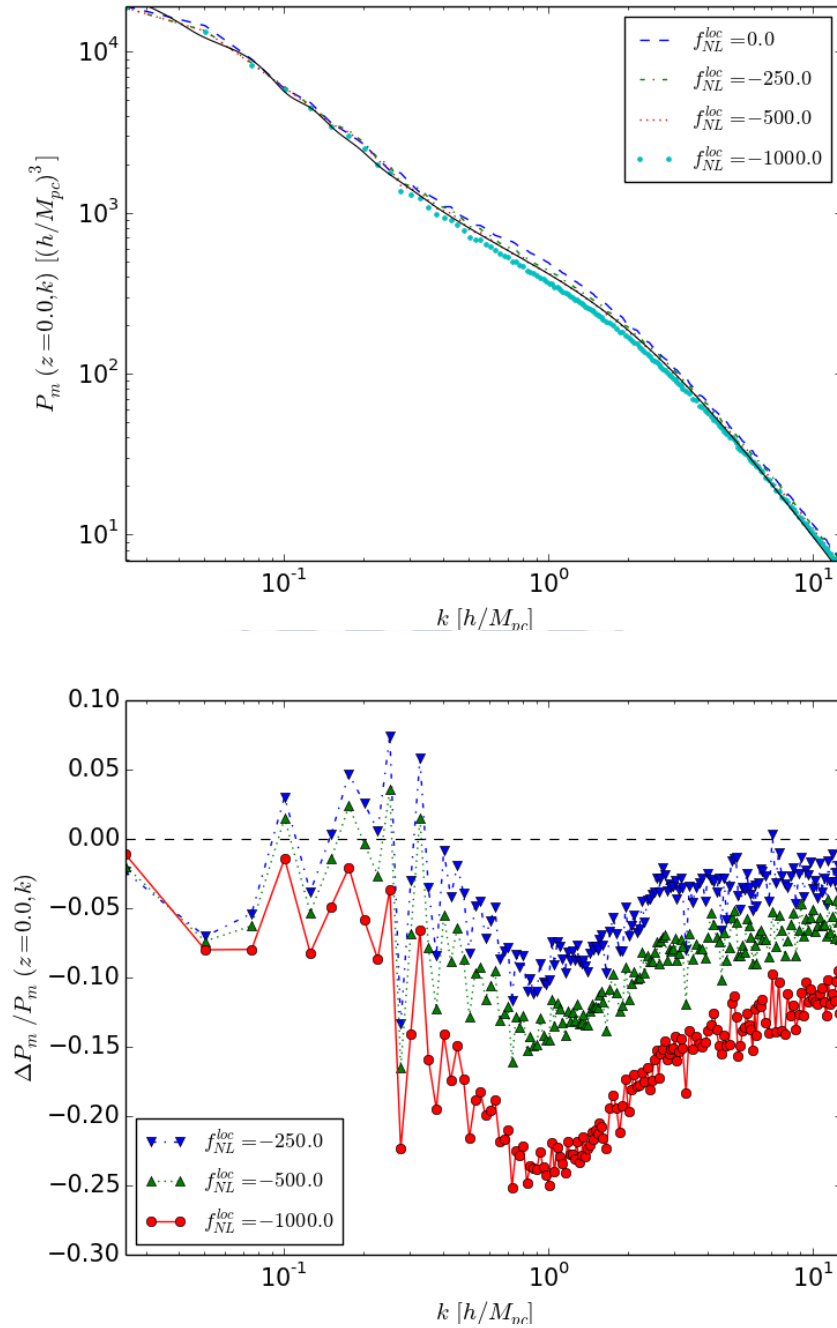


FIGURE 4.21: *Upper*: Non-linear power spectrum for different non-Gaussianity parameter $f_{NL}^{loc} = 0.0, -250.0, -500.0, -1000.0$ at redshift $z = 0.0$. Black solid line represents CAMB Halo-fit model prediction. *Lower*: Non-linear power spectrum residual with respect to Gaussian Λ CDM model at redshift $z = 0.0$.

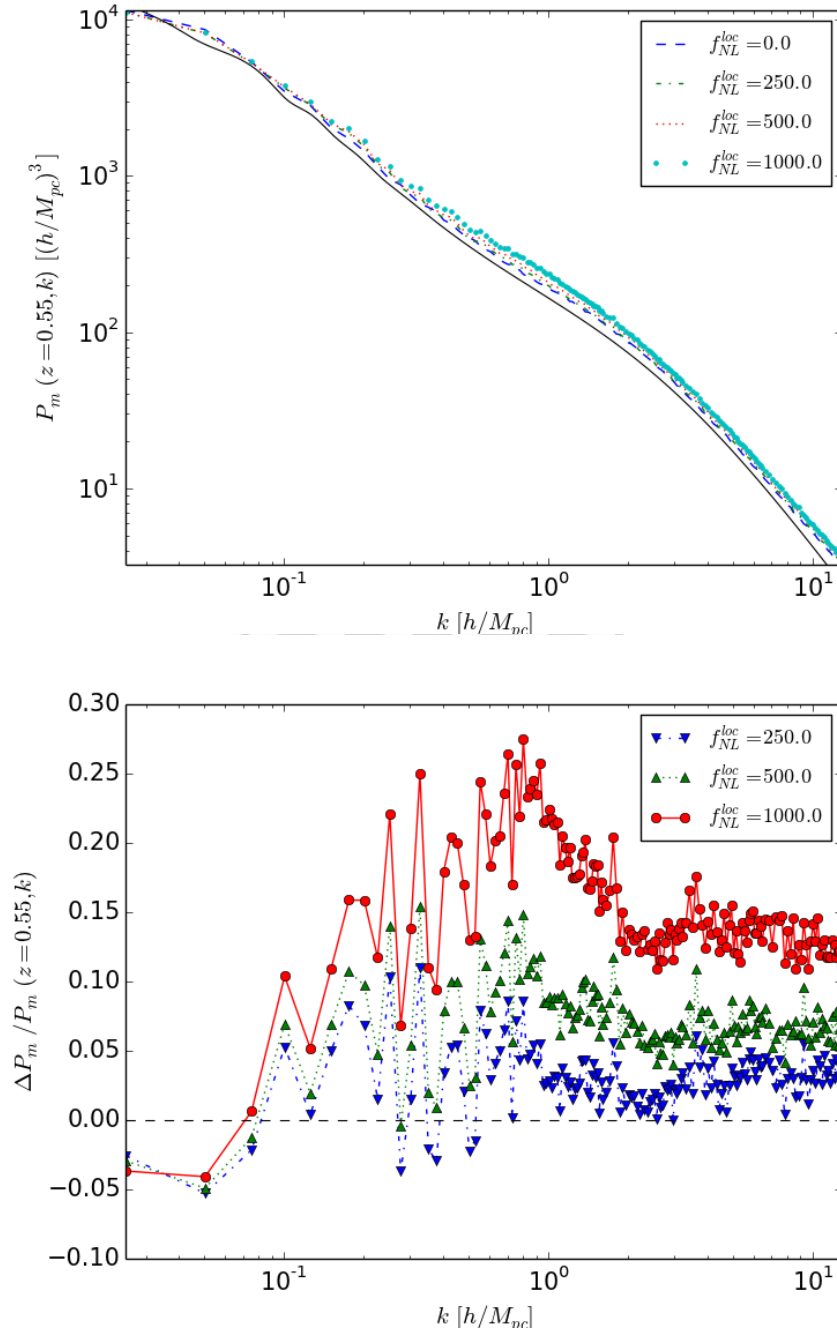


FIGURE 4.22: *Upper:* Non-linear power spectrum for different non-Gaussianity parameter $f_{NL}^{loc} = 0.0, 250.0, 500.0, 1000.0$ at redshift $z = 0.55$. Black solid line represents CAMB Halo-fit model prediction. *Lower:* Non-linear power spectrum residual with respect to Gaussian Λ CDM model at redshift $z = 0.55$.

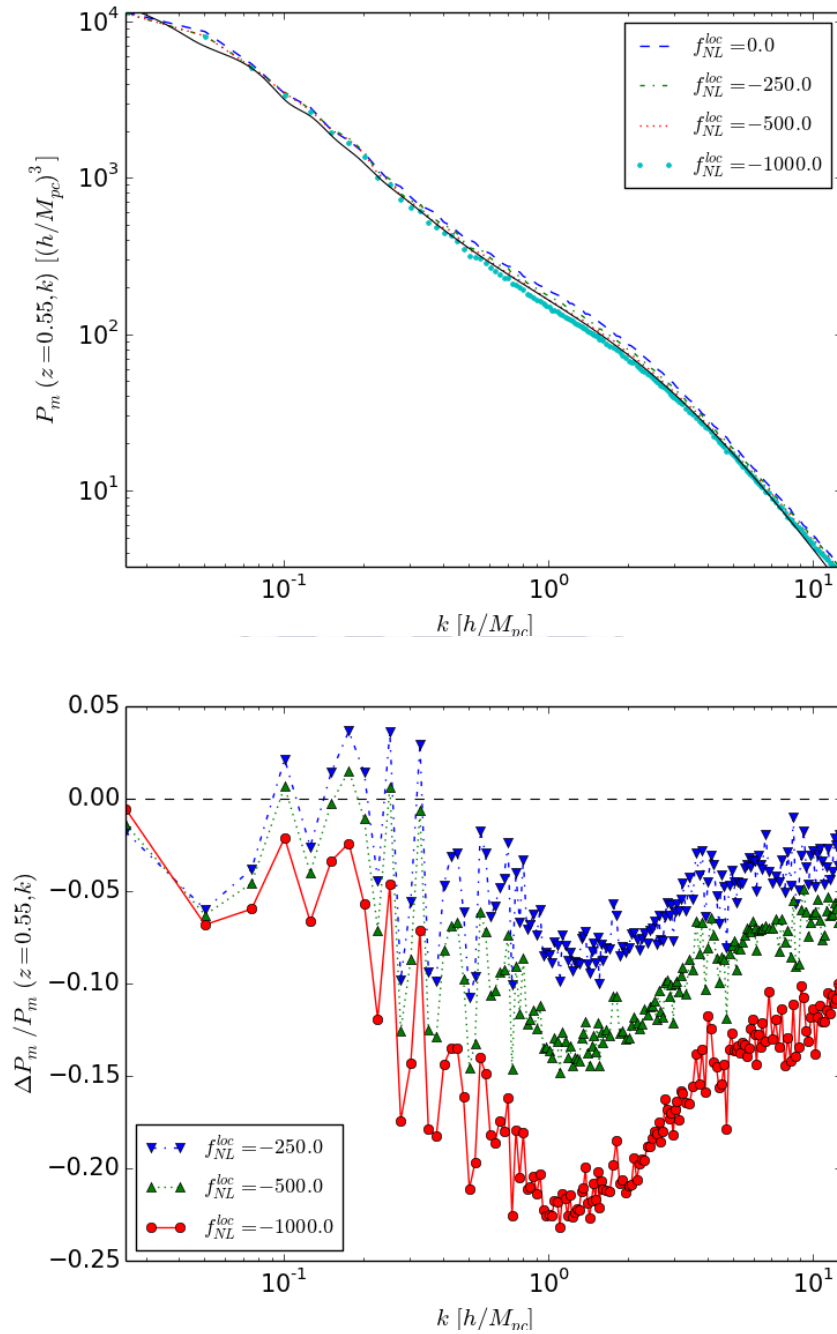


FIGURE 4.23: *Upper*: Non-linear power spectrum for different non-Gaussianity parameter $f_{NL}^{loc} = 0.0, -250.0, -500.0, -1000.0$ at redshift $z = 0.55$. Black solid line represents CAMB Halo-fit model prediction. *Lower*: Non-linear power spectrum residual with respect to Gaussian Λ CDM model at redshift $z = 0.55$.

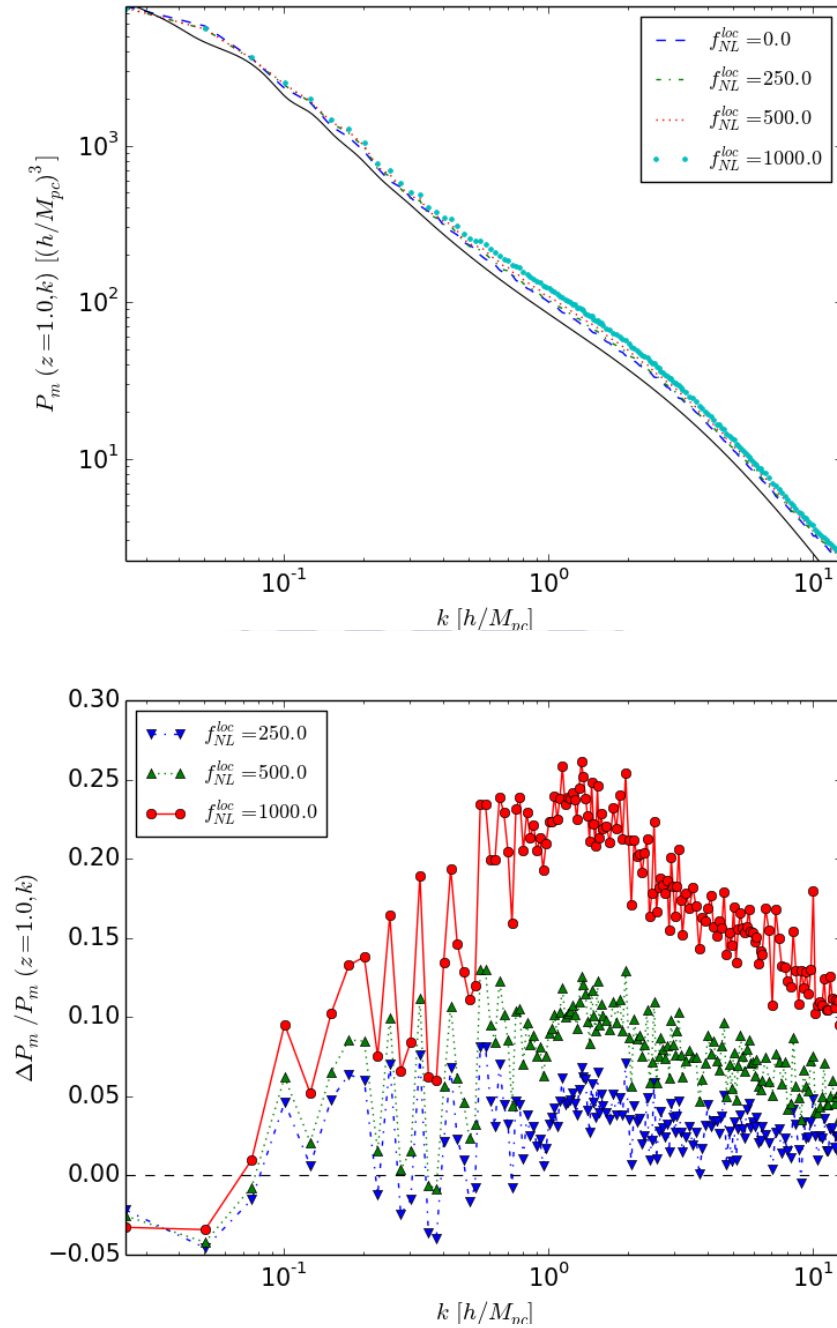


FIGURE 4.24: *Upper*: Non-linear power spectrum for different non-Gaussianity parameter $f_{NL}^{loc} = 0.0, 250.0, 500.0, 1000.0$ at redshift $z = 1.0$. Black solid line represents CAMB Halo-fit model prediction. *Lower*: Non-linear power spectrum residual with respect to Gaussian Λ CDM model at redshift $z = 1.0$.

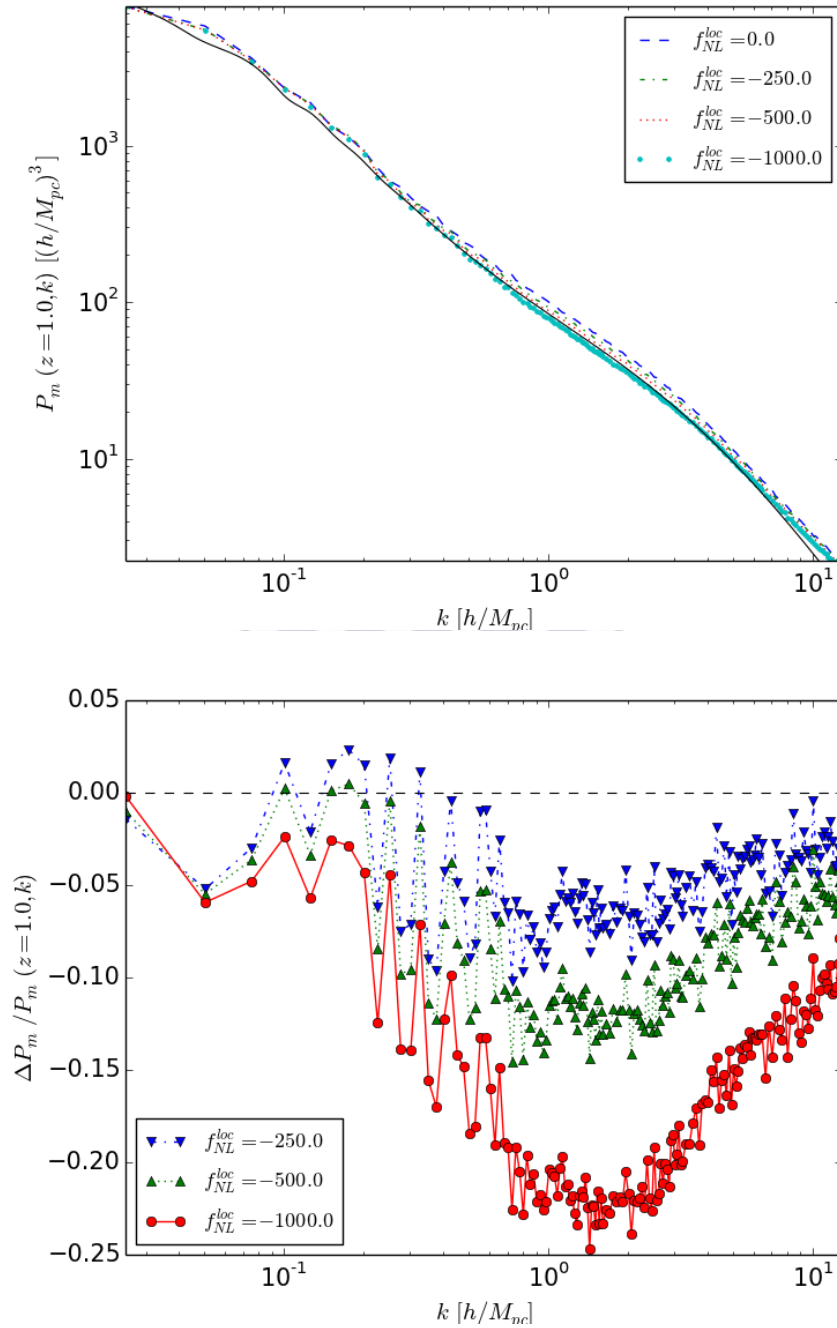


FIGURE 4.25: *Upper*: Non-linear power spectrum for different non-Gaussianity parameter $f_{NL}^{loc} = 0.0, -250.0, -500.0, -1000.0$ at redshift $z = 1.0$. Black solid line represents CAMB Halo-fit model prediction. *Lower*: Non-linear power spectrum residual with respect to Gaussian Λ CDM model at redshift $z = 1.0$.

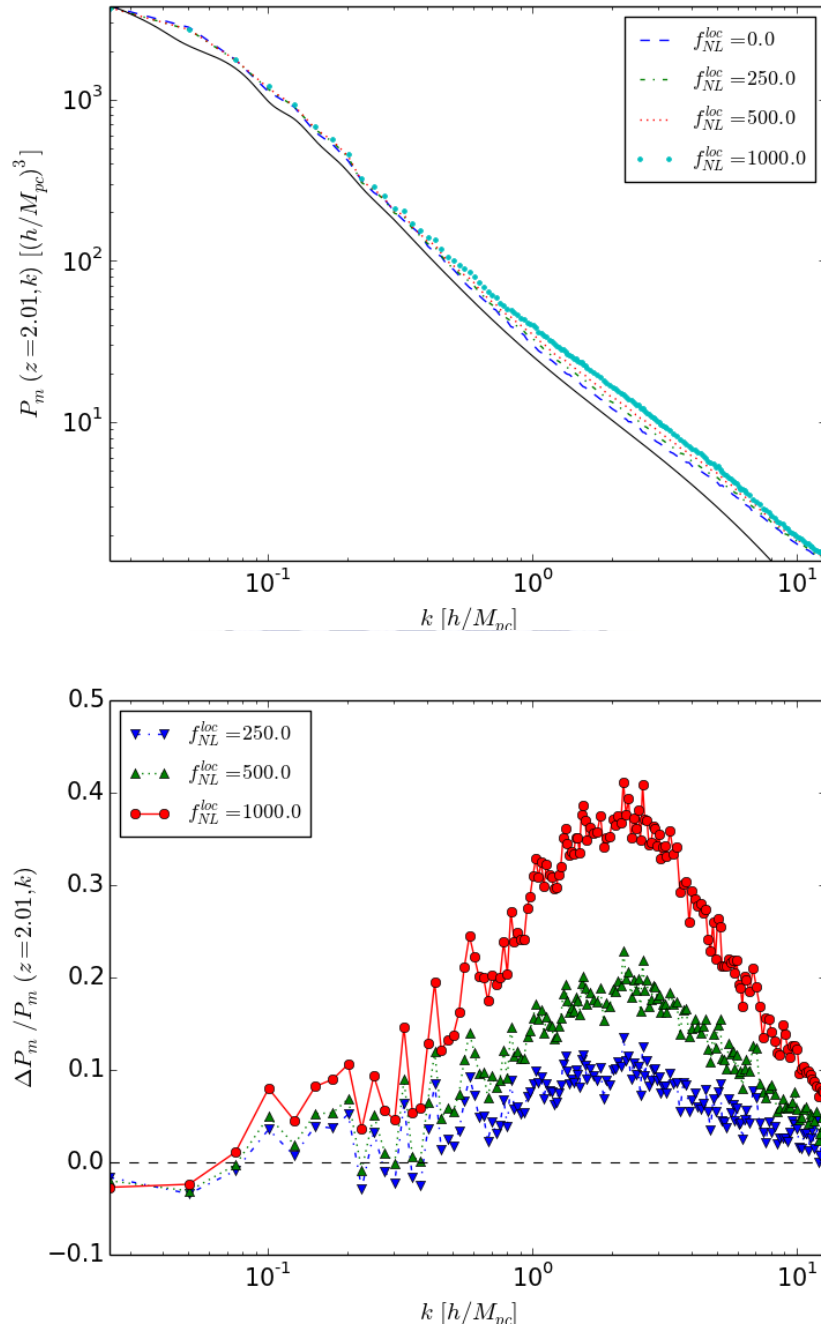


FIGURE 4.26: *Upper*: Non-linear power spectrum for different non-Gaussianity parameter $f_{NL}^{loc} = 0.0, 250.0, 500.0, 1000.0$ at redshift $z = 2.01$. Black solid line represents CAMB Halo-fit model prediction. *Lower*: Non-linear power spectrum residual with respect to Gaussian Λ CDM model at redshift $z = 2.01$.

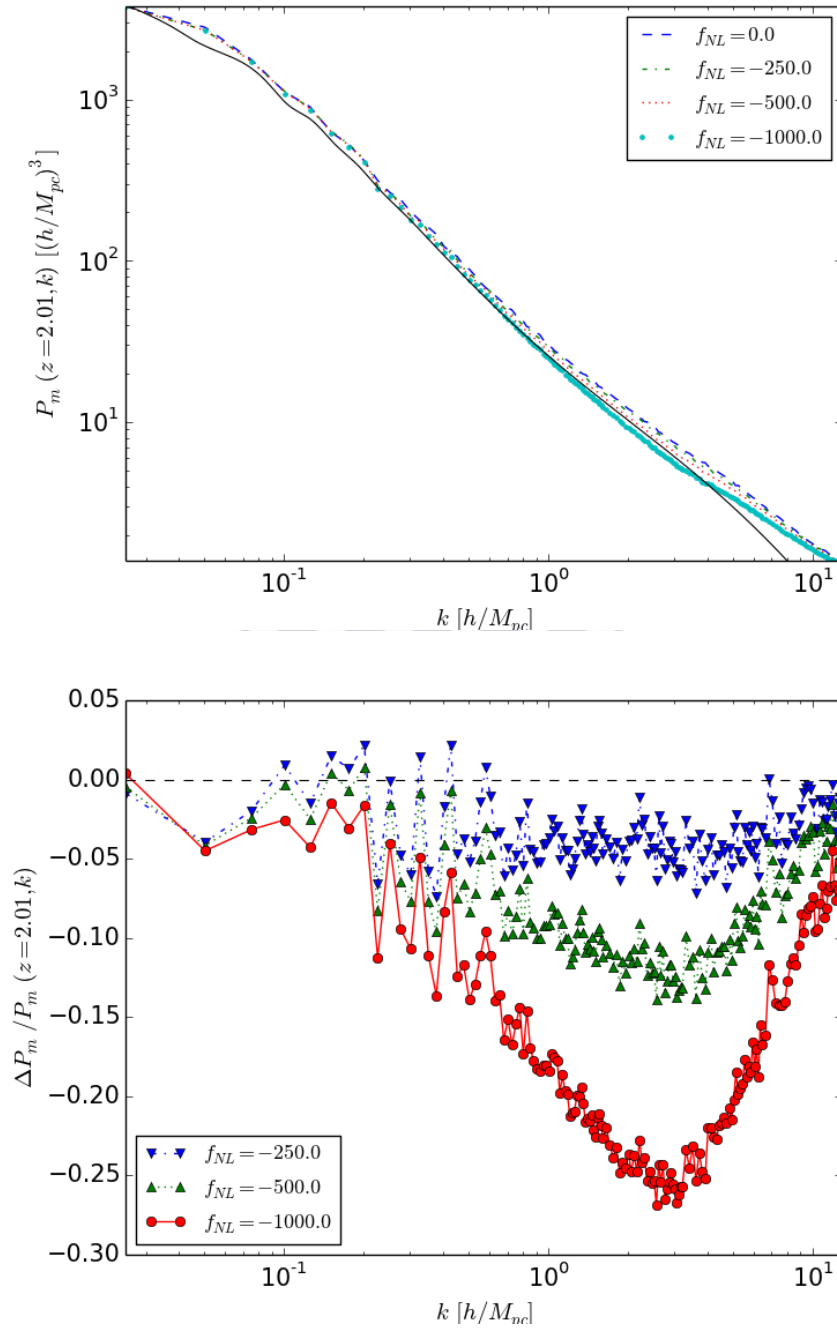


FIGURE 4.27: *Upper*: Non-linear power spectrum for different non-Gaussianity parameter $f_{NL}^{loc} = 0.0, -250.0, -500.0, -1000.0$ at redshift $z = 2.01$. Black solid line represents CAMB Halo-fit model prediction. *Lower*: Non-linear power spectrum residual with respect to Gaussian Λ CDM model at redshift $z = 2.01$.

4.3 Qualitative comparison with interacting dark energy simulations

Numerical N-body simulations have been tested so far for the simplest standard Λ CDM model with much agreement with analytical predictions. For more complex cosmological dark energy models, the use of N-body simulation becomes more relevant to identify small deviations from the standard model on non-linear scales. The significant progress made to the numerical simulations allows to investigate the nature of dark energy and to study different scenarios of interaction between dark energy and dark matter [53].

Interacting dark energy N-body simulations have been done firstly by [57] using a modified AMR code, which consider a range of scalar field dark energy models interacting with dark matter only. The first hydrodynamic simulations of interacting dark energy models are done by [9]. The evolution of the halo mass function with respect to redshift has been studied in [26] showing a significant effect of the interaction between dark energy and dark matter at high mass tail.

4.3.1 CoDECS simulations

For our qualitative comparison with interacting dark energy simulations, we are going to use the CoDECS simulations [7]. It includes interacting quintessence model simulations with interaction term of the form (3.54) with variable interaction rate $\beta(\phi)$ given as follows,

$$\beta(\phi) = \beta_0 \exp(\beta_1 \phi), \quad (4.1)$$

where β_0 and β_1 are constants. In our analysis we only consider simulations with constant interaction rate, i.e. $\beta_1 = 0.0$. There are different simulations runs within CoDECS including investigation of the effect of baryon dynamics via hydrodynamical simulations. Since this is out of the scope of the thesis, we only consider the L-CoDECS, see Table 4.3, runs which only represent interacting dark energy-dark matter simulations with the existence of baryons but without hydrodynamics. It consists of 2×1024^3 dark matter and baryon particles in a periodic cosmological box of $1^3 [(h^{-1} \text{Gpc})^3]$ size. The simulations are done using the modified TreePM N-body GADGET code [9]. The mass resolution of L-CoDECS simulations are $m_c = 5.84 \times 10^{10} h^{-1} M_\odot$ and $m_b = 1.17 \times 10^{10} h^{-1} M_\odot$ for dark matter and baryons respectively at $z = 0.0$.

The initial conditions for L-CoDECS simulations are generated using the Zel'dovich approximation on a homogeneous glass-like particle distribution [95]. The initial matter power spectrum are computed at $z_{ini} = 99.0$ via a modified Boltzmann code CAMB

Model	β_0	β_1	$w_\phi(z=0)$	$\sigma_8(z=0)$
L- Λ CDM	-	-	-1.0	0.809
L-EXP001	0.05	0	-0.997	0.825
L-EXP002	0.1	0	-0.995	0.875
L-EXP003	0.15	0	-0.991	0.967

TABLE 4.3: Set of L-CoDECS N-body simulation runs.

[54] for interacting quintessence cosmology with "WMAP7 only Maximum Likelihood" cosmological parameters [51].

4.3.2 Halo mass function

In order to compare primordial non-Gaussianity effect with interacting dark energy on non-linear scales, we compute the halo mass function for L-CoDECS simulations using the same halo finder we used for primordial non-Gaussianity simulations (see Sec. 4.2.1). We apply AHF halo finder [50] to L-CoDECS snapshots at $z = 2.01$ for three realizations of interaction parameter $\beta = 0.05, 0.1, 0.15$.

Fig. 4.28 shows halo mass function for interacting dark energy and the residual with respect to Λ CDM model. The halo mass function appears to show an increasing behaviour at high mass tail with the increasing interaction parameter β . At low mass tail, the halo mass function slightly deviates from the non-interacting case.

By qualitatively comparing with primordial non-Gaussian halo mass function Fig. 4.18, we notice that the high mass tail of the halo mass function apparently experience a similar effect from both primordial non-Gaussianity and interacting dark energy. This could lead to possible mutual degeneracy of primordial non-Gaussianity and interacting dark energy on non-linear scales.

4.4 Conclusion

In this chapter, we show that primordial non-Gaussianity leaves an imprint on non-linear scales of the structure formation of the universe. Via a set of cosmological mark matter N-Body simulations, we show that local primordial non-Gaussianity affects large mass halos. The calculation of the halo mass function indicates that large mass halos are very sensitive to primordial non-Gaussian initial conditions. This indicates that galaxy surveys are very good probes of primordial non-Gaussianity.

Non-linear power spectrum on scales $k \sim 1 h/\text{Mpc}$ are also sensitive to the value of non-Gaussianity. We show that for different non-Gaussianity realizations, non-linear power

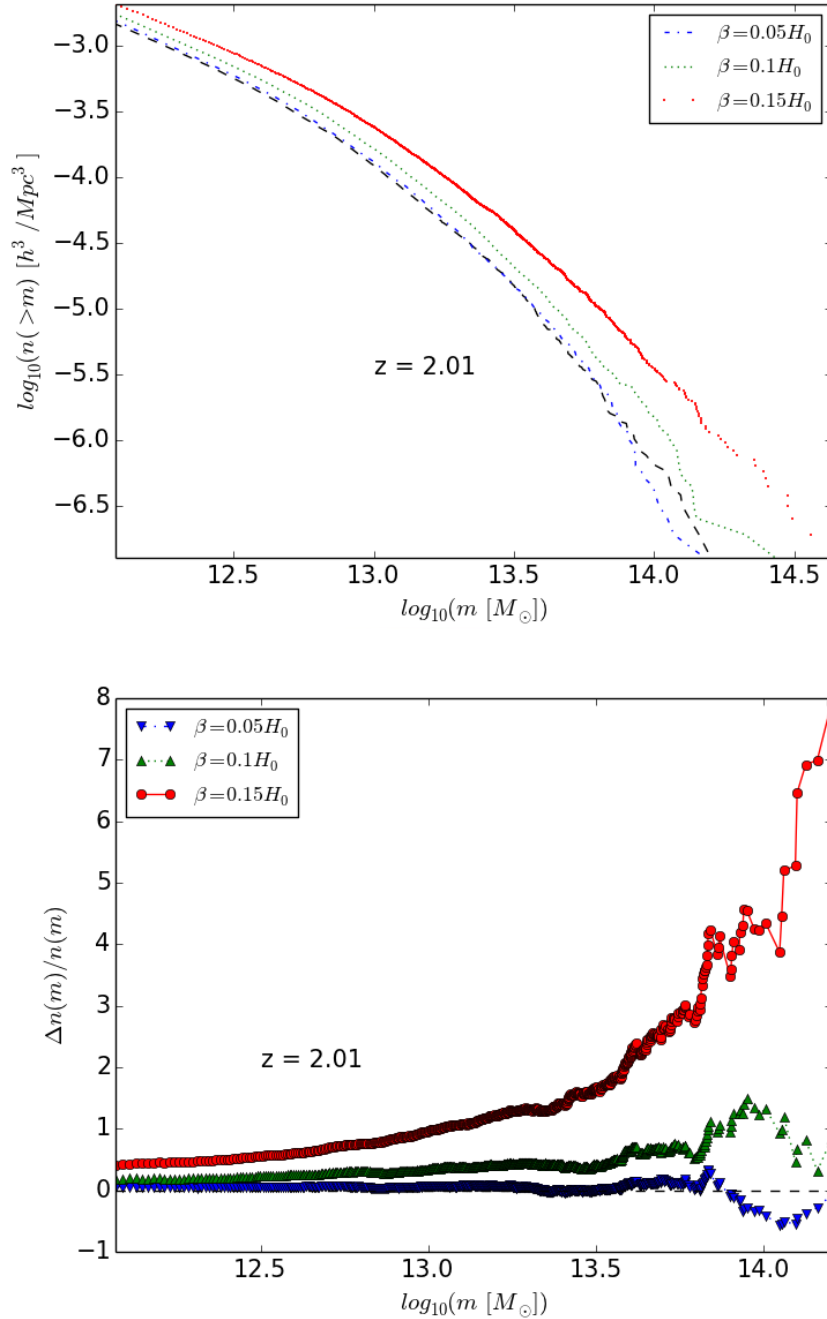


FIGURE 4.28: *Upper:* The halo mass function for L-CoDECS simulations of interacting dark energy at $z = 2.01$ for different interaction parameters $\beta = 0.05, 0.1, 0.15$. The solid-dashed line represents Λ CDM mode. *Lower:* The halo mass function residual with respect to Λ CDM model.

spectrum residual peaks around $k \sim 0.5 h/\text{Mpc}$ at redshift $z = 0.0$ and stabilize on very small scales.

In this chapter, we have used GADGET-2 and the initial condition code 2LPT-PNG with our CosmoSuite tool in order to investigate local primordial non-Gaussianity. This

work is part of a major project [42], which aims for the first time to include non-Gaussian initial conditions in N-body simulations with interacting dark energy. The project will advance our understanding from the large scales where perturbation theory is effective (see chapter 3) to small non-linear scales where N-body simulations are essential. The project combines the work presented in this chapter with previous work on N-body simulations with interacting dark energy and Gaussian initial conditions [9].



Chapter 5

Conclusion and future work

Large scale structure of the universe is a very promising tool for exploring the early universe physics. Mapping the universe on large scales gives us a very accurate constraint on many cosmological parameters including dark energy equation of state and primordial non-Gaussianity. In chapter one, we review the cosmic evolution history of the universe assuming the standard model. The dynamical evolution of the universe is described by the Friedmann equations derived by solving Einstein field equations for FLRW metric, assuming homogeneous and isotopic background. The expansion rate of the universe changes according to the different components of the cosmos. For accelerated expansion, the universe has to be filled with a negative pressure component.

In chapter 2 with discuss the dynamics of gravitational instability responsible for the evolution of the structure formation of the universe. Cosmological perturbation theory on linear/non-linear scales has been discussed with the derivation of perturbation equations for different dark energy cosmologies. We considered dynamical dark energy models with variable equation of state. We discussed the spherical collapse phenomenological model with the derivation of the mass function of collapsed objects. For statistical measure of the large scale structure, the 2-point correlation function has been discussed. In Fourier space, the power spectrum evolution of matter component of the universe has been derived using linear perturbation theory. According to inflation model, the quantum fluctuations are the physical seed of structure formation of the large scale structure in the universe. With the assumption of non-Gaussian curvature primordial field, we discussed the possible imprint of primordial non-Gaussian signature on late large scale structure. We showed that primordial non-Gaussianity leaves a scale-dependent effect of galaxy bias on very large scales.

Evolution is the interacting dark sector has been discussed in chapter 3. In this chapter, we derived the background and perturbation equations for interacting dark energy model

with constant interaction rate proportional to dark energy density. After numerical solution of the perturbation system we calculated the galaxy power spectrum. On very large scales, interacting dark energy perturbation leaves a scale-dependent signature similar to primordial non-Gaussianity. The two signals provide very similar features on very large scale galaxy power spectrum. At higher redshifts, the interacting dark energy signal decrease however primordial non-Gaussianity signal stay constant due to its primordial origin. So we can disentangle between the two signals by measuring the galaxy power spectrum at two different redshifts.

In chapter 4, we perform a set of cosmological N-body simulations to measure imprints of primordial non-Gaussianity on non-linear structure. Calculations of cumulative halo mass function show that it is sensitive to the value of primordial non-Gaussianity parameter f_{NL} on large mass tail. The change increase with higher redshifts. Non-linear power spectrum measurements also indicate that primordial non-Gaussianity affects non-linear power spectrum on scales $k \sim 1h/\text{Mpc}$. The change is stable with redshift changing however the peak of the residual change shifts towards small scales with higher redshifts. Future galaxy surveys are very good probes to the estimation of non-Gaussianity parameter to a high precision.

Measurements of halo mass function suggests that very large mass halos are affected by primordial non-Gaussianity. In the following section we discuss the future work investigating possible degeneracy between primordial non-Gaussianity an interaction in the dark sector via N-body numerical simulation.

5.1 Future work

Dark sector N-body simulations are a very promising tool to test the theoretical modelling of dark energy and dark matter components of the cosmos. The halo mass function are very sensitive to the nature of dark energy. The formation of dark matter halos on small scales is modulated by the primordial non-Gaussianity, leading to a scale-dependent bias on very large scales. Cosmological N-body simulations show that primordial non-Gaussianity strongly affects the clustering of rare objects on large scales and the mass function of massive halos.

Several scenarios have been proposed in the literature to account for the unexpected energy component of the cosmos - dark energy, responsible for the late time cosmic acceleration. This include the existence of a light minimally coupled scalar field called quintessence. Other proposed scenarios incorporate deviations form standard general relativity on cosmological scales. Recently, there has been a growing interest on whether

the physical nature of dark energy could be settled by the clustering of large-scale structures. This is also include the possible degeneracies between the clustering effect of interacting dark energy and the primordial non-Gaussianity constraint [43].

Numerical simulations used to investigate the evolution of the universe and the formation of cosmic structures beyond the linear regime has proven to be an extremely valuable tool. It has allowed to study the nature of dark matter and dark energy and its role in driving the growth of cosmic structures starting from the primordial density fluctuations generated in the early universe by the inflationary accelerated expansion. Many different codes have been developed for dark energy N-body simulations [7] and for alternative modified gravity scenarios [55]. This creates an essential studying tool and a link between theoretical modelling and direct observations for any present and future of the accelerated expansion of the universe.

In the presence of primordial non-Gaussianity, the formation of dark matter halos on small scales is modulated by the large-scale overdensity, leading to a scale-dependent bias on very large scales. Cosmological N-body simulations shows that primordial non-Gaussianity strongly affects the clustering of rare objects on large scales and the mass function of massive halos [28]. However dark sector interaction has its own imprint on the halo mass function as well [26] leading to a possible degeneracy between primordial non-Gaussianity and interacting dark energy on non-linear scales.

In future work, we will investigate different forms of primordial non-Gaussianity via its imprint on the halo mass function and the bias of the galaxies using N-body simulations, and determine how this form of non-Gaussianity is affected by various dark energy scenarios. Also, We will investigate a possible degeneracy between primordial Non-Gaussianity and Interacting dark energy on non-linear scales.

Bibliography

- [1] P. A. R. Ade et al. Planck 2015 results. XVII. Constraints on primordial non-Gaussianity. *arXiv:1502.01592*, 2015.
- [2] P. A. R. Ade et al. Planck 2015 results. XIII. Cosmological parameters. *arXiv:1502.01589*, 2015.
- [3] L. Amendola. Scaling solutions in general nonminimal coupling theories. *Phys. Rev.*, D60:043501, 1999. doi: 10.1103/PhysRevD.60.043501.
- [4] L. Amendola. Coupled quintessence. *Phys. Rev.*, D62:043511, 2000. doi: 10.1103/PhysRevD.62.043511.
- [5] L. Amendola. *Dark energy : theory and observations*. Cambridge University Press, New York, 2010.
- [6] J. Bahcall. *Dark matter in the universe*. World Scientific, Singapore Hackensack, N.J, 2004.
- [7] M. Baldi. The CoDECS project: a publicly available suite of cosmological N-body simulations for interacting dark energy models. *Mon. Not. Roy. Astron. Soc.*, 422: 1028–1044, 2012. doi: 10.1111/j.1365-2966.2012.20675.x.
- [8] M. Baldi. Dark Energy Simulations. *Phys. Dark Univ.*, 1:162–193, 2012. doi: 10.1016/j.dark.2012.10.004.
- [9] M. Baldi, V. Pettorino, G. Robbers, and V. Springel. Hydrodynamical N-body simulations of coupled dark energy cosmologies. *Mon. Not. Roy. Astron. Soc.*, 403: 1684–1702, 2010. doi: 10.1111/j.1365-2966.2009.15987.x.
- [10] J. M. Bardeen, P. J. Steinhardt, and M. S. Turner. Spontaneous Creation of Almost Scale - Free Density Perturbations in an Inflationary Universe. *Phys. Rev.*, D28: 679, 1983. doi: 10.1103/PhysRevD.28.679.
- [11] J. M. Bardeen, J. Bond, N. Kaiser, and A. Szalay. The Statistics of Peaks of Gaussian Random Fields. *Astrophys.J.*, 304:15–61, 1986. doi: 10.1086/164143.

- [12] N. Bartolo, E. Komatsu, S. Matarrese, and A. Riotto. Non-Gaussianity from inflation: Theory and observations. *Phys.Rept.*, 402:103–266, 2004. doi: 10.1016/j.physrep.2004.08.022.
- [13] D. Baumann. TASI Lectures on Inflation. In *Physics of the large and the small, TASI 09, proceedings of the Theoretical Advanced Study Institute in Elementary Particle Physics, Boulder, Colorado, USA, 1-26 June 2009*, pages 523–686, 2011. doi: 10.1142/9789814327183_0010.
- [14] A. J. Benson, C. Reichardt, and M. Kamionkowski. Statistics of Sunyaev-Zeldovich cluster surveys. *Mon. Not. Roy. Astron. Soc.*, 331:71, 2002. doi: 10.1046/j.1365-8711.2002.05139.x.
- [15] F. Bernardeau, S. Colombi, E. Gaztanaga, and R. Scoccimarro. Large scale structure of the universe and cosmological perturbation theory. *Phys. Rept.*, 367:1–248, 2002. doi: 10.1016/S0370-1573(02)00135-7.
- [16] E. Bertschinger. Simulations of structure formation in the universe. *Ann. Rev. Astron. Astrophys.*, 36:599–654, 1998. doi: 10.1146/annurev.astro.36.1.599.
- [17] G. R. Blumenthal, S. M. Faber, J. R. Primack, and M. J. Rees. Formation of Galaxies and Large Scale Structure with Cold Dark Matter. *Nature*, 311:517–525, 1984. doi: 10.1038/311517a0.
- [18] M. Bruni, R. Crittenden, K. Koyama, R. Maartens, C. Pitrou, et al. Disentangling non-Gaussianity, bias and GR effects in the galaxy distribution. *Phys.Rev.*, D85:041301, 2012. doi: 10.1103/PhysRevD.85.041301.
- [19] M. Bruni, R. Crittenden, K. Koyama, R. Maartens, C. Pitrou, et al. Disentangling non-Gaussianity, bias and GR effects in the galaxy distribution. *Phys.Rev.*, D85:041301, 2012. doi: 10.1103/PhysRevD.85.041301.
- [20] G. Caldera-Cabral, R. Maartens, and L. A. Urena-Lopez. Dynamics of interacting dark energy. *Phys. Rev.*, D79:063518, 2009. doi: 10.1103/PhysRevD.79.063518.
- [21] R. R. Caldwell, R. Dave, and P. J. Steinhardt. Cosmological imprint of an energy component with general equation of state. *Phys. Rev. Lett.*, 80:1582–1585, 1998. doi: 10.1103/PhysRevLett.80.1582.
- [22] T. Clemson, K. Koyama, G.-B. Zhao, R. Maartens, and J. Valiviita. Interacting Dark Energy – constraints and degeneracies. *Phys.Rev.*, D85:043007, 2012. doi: 10.1103/PhysRevD.85.043007.
- [23] S. Cole and N. Kaiser. Biased clustering in the cold dark matter cosmogony. *Mon. Not. Roy. Astron. Soc.*, 237:1127–1146, 1989.

- [24] S. Colombi, A. H. Jaffe, D. Novikov, and C. Pichon. Accurate estimators of power spectra in N-body simulations. *Mon. Not. Roy. Astron. Soc.*, 393:511, 2009. doi: 10.1111/j.1365-2966.2008.14176.x.
- [25] A. A. Costa, X.-D. Xu, B. Wang, E. G. M. Ferreira, and E. Abdalla. Testing the Interaction between Dark Energy and Dark Matter with Planck Data. *Phys.Rev.*, D89:103531, 2014. doi: 10.1103/PhysRevD.89.103531.
- [26] W. Cui, M. Baldi, and S. Borgani. The halo mass function in interacting Dark Energy models. *Mon. Not. Roy. Astron. Soc.*, 424:993, 2012. doi: 10.1111/j.1365-2966.2012.21267.x.
- [27] N. Dalal, K. Abazajian, E. E. Jenkins, and A. V. Manohar. Testing the cosmic coincidence problem and the nature of dark energy. *Phys. Rev. Lett.*, 87:141302, 2001. doi: 10.1103/PhysRevLett.87.141302.
- [28] N. Dalal, O. Dore, D. Huterer, and A. Shirokov. The imprints of primordial non-gaussianities on large-scale structure: scale dependent bias and abundance of virialized objects. *Phys. Rev.*, D77:123514, 2008. doi: 10.1103/PhysRevD.77.123514.
- [29] M. Davis, F. J. Summers, and D. Schlegel. Large scale structure in a universe with mixed hot and cold dark matter. *Nature*, 359:393–396, 1992. doi: 10.1038/359393a0.
- [30] V. Desjacques, U. Seljak, and I. Iliev. Scale-dependent bias induced by local non-Gaussianity: A comparison to N-body simulations. *Mon. Not. Roy. Astron. Soc.*, 396:85–96, 2009. doi: 10.1111/j.1365-2966.2009.14721.x.
- [31] S. Dodelson. *Modern cosmology*. Academic Press, An Imprint of Elsevier, San Diego, California, 2003.
- [32] D. Duniya, D. Bertacca, and R. Maartens. Clustering of quintessence on horizon scales and its imprint on HI intensity mapping. *JCAP*, 1310:015, 2013. doi: 10.1088/1475-7516/2013/10/015.
- [33] D. G. Duniya, D. Bertacca, and R. Maartens. Probing the imprint of interacting dark energy on very large scales. *Phys. Rev.*, D91:063530, 2015. doi: 10.1103/PhysRevD.91.063530.
- [34] R. Durrer. *The cosmic microwave background*. Cambridge University Press, Cambridge, UK New York, 2008.
- [35] K. Enqvist, S. Hotchkiss, and O. Taanila. Estimating f_{NL} and g_{NL} from Massive High-Redshift Galaxy Clusters. *JCAP*, 1104:017, 2011. doi: 10.1088/1475-7516/2011/04/017.

- [36] L. H. Ford. Cosmological constant damping by unstable scalar fields. *Phys. Rev.*, D35:2339, 1987. doi: 10.1103/PhysRevD.35.2339.
- [37] T. Giannantonio, A. J. Ross, W. J. Percival, R. Crittenden, D. Bacher, et al. Improved Primordial Non-Gaussianity Constraints from Measurements of Galaxy Clustering and the Integrated Sachs-Wolfe Effect. *Phys.Rev.*, D89:023511, 2014. doi: 10.1103/PhysRevD.89.023511.
- [38] S. P. D. Gill, A. Knebe, and B. K. Gibson. The Evolution substructure 1: A New identification method. *Mon. Not. Roy. Astron. Soc.*, 351:399, 2004. doi: 10.1111/j.1365-2966.2004.07786.x.
- [39] M. Grossi, L. Verde, C. Carbone, K. Dolag, E. Branchini, F. Iannuzzi, S. Matarrese, and L. Moscardini. Large-scale non-Gaussian mass function and halo bias: tests on N-body simulations. *Mon. Not. Roy. Astron. Soc.*, 398:321–332, 2009. doi: 10.1111/j.1365-2966.2009.15150.x.
- [40] A. H. Guth. The Inflationary Universe: A Possible Solution to the Horizon and Flatness Problems. *Phys. Rev.*, D23:347–356, 1981. doi: 10.1103/PhysRevD.23.347.
- [41] A. H. Guth and S.-Y. Pi. The Quantum Mechanics of the Scalar Field in the New Inflationary Universe. *Phys. Rev.*, D32:1899–1920, 1985. doi: 10.1103/PhysRevD.32.1899.
- [42] M. Hashim, M. Baldi, D. Bertacca, and R. Maartens. Interacting dark energy N-body simulations with non-Gaussian initial conditions. *In preparation*.
- [43] M. Hashim, D. Bertacca, and R. Maartens. Degeneracy between primordial non-Gaussianity and interaction in the dark sector. *Phys. Rev.*, D90(10):103518, 2014. doi: 10.1103/PhysRevD.90.103518.
- [44] S. Ho, C. Hirata, N. Padmanabhan, U. Seljak, and N. Bahcall. Correlation of CMB with large-scale structure: I. ISW Tomography and Cosmological Implications. *Phys. Rev.*, D78:043519, 2008. doi: 10.1103/PhysRevD.78.043519.
- [45] W. Hu and N. Sugiyama. Anisotropies in the cosmic microwave background: An Analytic approach. *Astrophys. J.*, 444:489–506, 1995. doi: 10.1086/175624.
- [46] W. Hu and N. Sugiyama. Small scale cosmological perturbations: An Analytic approach. *Astrophys. J.*, 471:542–570, 1996. doi: 10.1086/177989.
- [47] D. Huterer and M. Takada. Calibrating the nonlinear matter power spectrum: Requirements for future weak lensing surveys. *Astropart. Phys.*, 23:369–376, 2005. doi: 10.1016/j.astropartphys.2005.02.006.

- [48] A. Jenkins, C. S. Frenk, S. D. M. White, J. M. Colberg, S. Cole, A. E. Evrard, H. M. P. Couchman, and N. Yoshida. The Mass function of dark matter halos. *Mon. Not. Roy. Astron. Soc.*, 321:372, 2001. doi: 10.1046/j.1365-8711.2001.04029.x.
- [49] D. Jeong, F. Schmidt, and C. M. Hirata. Large-scale clustering of galaxies in general relativity. *Phys.Rev.*, D85:023504, 2012. doi: 10.1103/PhysRevD.85.023504.
- [50] S. R. Knollmann and A. Knebe. Ahf: Amiga’s Halo Finder. *Astrophys. J. Suppl.*, 182:608–624, 2009. doi: 10.1088/0067-0049/182/2/608.
- [51] E. Komatsu et al. Seven-Year Wilkinson Microwave Anisotropy Probe (WMAP) Observations: Cosmological Interpretation. *Astrophys. J. Suppl.*, 192:18, 2011. doi: 10.1088/0067-0049/192/2/18.
- [52] K. Koyama, R. Maartens, and Y.-S. Song. Velocities as a probe of dark sector interactions. *JCAP*, 0910:017, 2009. doi: 10.1088/1475-7516/2009/10/017.
- [53] M. Kuhlen, M. Vogelsberger, and R. Angulo. Numerical Simulations of the Dark Universe: State of the Art and the Next Decade. *Phys. Dark Univ.*, 1:50–93, 2012. doi: 10.1016/j.dark.2012.10.002.
- [54] A. Lewis, A. Challinor, and A. Lasenby. Efficient computation of CMB anisotropies in closed FRW models. *Astrophys. J.*, 538:473–476, 2000. doi: 10.1086/309179.
- [55] B. Li, G.-B. Zhao, R. Teyssier, and K. Koyama. ECOSMOG: An Efficient Code for Simulating Modified Gravity. *JCAP*, 1201:051, 2012. doi: 10.1088/1475-7516/2012/01/051.
- [56] A. R. Liddle and D. H. Lyth. The Cold dark matter density perturbation. *Phys. Rept.*, 231:1–105, 1993. doi: 10.1016/0370-1573(93)90114-S.
- [57] A. V. Maccio, C. Quercellini, R. Mainini, L. Amendola, and S. A. Bonometto. N-body simulations for coupled dark energy: Halo mass function and density profiles. *Phys. Rev.*, D69:123516, 2004. doi: 10.1103/PhysRevD.69.123516.
- [58] R. Mainini and S. Bonometto. Mass functions in coupled Dark Energy models. *Phys. Rev.*, D74:043504, 2006. doi: 10.1103/PhysRevD.74.043504.
- [59] S. Matarrese, L. Verde, and R. Jimenez. The Abundance of high-redshift objects as a probe of non-Gaussian initial conditions. *Astrophys.J.*, 541:10, 2000. doi: 10.1086/309412.
- [60] P. McDonald and U. Seljak. How to measure redshift-space distortions without sample variance. *JCAP*, 0910:007, 2009. doi: 10.1088/1475-7516/2009/10/007.

- [61] A. L. Melott, J. Einasto, E. Saar, I. Suisalu, A. A. Klypin, and S. F. Shandarin. Cluster Analysis Of The Nonlinear Evolution Of Large Scale Structure In An Axion / Gravitino / Photino Dominated Universe. *Phys. Rev. Lett.*, 51:935–938, 1983. doi: 10.1103/PhysRevLett.51.935.
- [62] M. J. Mortonson, W. Hu, and D. Huterer. Simultaneous Falsification of Λ CDM and Quintessence with Massive, Distant Clusters. *Phys. Rev.*, D83:023015, 2011. doi: 10.1103/PhysRevD.83.023015.
- [63] J. Peacock. *Cosmological physics*. Cambridge University Press, Cambridge, UK New York, 1999.
- [64] P. J. E. Peebles. Large scale background temperature and mass fluctuations due to scale invariant primeval perturbations. *Astrophys. J.*, 263:L1–L5, 1982. doi: 10.1086/183911.
- [65] P. J. E. Peebles. *Principles of physical cosmology*. Princeton University Press, Princeton, N.J, 1993.
- [66] W. J. Potter and S. Chongchitnan. A Gauge-invariant approach to interactions in the dark sector. *JCAP*, 1109:005, 2011. doi: 10.1088/1475-7516/2011/09/005.
- [67] W. H. Press and P. Schechter. Formation of galaxies and clusters of galaxies by selfsimilar gravitational condensation. *Astrophys. J.*, 187:425–438, 1974. doi: 10.1086/152650.
- [68] A. Raccanelli, D. Bertacca, O. Dor, and R. Maartens. Large-scale 3D galaxy correlation function and non-Gaussianity. *JCAP*, 1408:022, 2014. doi: 10.1088/1475-7516/2014/08/022.
- [69] B. Ratra and P. J. E. Peebles. Cosmological Consequences of a Rolling Homogeneous Scalar Field. *Phys. Rev.*, D37:3406, 1988. doi: 10.1103/PhysRevD.37.3406.
- [70] D. Reed, R. Bower, C. Frenk, A. Jenkins, and T. Theuns. The halo mass function from the dark ages through the present day. *Mon. Not. Roy. Astron. Soc.*, 374: 2–15, 2007. doi: 10.1111/j.1365-2966.2006.11204.x.
- [71] D. S. Salopek and J. R. Bond. Stochastic inflation and nonlinear gravity. *Phys. Rev.*, D43:1005–1031, 1991. doi: 10.1103/PhysRevD.43.1005.
- [72] V. Salvatelli, A. Marchini, L. Lopez-Honorez, and O. Mena. New constraints on Coupled Dark Energy from the Planck satellite experiment. *Phys. Rev.*, D88(2): 023531, 2013. doi: 10.1103/PhysRevD.88.023531.

- [73] V. Salvatelli, N. Said, M. Bruni, A. Melchiorri, and D. Wands. Indications of a late-time interaction in the dark sector. *Phys. Rev. Lett.*, 113(18):181301, 2014. doi: 10.1103/PhysRevLett.113.181301.
- [74] R. Scoccimarro, E. Sefusatti, and M. Zaldarriaga. Probing primordial non-Gaussianity with large - scale structure. *Phys.Rev.*, D69:103513, 2004. doi: 10.1103/PhysRevD.69.103513.
- [75] R. Scoccimarro, L. Hui, M. Manera, and K. C. Chan. Large-scale Bias and Efficient Generation of Initial Conditions for Non-Local Primordial Non-Gaussianity. *Phys. Rev.*, D85:083002, 2012. doi: 10.1103/PhysRevD.85.083002.
- [76] U. Seljak. Extracting primordial non-gaussianity without cosmic variance. *Phys. Rev. Lett.*, 102:021302, 2009. doi: 10.1103/PhysRevLett.102.021302.
- [77] U. Seljak and M. Zaldarriaga. A Line of sight integration approach to cosmic microwave background anisotropies. *Astrophys. J.*, 469:437–444, 1996. doi: 10.1086/177793.
- [78] R. K. Sheth and G. Tormen. Large scale bias and the peak background split. *Mon.Not.Roy.Astron.Soc.*, 308:119, 1999. doi: 10.1046/j.1365-8711.1999.02692.x.
- [79] A. Slosar, C. Hirata, U. Seljak, S. Ho, and N. Padmanabhan. Constraints on local primordial non-Gaussianity from large scale structure. *JCAP*, 0808:031, 2008. doi: 10.1088/1475-7516/2008/08/031.
- [80] R. E. Smith, J. A. Peacock, A. Jenkins, S. D. M. White, C. S. Frenk, F. R. Pearce, P. A. Thomas, G. Efstathiou, and H. M. P. Couchmann. Stable clustering, the halo model and nonlinear cosmological power spectra. *Mon. Not. Roy. Astron. Soc.*, 341:1311, 2003. doi: 10.1046/j.1365-8711.2003.06503.x.
- [81] V. Springel. The Cosmological simulation code GADGET-2. *Mon. Not. Roy. Astron. Soc.*, 364:1105–1134, 2005. doi: 10.1111/j.1365-2966.2005.09655.x.
- [82] J. L. Tinker, A. V. Kravtsov, A. Klypin, K. Abazajian, M. S. Warren, G. Yepes, S. Gottlober, and D. E. Holz. Toward a halo mass function for precision cosmology: The Limits of universality. *Astrophys. J.*, 688:709–728, 2008. doi: 10.1086/591439.
- [83] S. Tsujikawa, K. Uddin, S. Mizuno, R. Tavakol, and J. Yokoyama. Constraints on scalar-tensor models of dark energy from observational and local gravity tests. *Phys. Rev.*, D77:103009, 2008. doi: 10.1103/PhysRevD.77.103009.
- [84] S. Tsujikawa, A. De Felice, and J. Alcaniz. Testing for dynamical dark energy models with redshift-space distortions. *JCAP*, 1301:030, 2013. doi: 10.1088/1475-7516/2013/01/030.

- [85] J. Valiviita, E. Majerotto, and R. Maartens. Instability in interacting dark energy and dark matter fluids. *JCAP*, 0807:020, 2008. doi: 10.1088/1475-7516/2008/07/020.
- [86] J. Valiviita, R. Maartens, and E. Majerotto. Observational constraints on an interacting dark energy model. *Mon.Not.Roy.Astron.Soc.*, 402:2355–2368, 2010. doi: 10.1111/j.1365-2966.2009.16115.x.
- [87] C. Wagner, L. Verde, and L. Boubekur. N-body simulations with generic non-Gaussian initial conditions I: Power Spectrum and halo mass function. *JCAP*, 1010:022, 2010. doi: 10.1088/1475-7516/2010/10/022.
- [88] Y. Wang, D. Wands, G.-B. Zhao, and L. Xu. Post-*Planck* constraints on interacting vacuum energy. *Phys.Rev.*, D90:023502, 2014. doi: 10.1103/PhysRevD.90.023502.
- [89] N. N. Weinberg and M. Kamionkowski. Constraining dark energy from the abundance of weak gravitational lenses. *Mon. Not. Roy. Astron. Soc.*, 341:251, 2003. doi: 10.1046/j.1365-8711.2003.06421.x.
- [90] S. Weinberg. *Cosmology*. Oxford University Press, Oxford New York, 2008.
- [91] X.-D. Xu, B. Wang, P. Zhang, and F. Atrio-Barandela. The effect of Dark Matter and Dark Energy interactions on the peculiar velocity field and the kinetic Sunyaev-Zel’dovich effect. *JCAP*, 1312:001, 2013. doi: 10.1088/1475-7516/2013/12/001.
- [92] W. Yang and L. Xu. Cosmological constraints on interacting dark energy with redshift-space distortion after Planck data. *Phys.Rev.*, D89:083517, 2014. doi: 10.1103/PhysRevD.89.083517.
- [93] W. Yang and L. Xu. Testing coupled dark energy with large scale structure observation. *JCAP*, 1408:034, 2014. doi: 10.1088/1475-7516/2014/08/034.
- [94] J. Yoo, N. Hamaus, U. Seljak, and M. Zaldarriaga. Going beyond the Kaiser redshift-space distortion formula: a full general relativistic account of the effects and their detectability in galaxy clustering. *Phys. Rev.*, D86:063514, 2012. doi: 10.1103/PhysRevD.86.063514.
- [95] Ya. B. Zeldovich. Gravitational instability: An Approximate theory for large density perturbations. *Astron. Astrophys.*, 5:84–89, 1970.